Steam Explosions of Molten Ferrosilicon Drops Released into Water: Effects of Triggering, Alloying and Water Temperature

L.S. Nelson, P.W. Brooks, R. Bonazza, M.L. Corradini

February 2004

UWFDM-1224

FUSION TECHNOLOGY INSTITUTE

UNIVERSITY OF WISCONSIN

MADISON WISCONSIN

Steam Explosions of Molten Ferrosilicon Drops Released into Water: Effects of Triggering, Alloying and Water Temperature

L.S. Nelson, P.W. Brooks, R. Bonazza, M.L. Corradini

Fusion Technology Institute
University of Wisconsin
1500 Engineering Drive
Madison, WI 53706

http://fti.neep.wisc.edu

February 2004

UWFDM-1224

ABSTRACT

When 10 mm drops of molten ferrosilicon (75 wt.% Si and 25 wt.% Fe, with and without Al and Ca additives) at the liquidus temperature were released into liquid water at 8 ^{o}C, 20 ^{o}C (room temperature) and 80 ^{o}C, there were no spontaneous explosions. By generating pressure transients in the water with small hydrogen-oxygen explosions or with a mechanical impactor, steam explosions could be initiated at all three water temperatures, but only with the drops without additives. We recorded video and photographic images of the explosions and examined the debris that remained afterward.

By measuring the bubbles produced, we estimated the energy transferred to the water by the explosions to be 1 or 2% of the enthalpy available in the drops.

The video and photographic images indicate that the fragmented melt particles burn in the water, generating distinctive luminosities, bubbles of hydrogen and colloidal products. X-ray diffraction analyses of the debris suggest that molten ferrosilicon burns underwater largely via the vapor phase.

INTRODUCTION

Steam explosions sometimes occur when a hot molten material contacts liquid water. Even though these explosions have the potential to cause serious accidents in the metals, nuclear and other industries, they are not well understood. In order to provide information about the nature, energetics and possible suppression of these explosions, many experiments have been performed in which both large and small quantities of molten materials have been brought together with liquid water in various configurations (see reviews by Buxton and Nelson, 1975; Cronenberg and Benz, 1980; Reid, 1983; Corradini et al., 1988).

The release of single drops of molten materials into water is an important configuration for the experimental study of steam explosions. Because of the small scale, the experiments can provide good reproducibility and control of variables safely, at low cost and with rapid turnaround times. Also, these experiments usually combine high quality diagnostics during and after the experiments with the capability for quantitative collection of the fine debris and gases generated during the interactions. Moreover, single drop experiments can produce quantitative inputs for the development and validation of theories to predict the effects of full-scale steam explosions and thus reduce the need for more costly, hazardous and often difficult-to-interpret experiments with large amounts of melt.

Although single drops of some molten materials explode spontaneously when released into water, e.g., Sn, Pb, Bi (Flory et al., 1969; Dullforce et al., 1976; Shoji and Takagi 1983), drops of other melts fall benignly through the water and freeze without fragmentation or other violent interaction, e.g., Fe, Al, Al-Li alloys and FeO_x, where x is ~1.25 (Nelson and Duda, 1981, 1982, 1983; Nelson et al., 1994b; Nelson, 1995). Differences in the ability of various melts to explode spontaneously often occur even though the respective temperatures of both melt and water may lie in the same ranges.

When the freely falling molten globules do not explode spontaneously, explosions in many cases can be initiated by introducing pressure disturbances into the water; this process is often called triggering. We believe the pressure transients collapse the boiling film surrounding the drop of molten material and thus induce a steam explosion.

Several schemes have been developed for producing pressure transients in water for steam explosion triggering. These include application of mechanical impacts to the walls or bottom of the water chamber (Peppler and Till, 1986; Kim and Corradini, 1986; Schins et al., 1986; Epstein and Miller, 1987), the use of shock tubes (Sharon and Bankoff, 1981), underwater electrical discharges (Anderson and Armstrong, 1981; Arakeri et al., 1978; Nelson and Duda, 1981, 1982, 1985; Kondo et al., 1979; Ciccarelli, 1991; Ciccarelli and Frost, 1994), chemically enhanced electrical discharges (Nelson et al., 1994a) and the underwater detonation of small amounts of high explosives (Beck et al., 1991; Ciccarelli, 1991; Ciccarelli and Frost, 1994).

During 1996 and 1997, we began a laboratory study of single drops of molten ferrosilicon alloys (nominally 75 wt.% Si-25 wt.% Fe) released into water. This study, sponsored by SINTEF Materials Technology, Trondheim, Norway, was motivated by the desire to understand more about the water granulation technique for producing industrial quantities of solidified globules of the alloy. In this process, drops of the molten alloy are sprayed into water for quenching and cooling, a procedure in which steam explosions are potential hazards (Nygaard et al., 1995). Thus, we have been investigating both the behavior of the drops of melt as they enter and fall through water and also conditions that might give rise to steam explosions of individual drops of the molten material.

We learned in preliminary experiments that drops of the molten ferrosilicon alloys never exploded spontaneously as they fell through liquid water. Therefore, we have been generating pressure transients in the water in order to trigger steam explosions of the drops. For this purpose, we have developed two simple and inexpensive devices for generating typical initiating transients, one mechanical and the other chemical. As part of these procedures, we have characterized the pressure-time history of the transients with a quartz pressure transducer and a high-speed digital data recording system.

With the experiments described in this report, we investigated several aspects of the release of drops of molten ferrosilicon (75 wt.% Si and 25 wt.% Fe, with and without Al and Ca additives) into liquid water:

- We developed and improved our apparatus and techniques for releasing pendant drops of molten alloys into water.
- We studied the triggering of steam explosions of the melt drops with small underwater explosions of stoichiometric hydrogen-oxygen mixtures.
- We also studied the triggering of steam explosions of the melt drops with mechanical transients introduced into the water with an underwater impactor.
- We examined the effects of changing the temperature of the water into which ferrosilicon drops of three alloy compositions were released. Three water temperatures were used, nominally 8 ^{o}C, 20 ^{o}C (room temperature) and 80 ^{o}C.
- We estimated the energy transferred to the water during the steam explosions of molten alloy drops.
- We looked at the effects of increasing drop diameter with a few preliminary experiments.
- We studied the underwater combustion of drops of the molten alloys by examining video and photographic images that show the burning of the particles and also the production of colloidal products and bubbles of hydrogen. We also used X-ray diffraction to compare ferrosilicon starting materials with the debris recovered after steam explosions of drops in which underwater combustion is thought to have occurred.

EXPERIMENTAL

Formation and Release of Molten Ferrosilicon Drops

The use of the pendant drop technique to produce and release drops of molten ferrosilicon alloys into liquid water has been described earlier (Nelson et al., 1996, 1997a). The apparatus consists of a firebrick-insulated furnace heated with a silicon carbide element that surrounds a vertical mullite tube. A rod of the alloy is hung inside the furnace in a flowing inert atmosphere. The bottom of the furnace tube opens above a 1 m-deep water chamber. The chamber, in turn, is mounted above a 1 m-tall spill control container. The three components—furnace, water chamber and the spill control container—are mounted one above the other in a 3 m-tall steel framework.

Compared to the work performed in 1995 and 1996, we have made several changes to improve both the quality and reproducibility of the molten drop releases:

- A small round hole has been cut in the side of the mullite furnace tube at the center of the hot zone, as shown in Figure 1**.** Also, the space between the turns of the helical silicon carbide heating element that surrounds the tube has been repositioned slightly to allow us to look inside the furnace through this hole. This viewing allows the experimenter to carefully position the lower end of the ferrosilicon alloy rod in the hot zone of the furnace and to observe the pendant drop as it forms and ultimately drops off. For our imaging procedures, it is valuable to know, even approximately, when the drop is about to fall of its own weight.

  The spontaneous release of the drops is an important improvement over the 1995 and 1996 studies in which the pendant drops were shaken from the tip of the rod by mechanical action. It has added greatly to the reproducibility of drop weights. The somewhat random nature of the release times, however, has required the addition of a photodetector that senses the detachment of each drop and initiates an appropriate time delay relay that fires the triggering device after the drop has descended to the desired depth of water.

- The inert melting atmosphere has been improved by (a) reversing the direction of gas flow from upward in the 1995 and 1996 studies to downward in the current work, (b) eliminating the thin plastic foil "valve" through which the drop melted and (c) changing the flowing gas from "inert" commercial cylinder argon to a reducing mixture of 1% hydrogen in argon. We have also added a tubular extension beneath the furnace to extend the blanketing of the reducing atmosphere to within a few centimeters of the water surface, thus minimizing contact of the hot drops with air before entering the water. These modifications of the furnace atmosphere have been made to reduce or eliminate the black, sometimes patchy, oxidic coatings found on many of the drops quenched in the 1995 and 1996 studies.

Also, the interaction chamber used during the 1996 experiments (Nelson et al., 1997a) was reinforced with angle irons and threaded rods in preparation for the triggering and steam explosion experiments planned for 1997.

Materials

We used deionized water obtained from the Lindsay Water Company, Madison, WI. We normally used a single filling of water (about 90 liters for the 1 meter-deep chamber) for three or four experiments before discarding it.

The furnace purge gases were argon or a special mixture of 1% hydrogen in argon obtained from BOC Gases, Madison, WI. Both were obtained in cylinders at high pressures that were reduced by commercial regulators. The gas flow was monitored by a Matheson Type 605 flowmeter.

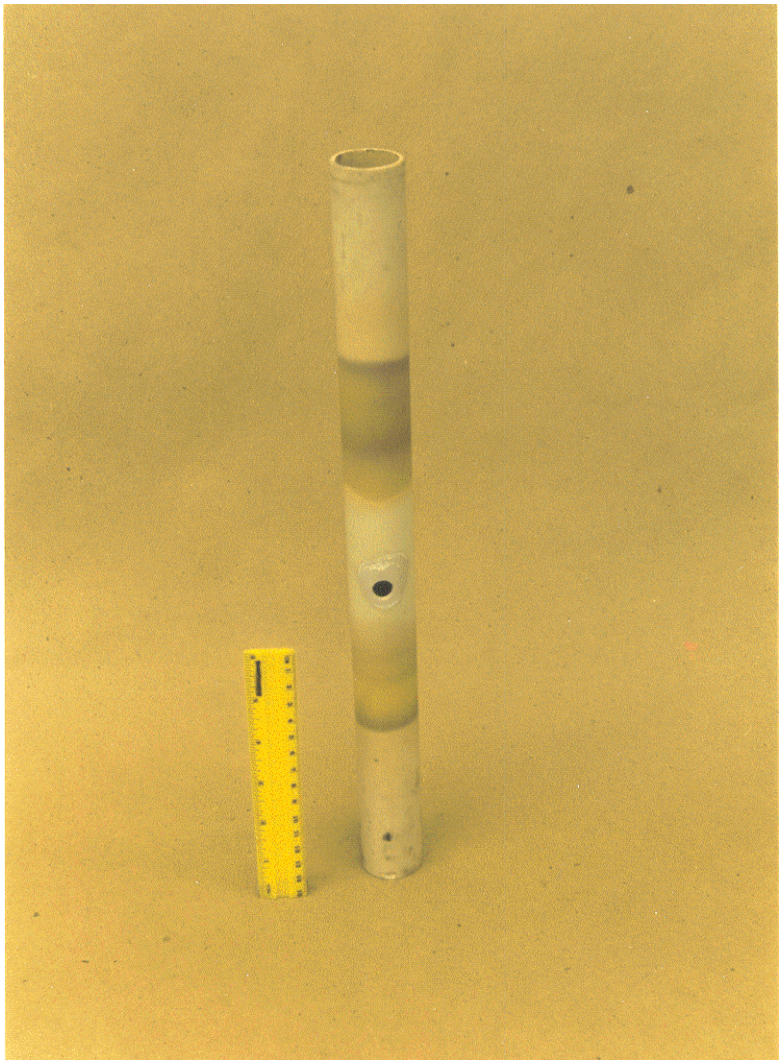

Figure 1. Photograph of the mullite furnace tube after being removed from the furnace. The hole through which the pendant drop is observed during melting can be seen at about the midpoint of the tube. (C-225-1).

The ferrosilicon alloys used here were obtained from SINTEF Materials Technology, Trondheim, Norway, in the form of several batches of rods 10 mm in diameter and nominally 100 mm long. The compositions of these rods are presented in Table 1 (the lesser constituents other than Al and Ca have been omitted).

Table 1. Ferrosilicon Rods Supplied by SINTEF Materials Technology, Trondheim, Norway

SINTEF No.	UW No.	Si (w/o)	Fe (w/o)	Al (w/o)	Ca (w/o)
None*	C-34-1	75.4	24.0	0.37	0.014
F1/F2	C-121-1	73.8	25.1	<0.001	0.001
F7	C-133-1	73.8	25.0	0.020	0.011
F8	C-133-2	73.9	24.9	0.002	0.007
F4	C-121-2	73.5	24.6	1.40	0.63
F5	C-121-3	73.8	25.4	0.34	0.074

* This material was supplied during 1996.

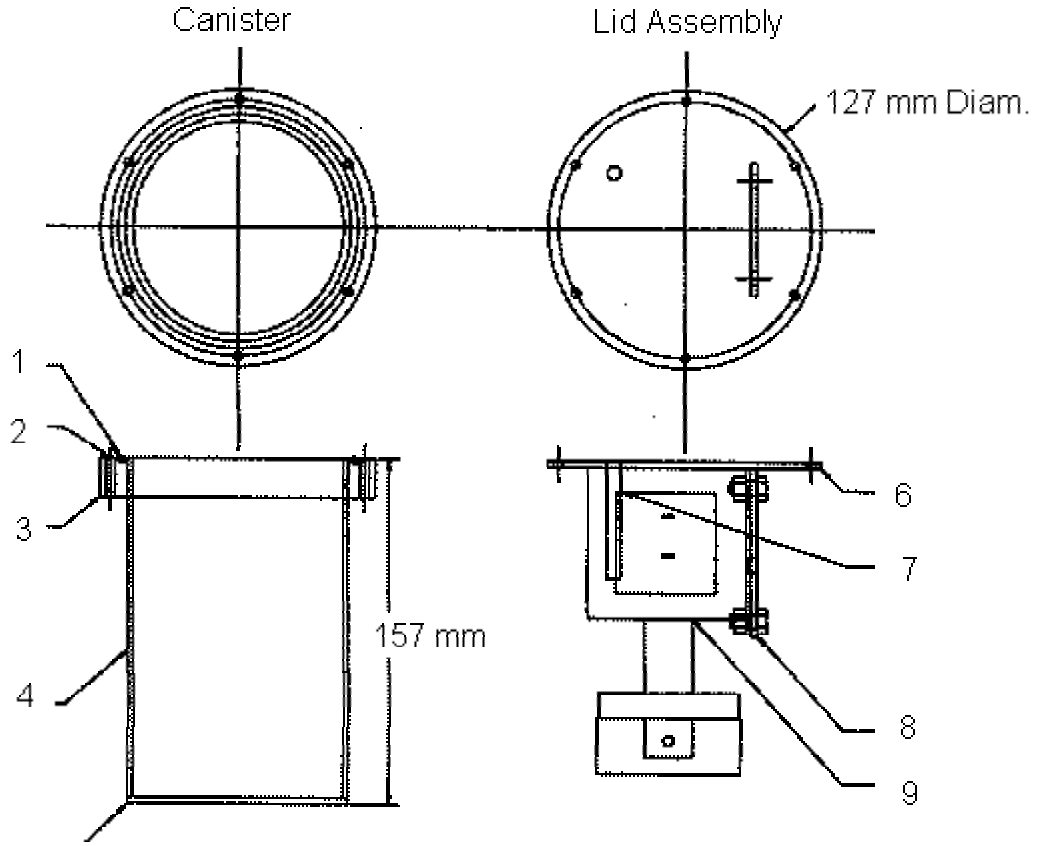

Figure 2. Schematic diagram of the solenoid-driven impactor. Key: 1. 2.5 mm O-ring and groove. 2. Tapped 8-32 for 6 screws. 3. 19.1 mm-thick steel ring welded on. 4. 102 mm OD X 2.2 mm wall 304 stainless steel tube. 5. 3.2 mm-thick 304 stainless steel plate welded on. 6. 3.2 mm-thick steel lid with 6 thru holes. 7. 6.4 mm tube for thru wires. 8. 3.2 mm-thick steel plate welded to lid. 9. Solenoid with 417 g steel weight welded to the armature.

Triggering Techniques

Two triggering techniques were used; these involved a solenoid-driven mechanical impactor and a hydrogen-oxygen combustion tube.

Impactor

This device consists of a pull-type solenoid (Dormeyer Model 3000-M-1, 12 ampere rating)) with a 408 g steel weight welded to its armature. The solenoid is positioned within a 158 mm-tall stainless steel capsule to permit operation under water. It is bolted to a steel plate welded perpendicular to a circular 127 mm-OD, 3.2 mm-thick steel plate that also closes the top of the capsule against an O-ring to seal it water-tight. This circular plate also has a hole near one edge through which a pair of 110 V AC leads pass. The leads are sealed in place with a silicone sealant. A schematic diagram of the unit is shown in Figure 2. The unit is shown before assembly in Figure 3 (the armature and weight are in the “out” or “down” position) and Figure 4 (the armature and weight are in the “in” or “up” position); it is shown assembled in Figure 5. To generate pressure transients, the coil of the solenoid is activated with a high amperage switch. This causes the armature and the weight to rise quickly and strike the underside of the circular steel plate. If the sealed unit is submerged, the impact generates a pressure transient that passes from the plate upward through the water.

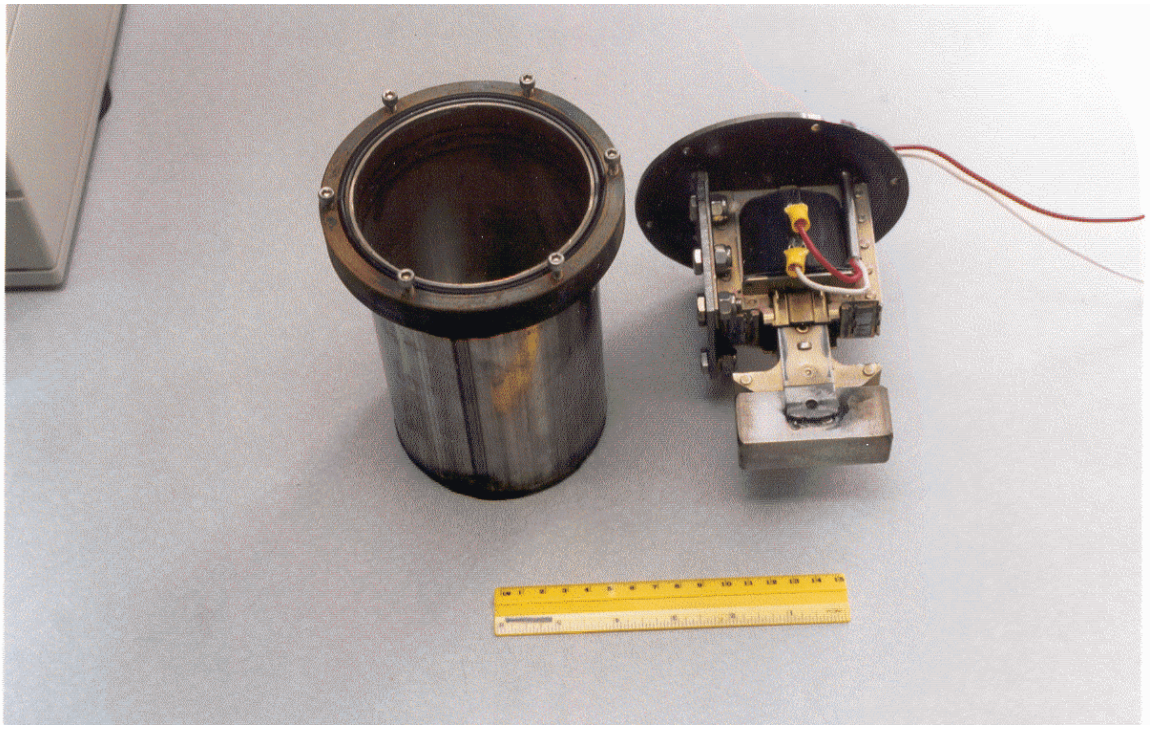

Figure 3. Photograph of the solenoid-driven impactor before assembly. The armature and weight are shown in the "out" or "down" position. (C-100-1f).

Hydrogen-Oxygen Combustion Tube

We have developed and tested a second device for generating transients in water that have somewhat different pressure-time signatures and the potential for producing significantly higher peak pressures than the impactor. This device is chemically driven, and is also simple and inexpensive.

The device consists of a vertical combustion tube that contains 100 ml of a stoichiometric mixture of gaseous hydrogen and oxygen at local atmospheric pressure. When the mixture is ignited at the bottom of the tube with a small electrical spark, a vigorous combustion results that is thought to undergo deflagration-detonation transition (DDT) as the flame front passes upward through the tube. This energetic reaction then produces an intense pressure pulse and movement of water and a train of bubbles upward into the water in the chamber above. It is believed that this upward water motion and pressure transient will destabilize the boiling film surrounding a drop of molten ferrosilicon alloy and thus induce a steam explosion.

The unit tested in these experiments is shown schematically in Figure 6; it consists of a 25 mm-ID X 230 mm-long transparent polymethylmethacrylate tube. The bottom of the tube is open, while the upper end of the tube is closed gas-tight with a thin polyethylene membrane held in place with a rubber band. The tube is suspended with its upper end 30 cm below the surface of the water. Marks were placed on the tube 68 mm and 203 mm below the upper end of the tube.

The tube is hung on the lower end of a bundle of two 6.4 mm copper tubes and an electrical cable that have been bent together into a gently curved U-shape. The tube is held on this "hooked" bundle with a strip of waterproof tape. The vertical tube bundle with the combustion tube in place is mounted on a steel framework that permits them to be positioned at various depths in the 1 m-deep water chamber.

The copper tubes are attached with 6.4 mm polypropylene tubing to an oxygen cylinder or to a hydrogen cylinder. Both are high pressure commercial gas cylinders, each fitted with an appropriate pressure regulator and a needle valve.

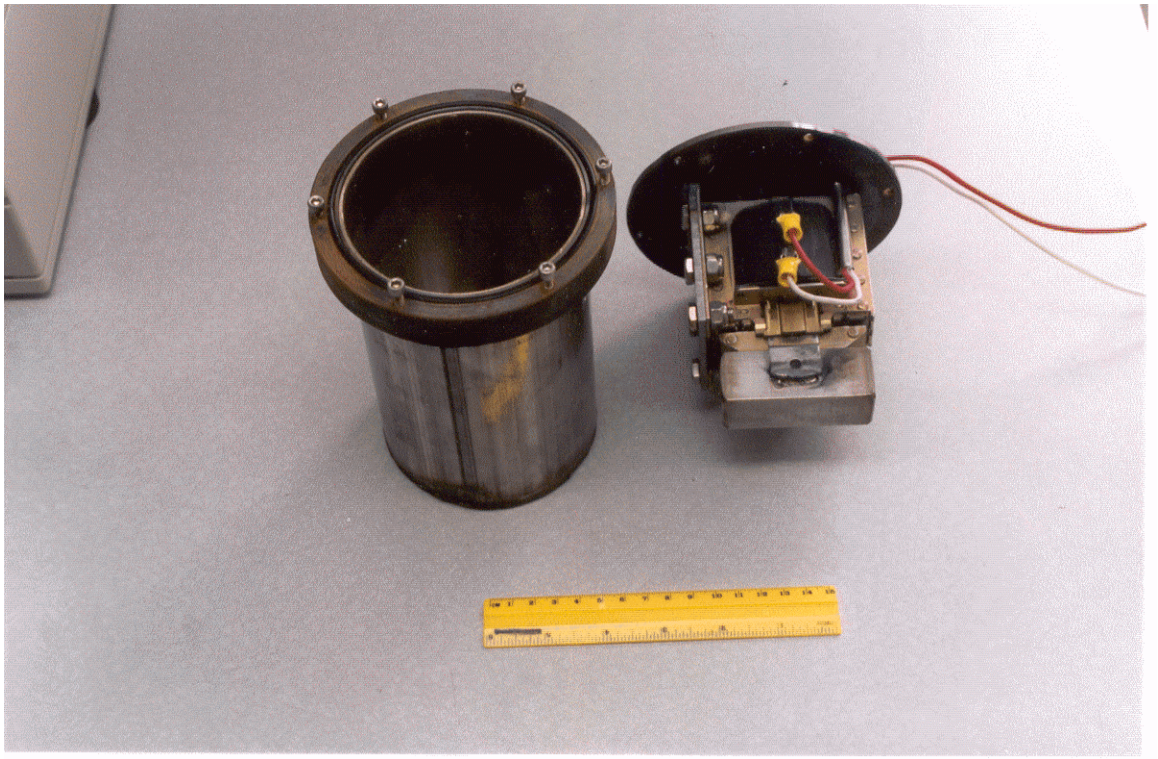

Figure 4. Photograph of the solenoid-driven impactor before assembly. The armature and weight are shown in the "in" or "up" position. (C-100-1e).

The combustion tube is filled with the stoichiometric hydrogen-oxygen mixture as follows: The transparent tube with plastic diaphragm closure at the top is inverted, submerged and carefully filled with water. Next, the tube is turned diaphragm-side up under water, and fastened in place on the "hook" of the tube-cable bundle. (The lower end of the tube is open.) Oxygen is then bubbled into the tube until the level of the water in the tube is lowered to the 1/3 marker (68 mm below the top) and finally hydrogen is cautiously bubbled upward into the oxygen already in the tube until the level of the water is lowered to the 3/3 level (203 mm). The tube now contains a mixture of one volume of gaseous oxygen and two volumes of gaseous hydrogen at local atmospheric pressure with a total volume of 100 ml. The mixture is now ready to ignite.

The electrical cable in the U-shaped bundle shown in Figure 6 is attached to a 110 VAC source via an appropriate switch. The upper ends of the electrical leads inside the combustion tube are shorted with an 0.15 mm-diameter copper filament that explodes when the switch is closed. This produces a strong arc that ignites the hydrogen-oxygen mixture.

Transducer

The pressure transients produced in the water by the impactor or the combustion tube are measured as a function of time with a Model 112AO3 quartz transducer (PCB Corporation, DePew, NY,), the tip of which is hung a few millimeters below the surface of the water. The pressure generation source under study is placed at various depths below the transducer. Both transducer and source are positioned approximately along the vertical centerline of the chamber.

The output of the transducer is passed through a PCB Model 462A charge amplifier and recorded as a function of time with a Type 4094A digital oscilloscope (Nicolet Corporation, Madison, WI) with 0.5

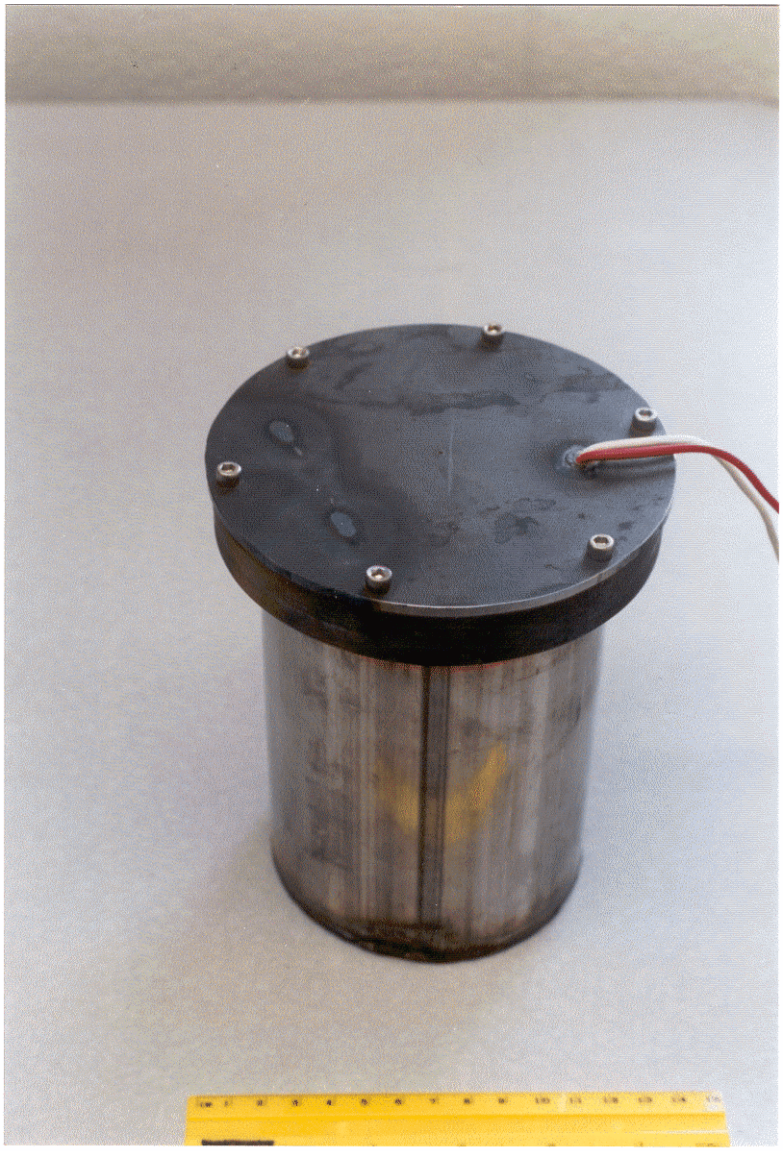

Figure 5. Photograph of the solenoid-driven impactor assembled. (C-100-1d).

microsecond separation between points, ±1.0 or ±2.0 V full scale. Cursor triggering, set at delays of 0.5 to 2.5 ms as appropriate, is used to capture the entire trace.

The digital record from the oscilloscope (7938 data points) is converted into a voltage-time trace using the DATRAN code installed on a Compu-Add computer. The appropriate 4000 data points centered around the peak pressure are then plotted via the Microsoft Excel Chart Wizard to produce a graphical pressure-time trace.

Imaging

We have tested four ways to produce images that will help us understand and quantitatively analyze the steam explosions of single drops of melt:

Time-Exposure Photography

The simplest way to produce images during the release, fall through water and steam explosions of drops of molten ferrosilicon alloys is to use open shutter, time-exposure photography in a darkened room.

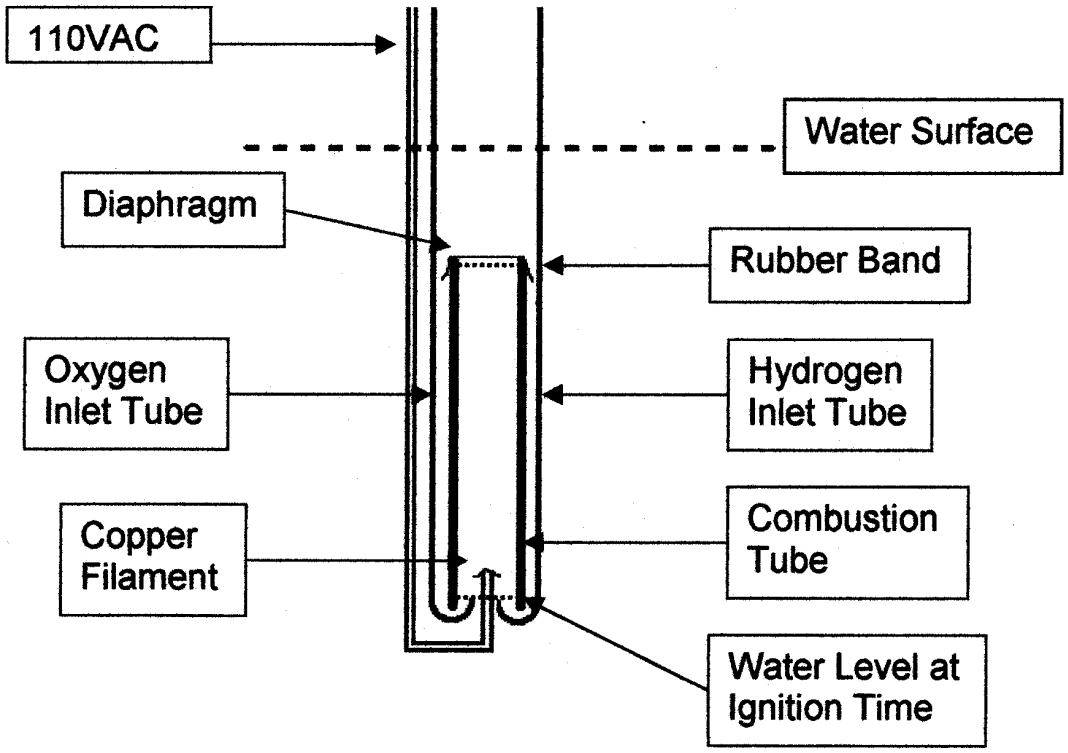

Figure 6. Schematic diagram of the hydrogen-oxygen combustion tube.

We recorded the behavior of non-exploding drops with this technique in the 1996 studies (Nelson et al., 1997a).

The technique is particularly suitable for drops of the molten ferrosilicon alloys because of their strong emission of visible radiation in the yellow, orange and red wavelengths where photographic emulsions are most sensitive.

We used 35 mm Kodak ASA 200 Gold negative film that may be processed and printed locally, in one hour if desired. For reporting purposes, the negatives may be enlarged quickly and reliably by various commercial establishments. And for preparing presentations, the negatives may be converted into high quality 35 mm color transparencies by the same local photographic processors.

Because it is important to determine true dimensions in the image planes of these photographs, we hung a pair of 3 mm-OD X 177 mm-long stainless steel rods vertically on threads in the image plane in the water at either side of the interaction volume. The spacing between the rods, about 135 mm apart horizontally, was measured carefully for each experiment. The spacing between the rods on our photographic images provides a fiducial for calibrating distances that is independent of the degree of enlargement. The shiny, reflective surfaces of the rods make them easily detectable, even on poorly exposed images.

Although the time-exposed photographic images usually have very high quality, they also have the disadvantage of being time-integrated, giving little information about the dynamic processes involved during the explosions. Therefore, we have investigated other procedures in order to obtain time-resolved images.

Video Imaging

Our VHS camcorder (Sylvania Model HQ-VHS) operates at 60 frames per second and produces reasonable time resolution, moderate image quality, color representation and sound. We have used it to determine fall and triggering distances and times, the occurrence and approximate magnitude of the explosions and the duration of luminous and non-luminous phenomena associated with the interactions both before and after they are triggered. The video images also provide information about bubble behavior and water motion that accompany the explosions.

The fiducials provided by the two stainless steel rods hung in the image plane are used to determine true distances on the video records as well as on the photographic images.

CCD Camera

We have access to a Dalsa Model CA-D1-0256 CCD (charge-coupled device) camera with an image resolution of 256 x 256 pixels that is capable of recording up to 30 images at 200 Hz. We have examined its characteristics and possible use in these studies. It has the advantage of promptly producing digitized black and white digital images that may be transferred directly to a computer for analyses. It has the disadvantages of generating only a few low resolution images at a framing rate not much greater than our video camera; also, it is a fairly complicated device to set up and sequence with other events. Therefore, we have not used it extensively.

High-Speed Photography

We also have access to a Hycam I high-speed 16 mm camera with 30.5, 71 or 142 meter film capacity and framing rates as high as 10,000 pictures per second. It has the important advantages of high spatial image resolution and good color rendition. Its drawbacks are the time required for processing and the relatively high cost of the film. We have, therefore, done as much as possible with the video imaging techniques to carefully determine appropriate time delays, framing rates, exposure times and light levels needed to produce usable images before attempting the high-speed photography. As in the 1996 studies (Nelson et al., 1997a), we used 30.5 meter rolls of film exposed at 500 or 1000 frames per second.

The Hycam camera requires about one second to accelerate to these framing rates and to place the images properly on the roll of film. This is difficult to achieve with spontaneous drop releases, however. Therefore, the experimenter who views the melting of the rod through the optical pyrometer can switch on both the camera and the photolights just as the pendant drop appears ready to fall. After a delay of one second, determined by a time delay relay, the rod is shaken with a solenoid to assist in its detachment.

As with the video records and the time-exposed photographs described above, the fiducials provided by the two stainless steel rods hung in the image plane are used to determine true distances on the high-speed photographic images.

Rod and Debris Diagnostics

As reported for the 1996 studies (Nelson et al., 1997a), extensive use is made of 35 mm still photography to record both the condition of the rods before and after each experiment and of the debris generated during each interaction. We normally used long exposures at f/22 with existing room light to obtain the sharpest images possible. Moreover, rod losses are determined from changes in weight and from changes in length determined from photographs and by direct caliper measurements of the rods. Also, the debris is weighed for each experiment.

We have used X-ray diffraction analyses to look for oxidic products in the debris, an indication that metal-water chemical reaction had occurred during the steam explosions. (These analyses were performed collaboratively with the Department of Metallurgical and Materials Engineering, Michigan Technological University, Houghton, MI, USA.) The fine, powdery nature of some of the debris is well suited for producing X-ray powder patterns.

RESULTS

During 1997, we completed 51 experiments in which drops of molten ferrosilicon alloys were released into about 90 L of deionized water contained in a 1 m-tall chamber. These experiments are summarized in Tables 2, 3 and 4. Some of the experiments were performed with several drops released one after the other from the same rod without allowing the furnace to cool.

Drop Characteristics

Compared to the 1996 work (Nelson et al., 1997a), the changes in techniques for melt preparation and release produced more reproducible drop weights. This can be seen in the early, non-triggered experiments outlined in Table 2, where the differences between the weights of the spontaneously released drops produced from a given alloy usually deviated by less than 1%. In the 1996 experiments, the deviations between drop weights in repeat experiments were sometimes as great as a factor of four.

Also, the changes in the melting atmosphere made early in the 1997 work (a reducing argon-1% hydrogen gas mixture instead of argon alone, downward instead of upward gas flow, extension of the inert zone almost to the water level and elimination of the burn-through plastic foil "valve") produced significant changes in the appearance of the quenched spherules. In particular, the black, patchy coatings on the exteriors of the drops observed during the 1996 studies (Nelson et al., 1997a) were no longer present. When the melt contained Al and Ca additives, however, black coatings still formed on the quenched drops, but these were smooth and uniform over the entire surface, not patchy.

A striking difference between the spherules generated during the current and the previous years is the considerably lower weights of the 1997 spherules. As indicated in Tables 1 and 2 of the 1996 report (Nelson et al., 1997a), globules as large as 8 or 9 g were recovered in several experiments, whereas in the 1997 experiments, the weights of the spontaneously released drops were 1 to 1.5 g. Moreover, the reproducibility of weights between drops formed from a given alloy was poor in 1996 and good in 1997, even though all rods from which the drops detached had diameters of 10 mm.

It can also be seen from Tables 2, 3 and 4 of this report that the weights of the drops formed from the ferrosilicon alloyed with Al and Ca were about 0.5 g lower than those formed from the unalloyed material. This occurred even though the diameters of all rods, both alloyed and non-alloyed, were the same—10 mm. From the literature on the self-detachment of pendant drops (see, for example, Vinet et al., 1993), the parameters that govern the weights of the detached drops are primarily the density and surface tension of the melt. Because major changes in density are not likely in alloys as dilute as these, it is probable that the surface tensions of the alloyed melts are significantly lower than that of the non-alloyed melt.

Interactions of Drops of Molten Ferrosilicon with Water

The primary objective of this program is to understand the explosive melt-water interactions, also called steam explosions, that may occur when single drops of molten ferrosilicon alloys are released in free fall into water.

Spontaneous Explosions

Drops of some molten metals explode spontaneously when released into water, for example, Sn, Bi and Pb. Drops of other molten metals, for example, Al and Fe, seem completely non-explosive when they fall into water, even though the respective melt and water temperatures may lie in the same ranges as those for the metals that explode spontaneously.

In the 1997 work, we found that nominally 1 gram drops of molten ferrosilicon (75 w/o Si, 25 w/o Fe) and alloys of this material with small amounts of Al and Ca do not explode spontaneously when released at their liquidus temperatures into 1 meter-deep water at room temperature. This also was observed in the 1996 studies (Nelson et al., 1997a) when drops of a similar ferrosilicon alloy with Al and Ca additives were

Table 2. Summary of Releases of Drops of Molten Ferrosilicon Alloys into Water

Experiments were performed without pressure transient triggering.

		T(water)	T(furnace)	Furnace	Rod Loss		Debris	Triggering			Type of	Nature of					
Expt, No.	Alloy	(^{o}C)	(^{o}C)	Atm.	Lgth (mm)	Wt (g)	Wt. (g)	Unit	Depth(cm)	Delay(ms)	Interaction	Debris	Imaging	Remarks			
C 122-2	C-34-1	21.0	1550	Ar + 1%H_2	18	4.76	See Rmrks	None	NA	NA	Solidified	Spherules	OS, VCR	3 spontaneous drops (1.39, 1.38, 1.43 g), 1			
	0.37w/o Al													shaken drop (0,62 g); shutter wheel;			
														oscillatory trace			
C-123-1	C-34-1	RT	1440	Ar + 1%H_2	Total	Total	1.43	None	NA	NA	Solidified	See Rmks	OS, VCR	2 spontaneous drops (1.48, 1.45 g), 1			
	0.37w/o Al													shaken drop (0.30 g); then rod fell; shutter			
														wheel			
C-125-1	C-34-1	20.1	1445	Ar + 1%H_2	6	1.39	1.43	None	NA	NA	Solidified	Spherule	OS, VCR	Single black spherule; shutter wheel			
	0.37w/o Al																
C-127-1	C-121-1	22.5	1465	Ar + 1%H_2	5	1.11	1.11	None	NA	NA	Solidified	Spherule	OS, VCR	Single metallic spherule + tiny spheres;			
	0 w/o Al													shutter wheel			
C-129-1	C-121-1	24.5	1460	Argon	15	3.70	See Rmrks	None	NA	NA	Solidified	Spherules	OS, VCR	3 spontaneous drops ((1.26, 1.20, 1.27 g);			
	0 w/o Al													no shutter wheel			

Table 3. Summary of Releases of Drops of Molten Ferrosilicon Alloys into Water.
Experiments were triggered with stoichiometric hydrogen-oxygen explosions.

		T(water)	T(furnace)	Furnace	Rod Loss		Debris	Triggering			Type of	Nature of		
Expt, No.	Alloy	(^{o}C)	(^{o}C)	Atm.	Lgth(mm)[a]	Wt (g)	Wt. (g)	Unit	Depth(cm)	Delay(ms)	Interaction	Debris	Imaging	Remarks
C-150-1	C-133-1	21.6	1460	Ar + 1%H_2	NM	1.15	1.12	$H_2 + O_2$	30	350	Explosion	Powder	VCR only	Spherical explosion; debris not as fine as
	0 w/o Al													C-135-1, etc.
C-154-1	C-133-1	22.0	1465	Ar + 1%H_2	7	1.45	0.99	$H_2 + O_2$	30	350	Explosion	Powder	OS, VCR	V. loud spherical explosion; good video and
	0 w/o Al				6.7[c]									OS photo; follower drop; fine debris
C-157-1	C-133-1	20.5	1460	Ar + 1%H_2	5	1.43	1.35	$H_2 + O_2$	30	350	Explosion	Powder	Hyc, VCR	Good spherical explosion, not as loud as
	0 w/o Al				5.7[c]									C-154-1; good video; fine debris
C-158-1	C-133-1	21.3	1460	Ar + 1%H_2	5	1.50	1.32	$H_2 + O_2$	30	350	Explosion	Powder	Dals, VCR	Good spherical explosion, not as vigorous
	0 w/o Al				4.9[c]									as C-157-1; good video; fine debris; H_2
														bubbles from explosion
C-163-1	C-121-3	21.5	1460	Ar + 1%H_2	3	1.10	1.06	$H_2 + O_2$	30	350	Mild explo.	Coarse frg	OS, VCR	Mild explosion; coarse debris; long luminos-
	0.34w/o Al				NM									ity afterward compared to unalloyed FeSi
C-166-1	C-121-2	21.6	1460	Ar + 1%H_2	3	1.05	1.06	$H_2 + O_2$	30	350	Mild explo.	Coarse frg	OS, VCR	Mild explosion; debris coarser than C-163-1;
	1.4 w/o Al				NM									OS photo about same as C-163-1; long
														luminosity afterward
C-168-1	C-121-3	22.4	1460	Ar + 1%H_2	5	1.05	0.95	$H_2 + O_2$	30	350	Mild explo.	Coarse frg	VCR only	
	0.34w/o Al				3.8[c]									
C-169-1	C-133-1	21.0	1460	Ar + 1%H_2		0.58	0.51	$H_2 + O_2$	30	350	Mild explo.	Coarse frg	Hyc, VCR	Downstroke to shake off; drop was small;
	0 w/o Al				1.3[c]									coarse frag.; 1st use of SS catcher pan
C-170-1	C-133-1	20.8	1460	Ar + 1%H_2		1.38	1.21	$H_2 + O_2$	30	350	Explosion	Powder	Hyc, VCR	Upstroke to shake off; good explosion; fine
	0 w/o Al				5.7[c]									debris. On video, luminosity of cloud fell
														1/2 s after triggering
C-171-1	C-121-3	21.2	1460	Ar + 1%H_2		1.24	1.21	$H_2 + O_2$	30	350	Mild explo.	Coarse frg	Hyc, VCR	Excellent video; combustion bubbles
	0.34w/o Al				5.2[c]									confuse fragmenation
C-177-1	C-133-1	20.4	1465	Ar + 1%H_2		1.38	1.45	$H_2 + O_2$	40	350	V. mild	V. coarse	VCR only	Attempt to separate $H_2 + O_2$ bubble stream
	0 w/o Al				4.8									from steam explosion bubble by increasing
														triggering distance

[a] Upper entries for losses of rod length are determined from photograph. [C] Lower entries are determined with a caliper.

Table 3. Summary of Releases of Drops of Molten Ferrosilicon Alloys into Water (continued)

Experiments were triggered with stoichiometric hydrogen-oxygen explosions.

Expt, No.	Alloy	T(water) (^{o}C)	T(furnace) (^{o}C)	Furnace Atm.	Rod Loss Lgth(mm)[a]	Rod Loss Wt (g)	Debris Wt. (g)	Triggering Unit	Triggering Depth(cm)	Triggering Delay(ms)	Type of Interaction	Nature of Debris	Imaging	Remarks
C-180-1	C-133-1	20.6	1470	Ar + 1%H_2		1.35	1.29	$H_2 + O_2$	30	350	V. small	Spherule	VCR only	Attempt to separate $H_2 + O_2$ bubble stream
	0 w/o Al				5.2									from steam explosion bubble by inserting
														steel plate. Failed.
C-181-1	C-133-1	20.7	1470	Ar + 1%H_2		1.25	1.13	$H_2 + O_2$	30	350	Explosion	Powder	VCR only	Attempt to separate $H_2 + O_2$ bubble stream
	0 w/o Al				4.4									from steam explosion bubble by inserting
														51 % screen. Successful.
C-182-1	C-133-1	20.9	1465	Ar + 1%H_2		1.17	1.30	$H_2 + O_2$	30	350	V. mild	V. coarse	VCR only	Attempt to separate $H_2 + O_2$ bubble stream
	0 w/o Al				2.8									from steam explosion bubble by inserting
														36 % screen. Failed.
C-184-1	C-133-1	20.7	1510	Ar + 1%H_2		1.24	1.12	$H_2 + O_2$	300	350	Explosion	Powder	VCR only	Attempt to separate $H_2 + O_2$ bubble stream
	0 w/o Al				1.7									from steam explosion bubble by inserting
														51 % screen. Successful.
C-186-1	C-133-1	21.8	1460	Ar + 1%H_2		1.50	1.46	$H_2 + O_2$	30	320	Mild	Lump, fine	VCR, Hyc	Attempt to separate $H_2 + O_2$ bubble stream
	0 w/o Al													from steam explosion bubble by inserting
														51 % screen. Failed.
C-187-1	C-133-1	21.0	1520	Ar + 1%H_2		1.58	1.55	$H_2 + O_2$	30	340	Mild	Lump, fine	VCR only	Attempt to separate $H_2 + O_2$ bubble stream
	0 w/o Al				NM									from steam explosion bubble by inserting
														51 % screen. Failed.
C-189-1	C-133-1	23.5	1470	Ar + 1%H_2		1.39	1.14	$H_2 + O_2$	30	350	Explosion	Powder	OS, VCR	Excellent explosion; very fine debris; good
	0 w/o Al				6.2									OS photo; water used 3X before.
C-190-1	C-133-1	23.1	1480	Ar + 1%H_2		1.21	1.05	$H_2 + O_2$	30	350	Mild	Coarse frg.	OS, VCR	Moderate explosion; debris coarser than
	0 w/o Al				1.6									C-189-1; good OS photo; water used 4 X
														before. New rod.
C-191-1	C-133-1	21.8	1465	Ar + 1%H_2		1.39	1.31	$H_2 + O_2$	30	350	Mild	Coarse frg.	OS, VCR	Mild interaction even though drop should
	0 w/o Al				2.9									have exploded vigorously. Water used 5 X
														5X before; shell-like debris. New rod.
C-193-1	C-133-1	18.3	1460	Ar + 1%H_2		1.38	1.27	$H_2 + O_2$	30	350	Mild	Coarse frg.	OS, VCR	Mild interaction even though drop should
	0 w/o Al				0.5									have exploded vigorously; fresh DI water;
														rod same as C-191-1.
C-195-1	C-133-2	14.7	1490	H_2 ??		1.37	1.33	$H_2 + O_2$	30	350	None	Split drop	OS, VCR	No explosion; drop split; new F8 rod; new
	0 w/o Al				3.4									gas gave flame beneath furnace;
														demonstration experiment.

[a] Upper entries for losses of rod length are determined from photographs; lower entries are determined with a caliper.

Table 4. Summary of Releases of Drops of Molten Ferrosilicon Alloys into Water.
Experiments were triggered with the solenoid-driven mechanical impactor.

		T(water)	T(furnace)	Furnace	Rod Loss		Debris	Triggering			Type of	Nature of		
Expt, No.	Alloy	(^{o}C)	(^{o}C)	Atm.	Lgth(mm)[a]	Wt. (g)	Wt. (g)	Unit	Depth(cm)	Delay(ms)	Interaction	Debris	Imaging	Remarks
C-131-1	C-34-1	24.0	1480	Argon	16	4.29	See Rmrks	Impactor	60	1000	Solidified	Spherules	OS, VCR	3 spontaneous drops (1.45, 1.43, 1.41 g);
	0.37w/o Al													spherules had black exterior; first use of
														optical sensor to trigger.
C-133-3	C-121-1	22.5	1470	Argon	17	4.52	See Rmrks	Impactor	60	1000	Solidified	Spherules	OS, VCR	4 spontaneous drops (1.15, 1.15, 1.15,
	0 w/o Al													1.17g), one without trigger; all had metallic
														luster.
C-135-1	C-133-1	23.3	1450	Argon	4	1.47	1.22	Impactor	20	300	Explosion	Powder	OS, VCR	Submillimeter debris; hemispherical
	0 w/o Al													explosion.
C-137-1	C-133-1	24.9	1460	Argon	13	2.99	See Rmrks	Impactor	20	See Rmrks	See Rmrks	See Rmrks	VCR only	At 250 ms delay, popcorn spherule (1.45 g);
	0 w/o Al													at 300 ms delay, explosion, powder (1.26 g).
C-141-1	C-133-1	23.1	1460	Argon	15	4.20	See Rmrks	Impactor	20	See Rmrks	See Rmrks	See Rmrks	OS, VCR	At 280 ms delay, spongy spherule (1.13 g);
	0 w/o Al													at 290 ms delay, explosion (1.49 g); repeat,
														blowout (1.44 g).
C-143-1	C-133-1	23.5	1465	Argon	4	1.53	1.24	Impactor	20	350	Explosion	Powder	OS, VCR	Explosion more violent than before; good
	0 w/o Al													OS photo; hemispherical explosion; egg
														shell piece in debris.
C-145-1	C-121-2	22.5	1460	Argon	2	1.10	1.10	Impactor	20	350	Very mild	See Rmrks	VCR only	Debris: 3 chunks plus small spherules
	1.4 w/o Al													
C-147-1	C-121-3	21.9	1460	Argon	5	1.13	1.22?	Impactor	20	350	Mild	See Rmrks	VCR only	Debris is fairly fragmented, in many pieces.
	0.34w/o Al													
C-173-1	C-133-1	22.4	1460	Ar + 1%H_2		1.41	1.21	Impactor	30	350	Explosion	Powder	Hyc, VCR	Vigorous explosion; very fine debris.
	0 w/o Al				5.9c									
C-175-1	C-121-3	21.6	1465	Ar + 1%H_2		1.74	1.74	Impactor	30	350	No explo.	Solid drops	Hyc, VCR	No explosion; drop landed off-center; small
	0.34w/o Al				1.1c									round satellite drop.
C-197-1	F8/C-133-2	16.2	1465	Ar + 1%H_2	18	4.27	4.08	Impactor	20	350, 370	Explosion	Powder	OS, VCR	Two drops failed to explode at 350 ms; 3rd
	0 w/o Al				18.3									drop exploded above surface at 370 ms.
C-199-1	F8/C-133-2	17.7	1480	Ar + 1%H_2	19	NM	Combined	Impactor	20	370	Explosions	Powder	VCR only	4 drops released; 3 exploded, 1 did not;
	0 w/o Al				NM		w. C-201-1							forgot to load film into camera; combined
														debris with C-201-1.
C-201-1	F8/C-133-2	19.0	1460	Ar + 1%H_2	49	12.01	13.29 with	Impactor	20	370	Explosions	Powder	OS, VCR	2 drops released; both exploded with OS
	0 w/o Al				NM		C-199-1							and VCR imaging; then rod fell and
														exploded with VCR only.

[a] Upper entries for losses of rod length are determined from photographs; lower entries are determined with a caliper.

Table 4. Summary of Releases of Drops of Molten Ferrosilicon Alloys into Water (continued).

Experiments were triggered with the solenoid-driven mechanical impactor.

Expt, No.	Alloy	T(water) (^{o}C)	T(furnace) (^{o}C)	Furnace Atm.	Rod Loss Lgth(mm)[a]	Rod Loss Wt. (g)	Debris Wt. (g)	Triggering Unit	Triggering Depth(cm)	Triggering Delay(ms)	Type of Interaction	Nature of Debris	Imaging	Remarks
C-203-1	F8/C-133-2	79 to 83	1480	Ar + 1%H_2	20, 15	2.79, 4.17	Globs 2.74	Impactor	20	370	Mild explo.	Coarse	OS, VCR	Hot water series. 2 drops fell from 1st rod,
	0 w/o Al				NM, 15.8		Fines 4.24							no interactions; then rod fell. Inserted 2nd
														rod, 3 drops fell, mild explosions, weird,
														seaweed-like images as tiny drops burned.
C-205-1	F8/C-133-2	6.5	1490	Ar + 1%H_2	25	5.98	5.22	Impactor	20	370	Explosions	Powder	OS, VCR	Cold water series; 4 drops, 3 OS photos
	0 w/o Al				23.8									(good ones) fine debris.
C-207-1	F4/C-121-2	21.7	1465	Ar + 1%H_2	19	4.43	4.46	Impactor	20	370	V. mild	V. coarse	OS, VCR	RT water series with high Al melt; 4 drops
	1.4 w/o Al				17.3									and photos; debris is coarse chunks.
C-209-1	F4/C-121-2	80.4	1460	Ar + 1%H_2	15	2.96	1.87	Impactor	20	370	Slight	Globule	OS, VCR	Hot water series; one drop fell without
	1.4 w/o Al				NM									interaction, then rod with drop fell without
														interaction; no fragmentation.
C-211-1	F8/C-133-2	21.1	1465	Ar + 1%H_2	17	4.63	4.39	Impactor	20	370	Nil + Expl.	Globules +	VCR, Hyc	New F8 rod; 1st two drops, no explosion;
	0 w/o Al				18.0							powder		3rd drop exploded. Hycam on 1st drop saw
														no explosion.
C-213-1	F8/C-133-2	22.3	1470	Ar + 1%H_2	32	10.70	9.85	Impactor	20	370	Explo.+big	Powder	VCR, Hyc	Reused F8 rod: 1st drop, good explosion
	0 w/o Al				NM						explosion			seen by Hycam; then rod fell, gave big
														triggered explosion with most of rod.
C-215-1	F8/C-133-2	81.1	1460	Ar + 1%H_2	9	2.98	2.91	Impactor	20	370	Mild explo.	Coarse	VCR, Hyc	Hot water; 1st drop fell spontansously,
	0 w/o Al				NM									mild fragmentation + burning; 2nd drop
														released with Hycam; same burning, rising.
C-217-1	F4/C-121-2	9.5	1460	Ar + 1%H_2	17	4.93	4.99	Impactor	20	370	Nil	Globules	OS, VCR	Cold water; 4 drops without interaction;
	1.4 w/o Al				NM									globules formed. Good OS photos.
C-219-1	F5/C-121-3	18.7	1455	Ar + 1%H_2	15	3.76	3.75	Impactor	20	370	V. mild	V. coarse	OS, VCR	RT water series with intermed. Al content;
	0.34 w/o Al				20.3									3 drops, each with small burning drops that
														rise.
C-221-1	F5/C-121-3	8.5	1460	Ar + 1%H_2	18	4.21	4.34 w.	Impactor	20	370	Almost nil	Chunks	OS, VCR	Cold water with intermediate Al; 3 drops,
	0.34 w/o Al				17.0	(3 drops)	silica							each with fewer burning drops than C-219-1.
														Debris is in chunk form.
C-223-1	F5/C-121-3	84	1455	Ar + 1%H_2	20	8.33	4.06	Impactor	20	370	V. little	Coarse &	OS, VCR	Hot water with intermediate Al; 1st drop, no
	0.34 w/o Al				NM							spherical		fragmentation, good OS photo; 2nd drop, no
														OS photo; 3rd drop, good OS photo with
														burning particles; then lost rod. Coarse
														drops.

[a] Upper entries for losses of rod length are determined from photographs; lower entries are determined with a caliper.

released into the same depth of water at several temperatures between 7.5 ^{o}C and 90 ^{o}C. (There was patchy black oxide on the exteriors of many of those drops, however.)

During 1997, five experiments were performed to test for spontaneous explosions, as indicated in Table 2; none occurred.

Triggered Explosions

Because spontaneous explosions were never observed with any of the ferrosilicon drops, either non-alloyed or alloyed, we turned to triggering the steam explosions by introducing pressure transients into the water shortly after the drops were released. We generated the transients with the small hydrogen-oxygen combustion tube and the solenoid-driven impactor described in the experimental section above.

The Hydrogen-Oxygen Combustion Tube. This triggering technique uses the underwater explosion of 100 ml (STP) of a stoichiometric hydrogen-oxygen mixture contained in a vertical combustion tube. This tube is placed in the path of drops of molten ferrosilicon alloys as they fall through the water. By positioning the tube at a proper depth in the water and choosing an appropriate delay time, the gaseous explosion can be initiated when a falling drop is a few centimeters above the tube. A time-exposed photograph of an explosion triggered this way is shown in Figure 7 (C-189-1).

General Observations. The underwater ignition and combustion of 100 ml of a stoichiometric hydrogen-oxygen mixture at local atmospheric pressure is a vigorous event. To assure ourselves of the overall safety of the apparatus, several trial experiments were first performed at the University of Wisconsin's remote laboratory in Stoughton, Wisconsin. These initial experiments were carried out in an area of the laboratory surrounded by heavy concrete walls, with the combustion apparatus and water chamber shielded with heavy plywood panels. In the first test, the combustion tube was submerged in water contained in a 244 mm-OD X 279 mm-tall stainless steel beaker. (Stainless steel was chosen because of its tendency to yield plastically rather than shatter when exposed to strong pressure transients.) After the first test indicated only moderate potential for damage, subsequent experiments were performed in the 1 m-tall polycarbonate water chamber (this chamber, used in the 1996 studies (Nelson et al., 1997a), was newly reinforced with steel angle irons and threaded rods).

After several further experiments at the Stoughton site indicated the safety of the apparatus, we moved the entire system to Room 1408 in the Engineering Research Building in Madison, where the 1996 experiments had been performed. Further tests were performed with the chamber mounted in the 3 m-tall tower to take advantage of the spill control system installed there in case the water chamber fractured or developed leaks. No difficulties were encountered with the chamber even after several dozen hydrogen-oxygen combustion experiments had been carried out. On the basis of these experiments, we concluded that the triggering system posed no significant danger to personnel or the surroundings.

During a number of the experiments, we recorded video images during the combustion with a VHS camcorder (60 frames/second). We imaged in two ways: (a) from the front through the transparent wall of the combustion chamber and perpendicular to the axis of the combustion tube, and (b) from above the water surface, at an angle of about 30 degrees downward from horizontal. View (a) showed details of the ignition, combustion and behavior of any gaseous products, while (b) showed the motion of the water surface produced by the combustion.

Frame-by-frame examination of the video images obtained from view (a) showed a brilliant flash of light in the first frame and what appears to be an underwater puff of steam that moves upward from the tube for the next few frames. Steam also seems to fill the combustion tube during these same frames. Also, a much smaller puff of steam seems driven downward from the open lower end of the combustion tube. The upper puff travels about 200 mm upward, then slows and disperses, presumably due to condensation in the water.

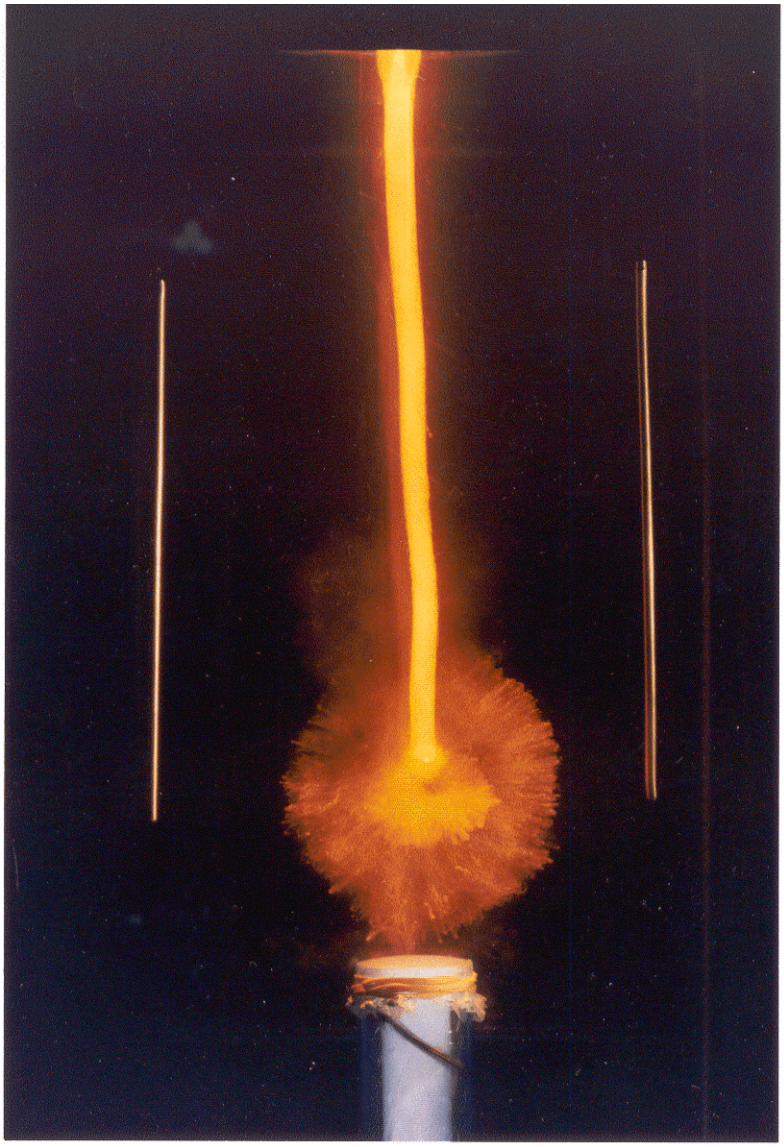

Figure 7. Time-exposed image of a drop of molten ferrosilicon alloy that exploded after being triggered by the underwater explosion of 100 ml of a stoichiometric hydrogen-oxygen mixture. Alloy contained 0.020 w/o Al and 0.011 w/o Ca. Note the brighter, smaller circular image superimposed on the darker, larger image. Fiducial rods to either side of the image are 135 mm apart. (C-189-1).

This entire process takes 6 or 8 frames, or about 0.1 s. During this same period, the downward puff travels only a few centimeters and then breaks into large, discrete bubbles which gradually rise to the surface over the next few seconds.

View (b) of the water surface shows light from the flash scattered at the surface in frame 1 followed by four linear jets of water emitted upward along the four straight edges of the top of the chamber. These jets show considerable structure, resembling Taylor instability fingers. The jets rise for a few video frames, with water drops being thrown as high as about 200 mm, before they begin to collapse. After collapse, the surface of the water shows intense ripples that rise and fall in a checkerboard pattern before dissipating gradually. Somehow, very little water is thrown over the edges of the chamber in spite of this vigorous water motion.

Transducer Measurements. Sixteen separate hydrogen-oxygen combustion reactions were performed with the tip of the transducer a few millimeters below the water surface and the combustion tube 286 mm, 310 mm or 470 mm below the transducer. The results were quite variable. The pressure-time records showed many shapes, as shown in Figures 8, 9 and 10, while the peak pressures normalized to100 mm fell in a wide range from less than 0.01 MPa to greater than 0.2 MPa, as shown in Table 5. The average peak pressure was 0.083 MPa at 100 mm, with a standard deviation of ±0.061 MPa, nearly as large as the average peak pressure itself. This variability occurred even though the burns seemed quite similar audibly and visually and in the video images.

Disadvantages and Advantages. Although the hydrogen-oxygen explosions can trigger steam explosions of the melt drops very efficiently, the technique has several disadvantages for our studies:

- The hydrogen-oxygen explosions inject a water jet and a stream of bubbles at high velocity into the same water volume in which the steam explosions occur. This often obscures video imaging and high-speed photography of the steam explosions with reflected light, both of which are desirable for time-resolved measurements of energetics, as discussed below. (Time-exposed images recorded with the self-illumination of the interaction, however, do not seem to be affected by these interferences.)

- The high velocity water jet can cause Weber-type breakup of the melt drop that may cause fragmentation unrelated to the steam explosion under study. We measured the water jet velocities from two consecutive frames in the video records of three different experiments (typical images are shown in Figure 11). The jet front moved 140 mm in two experiments and 99 mm in the third in the time interval for the video record to advance one frame. At 60 frames/second, or 16.7 ms per frame, this corresponds to jet velocities of 8.4, 8.4 and 5.9 m/s.

Table 5. Pressure Transients Generated in Water with the Hydrogen-Oxygen Combustion Tube PCB Transducer Type 112AO3, S/N 7617

Expt. No.	Distance (mm)	V_{max} (V)	V_{max} at 100 mm	P_{max} at 100mm (psi)	(Mpa)	
C-109-1	47.0	0.60	0.28	14.1	0.097	
C-109-2	47.0	0.34	0.16	8.0	0.055	
C-109-4	47.0	0.02	0.01	0.5	0.003	
C-109-5	47.0	0.53	0.25	12.5	0.086	
C-109-6	47.0	0.20	0.09	4.7	0.032	
C-112-1	47.0	0.42	0.20	9.9	0.068	
C-112-3	47.0	0.26	0.12	6.1	0.042	
C-114-1	28.6	1.18	0.34	16.9	0.116	
C-114-3	28.6	0.65	0.19	9.3	0.064	
C-114-4	28.6	0.22	0.06	3.2	0.022	
C-114-5	28.6	1.58	0.45	22.6	0.155	
C-120-1	31.0	0.78	0.24	12.1	0.083	
C-120-2	31.0	1.84	0.57	28.5	0.196	
C-120-3	31.0	0.25	0.78	3.9	0.027	
C-120-4	31.0	0.62	0.19	9.6	0.066	
C-120-5	31.0	2.02	0.63	31.3	0.215	
					Avg 0.083	SD 0.061

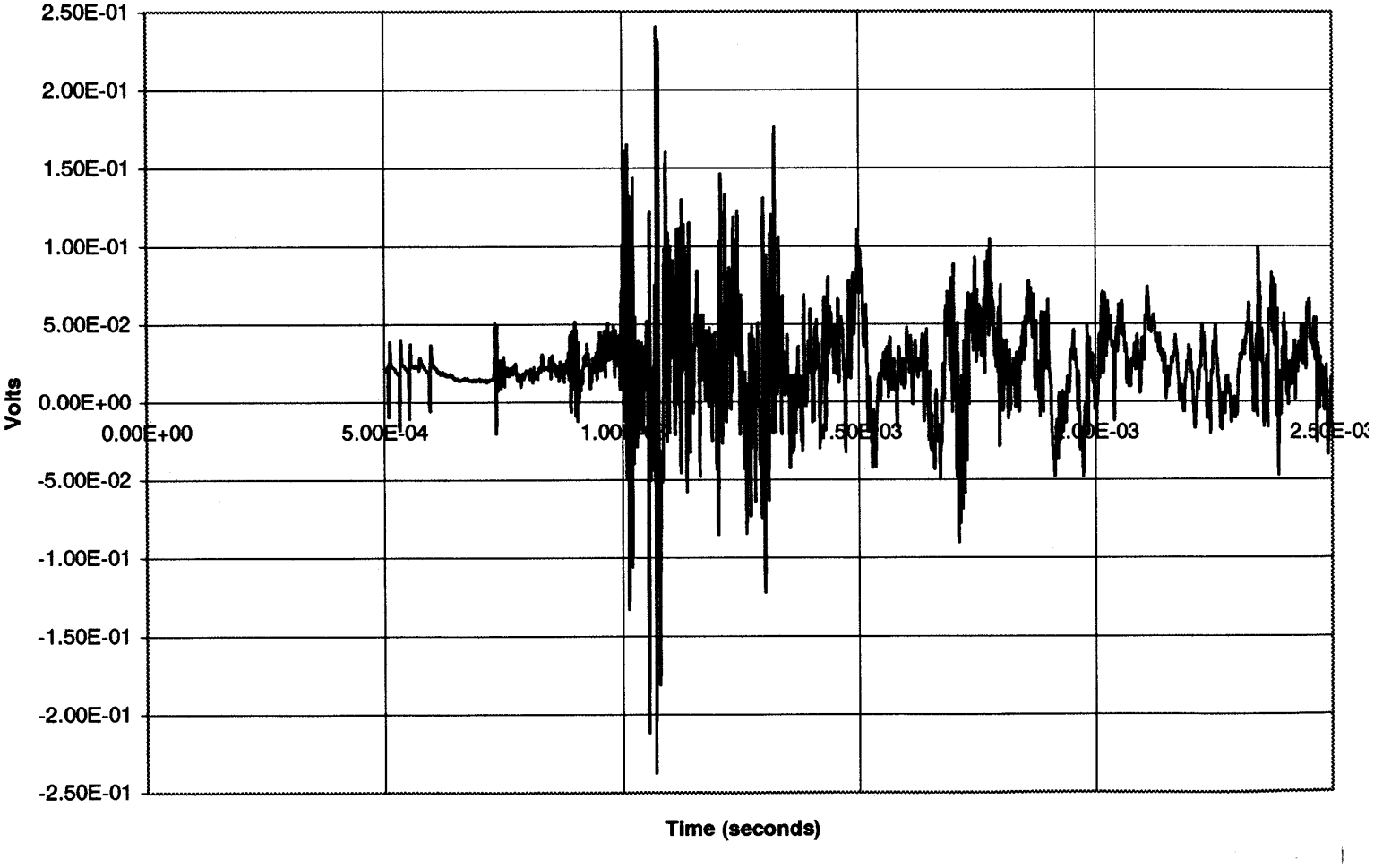

Figure 8. Voltage-time trace generated by underwater hydrogen-oxygen combustion. (Experiment C-112-3). Details of the conversion to pressures are presented in Table 5.

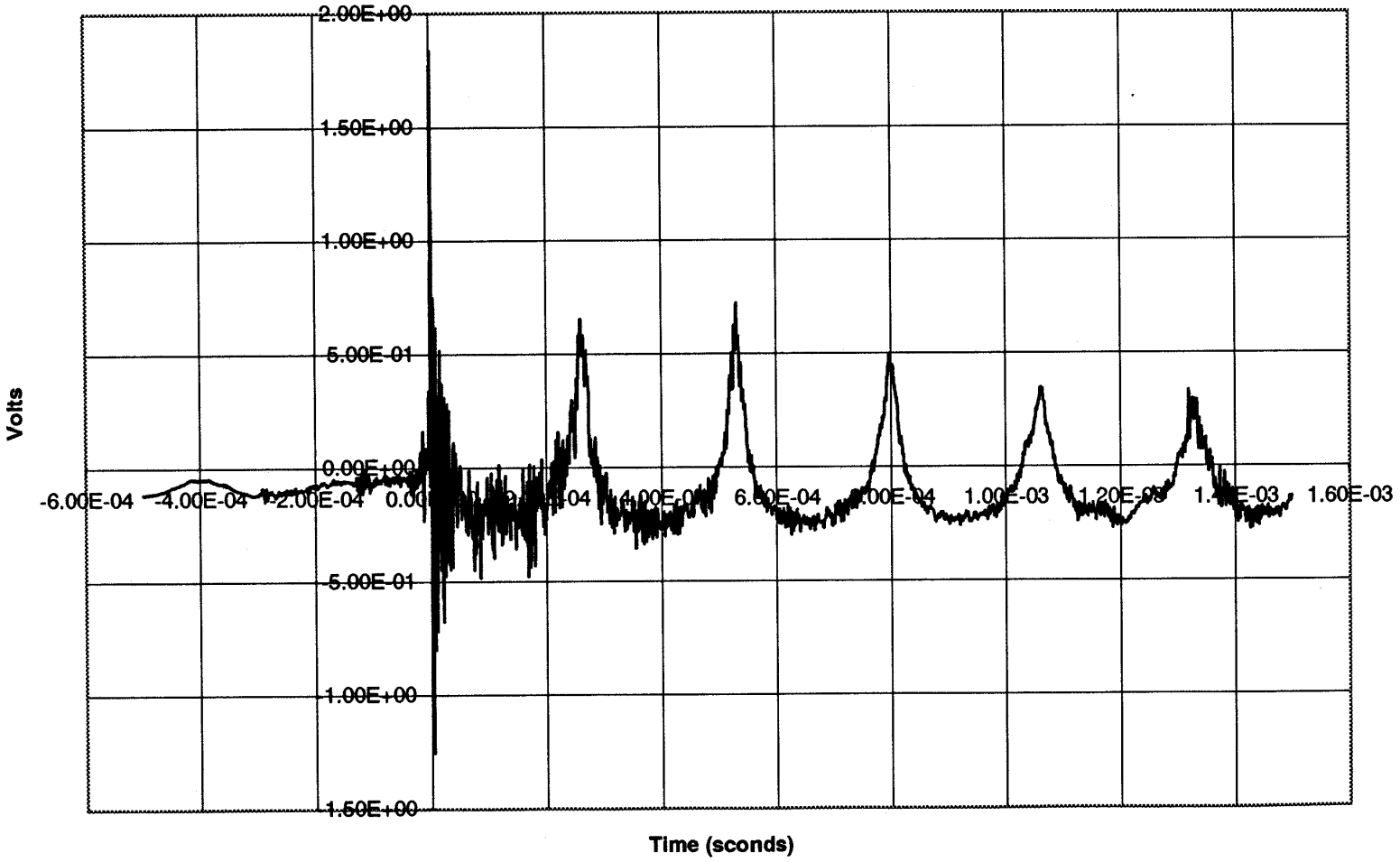

Figure 9. Voltage-time trace generated by underwater hydrogen-oxygen combustion. (Experiment C-120-2). Details of the conversion to pressures are presented in Table 5.

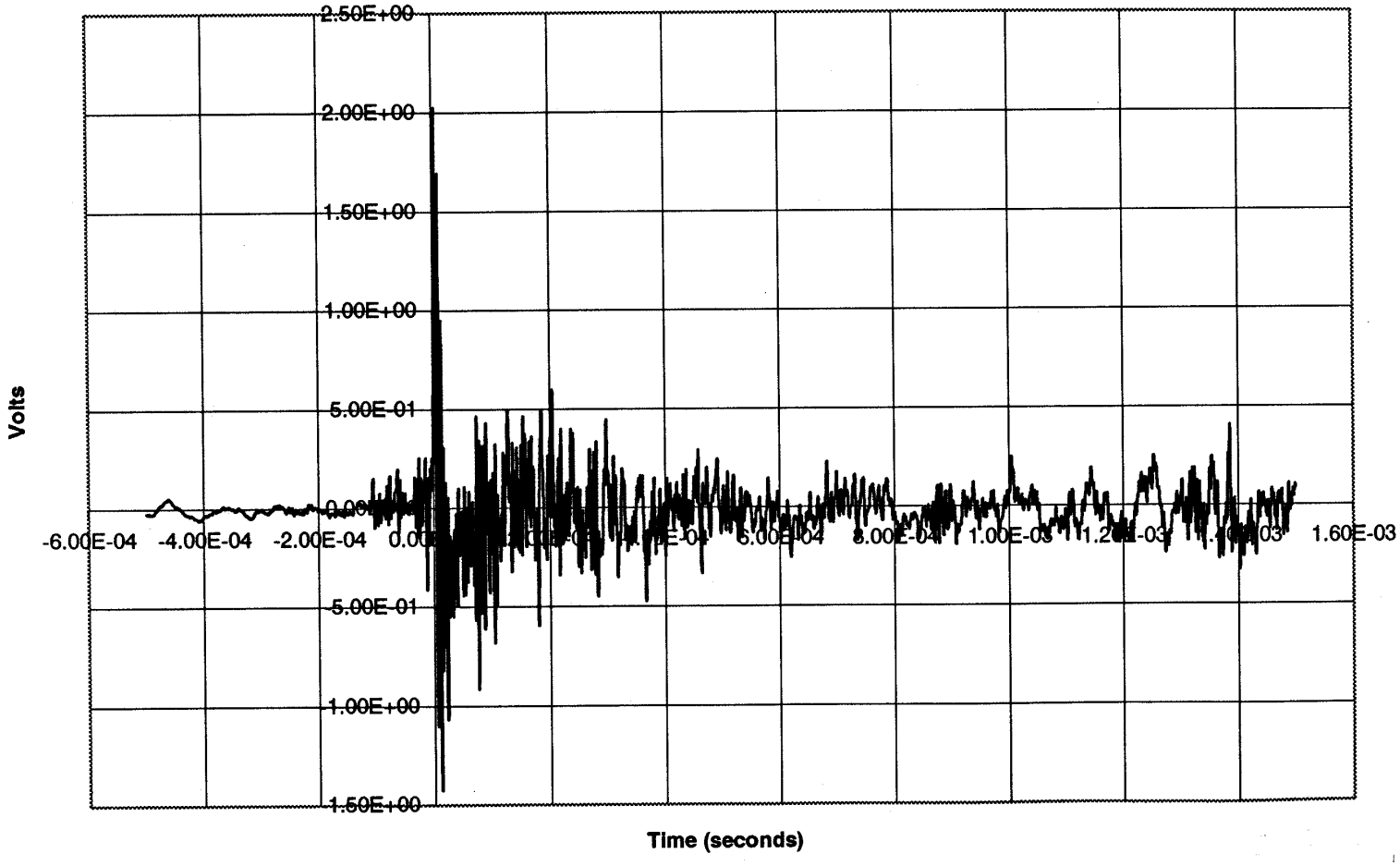

Figure 10. Voltage-time trace generated by underwater hydrogen-oxygen combustion. (Experiment C-120-5). Details of the conversion to pressures are presented in Table 5.

The Weber number, W_e, given in Equation (1), is a measure of the likelihood that a drop of liquid will break up when exposed to a high-speed flow of another fluid:

$$W_e = \rho V^2 D/\sigma \quad (1)$$

where ρ is the density of the streaming fluid, V is the velocity of the fluid stream past the drop, D is the diameter of the drop, and σ is the surface tension of the drop material. For a 9.2 mm (0.0092 m)-diameter melt drop with a surface tension of 750 dynes/cm (0.75 N/m) (Klevan, 1997) exposed to a water jet with a density of 1.0 g/cc (1000 kg/m^3) traveling at 8.4 m/s, the Weber number is 875. According to Pilch and Erdman (1987), when the Weber number is greater than 350, the molten drop is very likely to break up catastrophically, provided its viscosity is not too high, and the time it is exposed to the flowing stream is not too short.

The fragmentation predicted by this determination of the Weber number is confirmed by the breakup of nonexploding ferrosilicon drops with Al and Ca additives at two concentrations shown in Figures 12 and 13 (see also Figure 27).[1]

- The hydrogen-oxygen explosions are usually accompanied by incomplete combustion, placing unburned gaseous hydrogen and oxygen in the reaction volume. These gases could confuse measurements of hydrogen if it were used to estimate the extent of alloy-water chemical reaction.

- While the hydrogen-oxygen explosions generate vigorous pressure transients, they are poorly reproducible compared to those produced by the mechanical triggering system discussed below (compare Tables 5 and 6).

- When repetitive experiments are being performed, the hydrogen-oxygen combustion technique suffers from a slow turnaround time (about an hour) compared to the mechanical triggering procedure (several minutes).

The combustion triggering technique has one significant advantage, however, namely, the ability to produce steam explosions in a free volume of water, away from surfaces. As shown in Figure 7, these explosions are essentially spherical and are thought to simulate the steam explosions of drops of molten ferrosilicon that might occur in industrial granulation processes.

Triggering with the Hydrogen-Oxygen Combustion Tube. We devoted significant effort to achieving good reflected light photographic and video images of steam explosions of drops of ferrosilicon alloys triggered by hydrogen-oxygen combustion. Twenty-three experiments were performed with the hydrogen-oxygen combustion tube as trigger; they are summarized in Table 3.

The Impactor. Mechanical transient generators have few of the disadvantages of the hydrogen-oxygen combustion trigger. If their use can be optimized, they should provide the best and most reliable triggering sources for steam explosion studies with single drops of melt.

General Observations. The impactor is a sturdy, very reliable and easy-to-use source of pressure transients. It operates with only the closure of an electrical switch and resets by gravity for repeat operation simply by opening the switch again. Moreover, its operation produces only minimal disturbance of the water column in the chamber (e.g., splashing at the water surface, jet or bubble generation or flexure of the chamber walls). The only motion that can be observed is the upward jump by the entire unit of a few

[1]A discussion of the effect Weber-type breakup may have on the maximum diameter of commercially granulated ferrosilicon is presented in Appendix A.

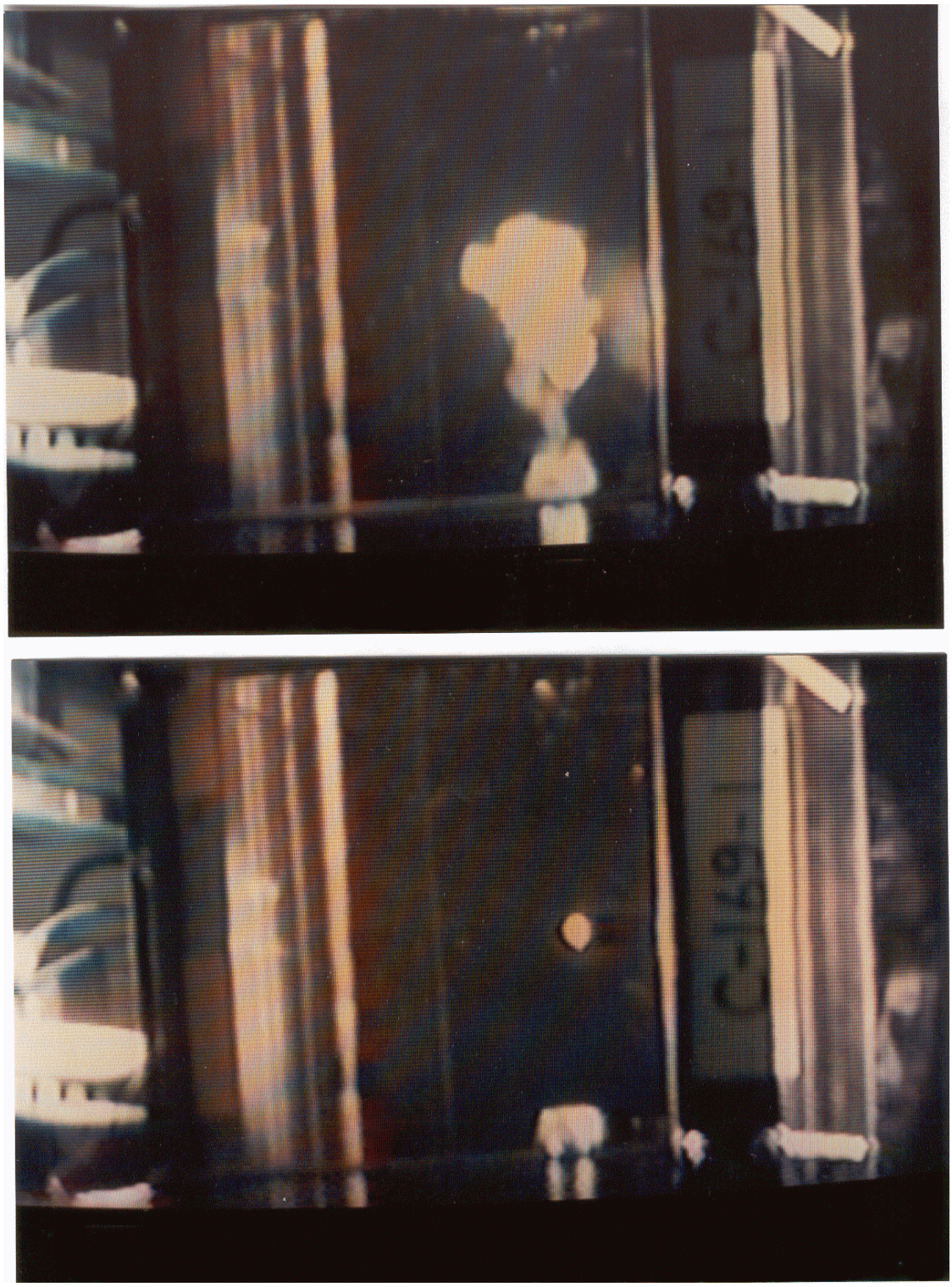

Figure 11. Video images of the top of the combustion tube with a molten ferrosilicon drop just above it (lower image) and one video frame later (16.7 ms), just after the hydrogen-oxygen explosion was initiated (upper image). From the distance the bubble front moved in this time interval (0.14 m), we estimated a jet velocity of 8.4 m/s. (C-169-1)

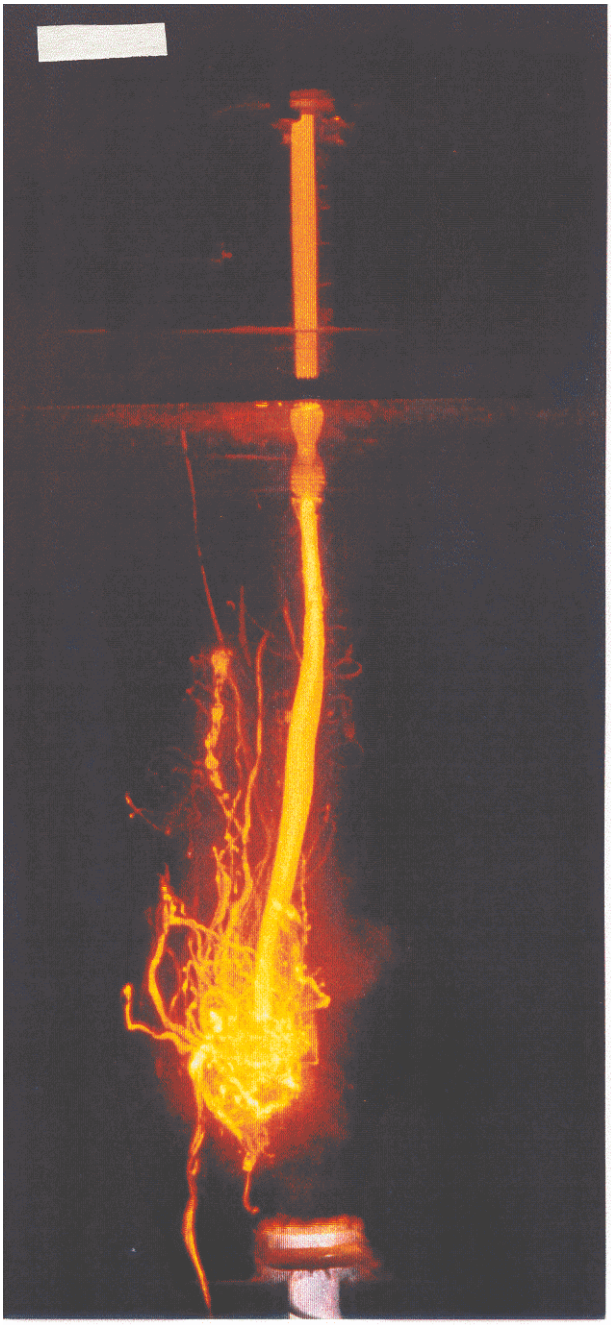

Figure 12. Time-exposed image of a drop of molten ferrosilicon alloy that fragmented a few centimeters above the underwater explosion of 100 ml of a stoichiometric hydrogen-oxygen mixture. The alloy contained 0.34 w/o Al and 0.074 w/o Ca. Breakup of the melt is thought to have been caused by Weber-type processes. Bar is 5 cm long. (C-163-1)

millimeters when the solenoid is activated. Clearly, the impactor is a benign, simple source of upward-directed pressure transients.

Transducer Measurements. In preliminary tests, we learned that the pressure-time traces generated by the impactor were sensitive to the nature of the current switching used to activate the solenoid. Unless the switch had a capacity of at least 20 A, there was considerable variation between peak pressures recorded in repeated experiments.

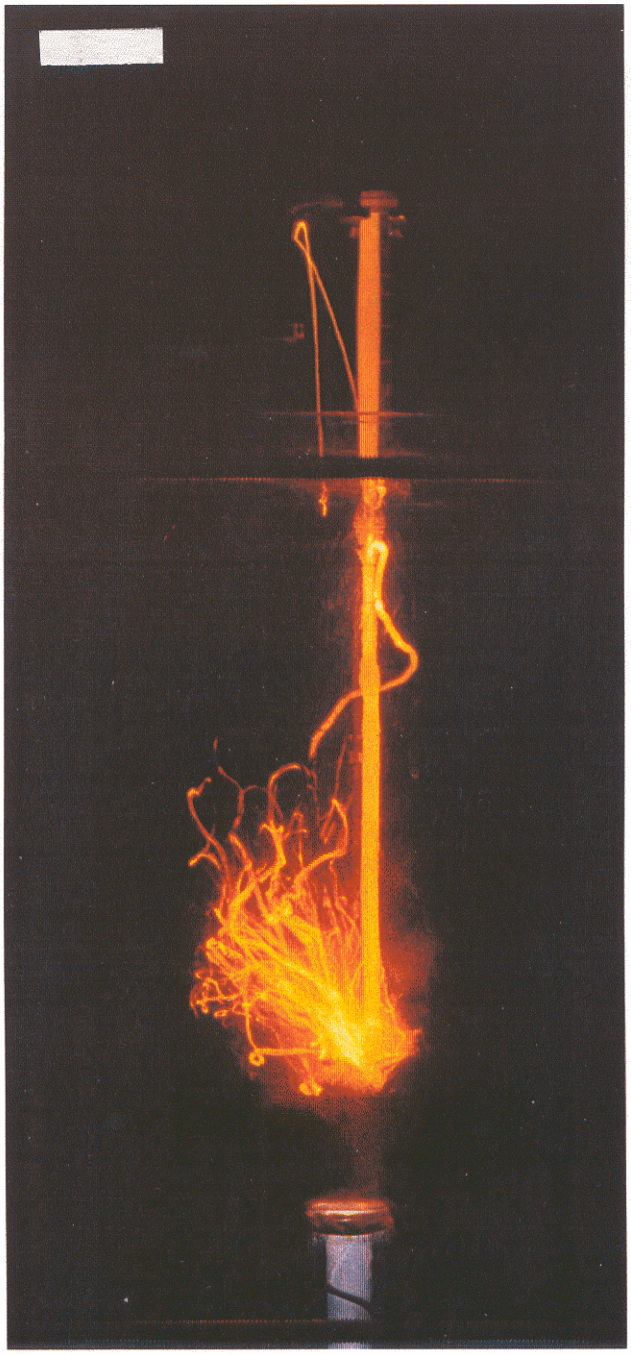

Figure 13. Time-exposed image of a drop of molten ferrosilicon alloy that fragmented a few centimeters above the underwater explosion of 100 ml of a stoichiometric hydrogen-oxygen mixture. The alloy contained 1.4 w/o Al and 0.63 w/o Ca. Breakup of the melt is thought to have been caused by Weber-type processes. Bar is 5 cm long. (C-166-1).

After we turned to a high amperage switch, we produced traces with good reproducibility; a typical trace is shown in Figure 14. Note that the duration of the transient is about 0.5 ms. In Table 6, we present the peak voltages, V_{max}, recorded when the impactor unit was positioned in the water at two distances below the transducer—74 mm and 148 mm. We also normalize the maximum voltages at the two distances to an

Table 6. Pressure Transients Generated in Water with the Mechanical Impactor
PCB Transducer Type 112AO3, S/N 7617

Expt. No.	Distance (mm)	V_{max} (V)	V_{max} at 100 mm	P_{max} at 100mm (psi)	(Mpa)	
C-118-1	74	1.36	1.00	50.0	0.343	
C-118-2	74	1.58	1.17	58.5	0.402	
C-118-3	74	1.52	1.12	56.0	0.385	
C-118-4	74	1.36	1.00	50.0	0.344	
C-118-5	74	1.63	1.21	60.5	0.416	
C-118-6	147	0.79	1.16	58.0	0.398	
C-118-7	147	1.20	1.76	88.0	0.605*	
C-118-8	147	0.88	1.29	64.5	0.443	
C-118-9	147	0.87	1.28	64.0	0.440	
C-118-10	147	0.88	1.29	64.5	0.443	
					Avg 0.422	SD 0.074
			*Omitting C-118-7		Avg 0.402*	SD0.039*

arbitrary 100 mm, using the inverse distance relationship (see Nelson et al, 1994a). And in the two right-hand columns, we convert these maximum voltages into peak pressures in psi and MPa, using the amplification of the recording system and the calibration provided by the manufacturer of the transducer.

It can be seen in Table 6 that peak pressures of 0.422 ± 0.074 MPa (normalized to 100 mm) were recorded in ten experiments, with five recorded at 74 mm and five at 148 mm. Note that the average peak pressure of 0.422 ± 0.074 MPa produced by the impactor is about five times the 0.083 ± 0.061 MPa produced at 100 mm by the combustion tube (see Table 5). For comparison, a typical transient generated by the underwater explosion of a gold bridgewire with a capacitor discharge of 282 J @ 3.36 kV produced a 1.0 MPa peak pressure at 100 mm (Nelson et al., 1994a). Pressure transients of this magnitude successfully triggered steam explosions of drops of molten iron oxide (Nelson and Duda, 1981, 1982, 1985) and aluminum (Nelson, 1995).

Triggering with the Impactor. In the earliest experiments with the mechanical impactor, we found that at certain combinations of depths and activation delay times, good steam explosions of the drops could be achieved if the impactor was activated shortly after they landed on its steel surface. A typical explosion triggered this way is shown in Figure 15. The presence of the surface caused the explosions to appear hemispherical, however. This led us to set aside the method temporarily in order to concentrate our efforts on the hydrogen-oxygen triggers to study spherical explosions, unaffected by the proximity of the surface.

After a few experiments, the difficulties encountered in achieving good reflected light photographic and video images of the steam explosions with the hydrogen-oxygen trigger discussed in the previous section then prompted us to return to the impactor to try to obtain explosions above its surface. By trial and error, we discovered that by selecting a depth of 20 cm and a delay time of 370 ms for firing the impactor, we could actually achieve spherical explosions several centimeters above the surface of the impactor. A time-exposed photograph of the first such explosion is shown in Figure 16 (C-197-1). We then continued to use the impactor with this combination of depth and delay for the remainder of the experiments performed during 1997.

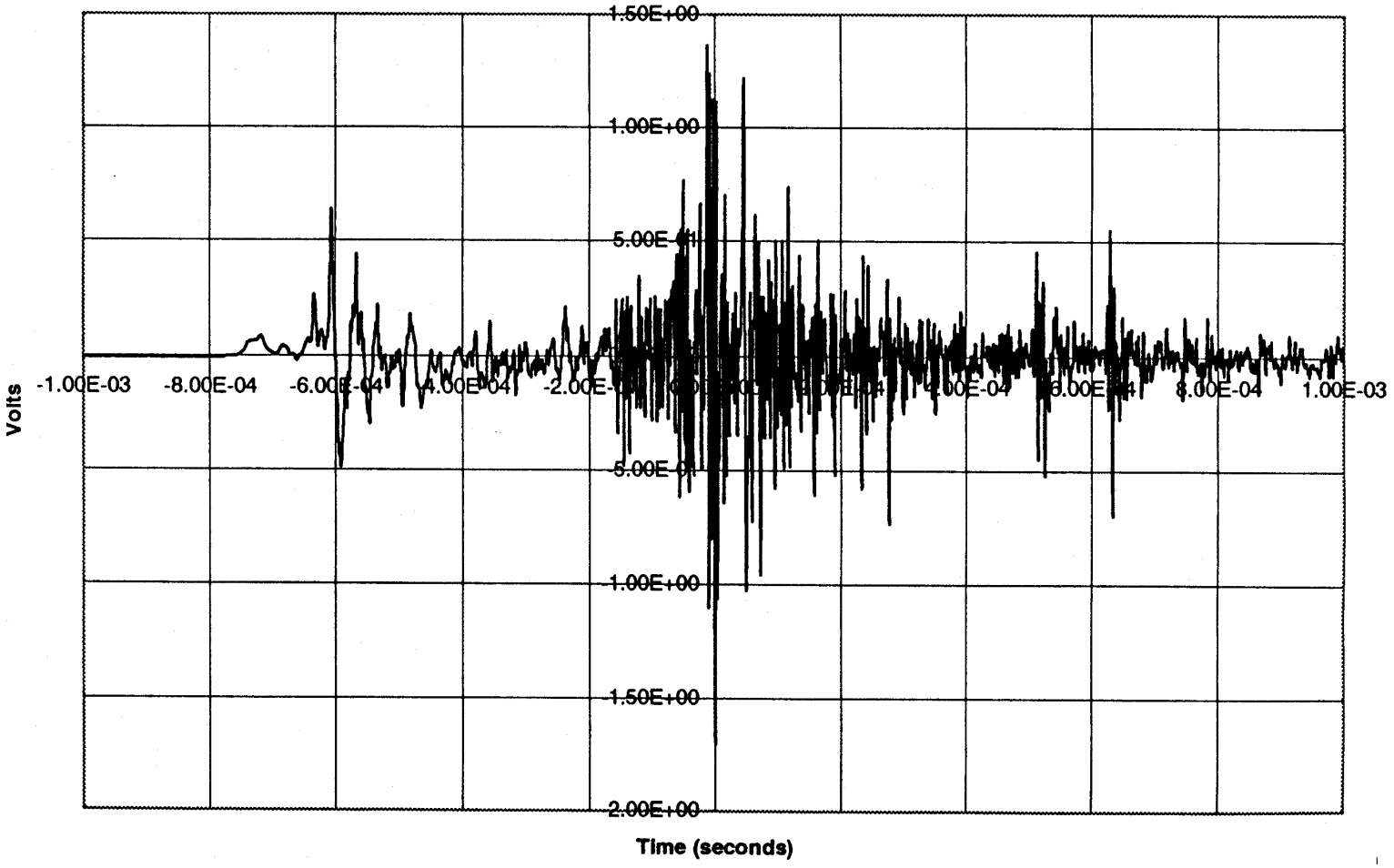

Figure 14. Typical voltage-time trace generated by the solenoid-driven impactor when activated underwater. (Experiment C-118-1). Details of the conversion to pressures are presented in Table 6.

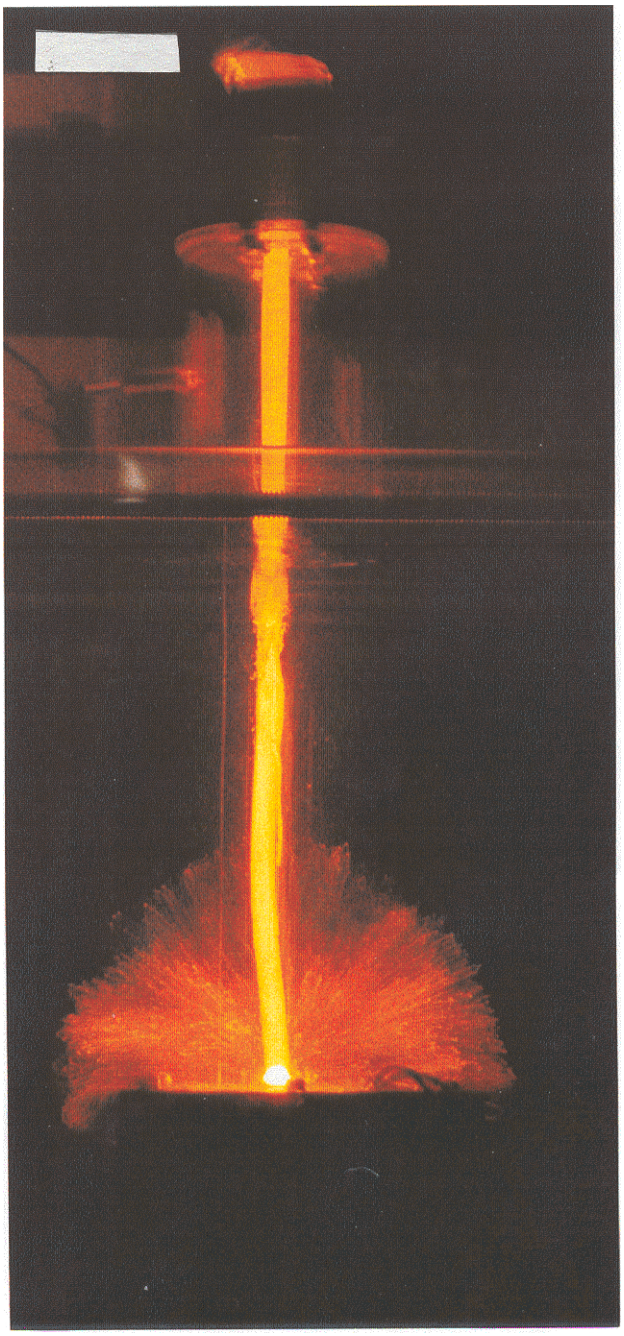

Figure 15. Time-exposed photograph of the hemispherical explosion of a drop of molten ferrosilicon that was triggered at the underwater surface of a solenoid-driven impactor. Bar is 5 cm long. (C-143-1).

Twenty-four experiments were performed with impactor triggering, as indicated in Table 4. Some of these experiments involved the release of several drops in succession from the same rod. (Repetitive experiments of this sort could not be performed easily with combustion tube triggering.)

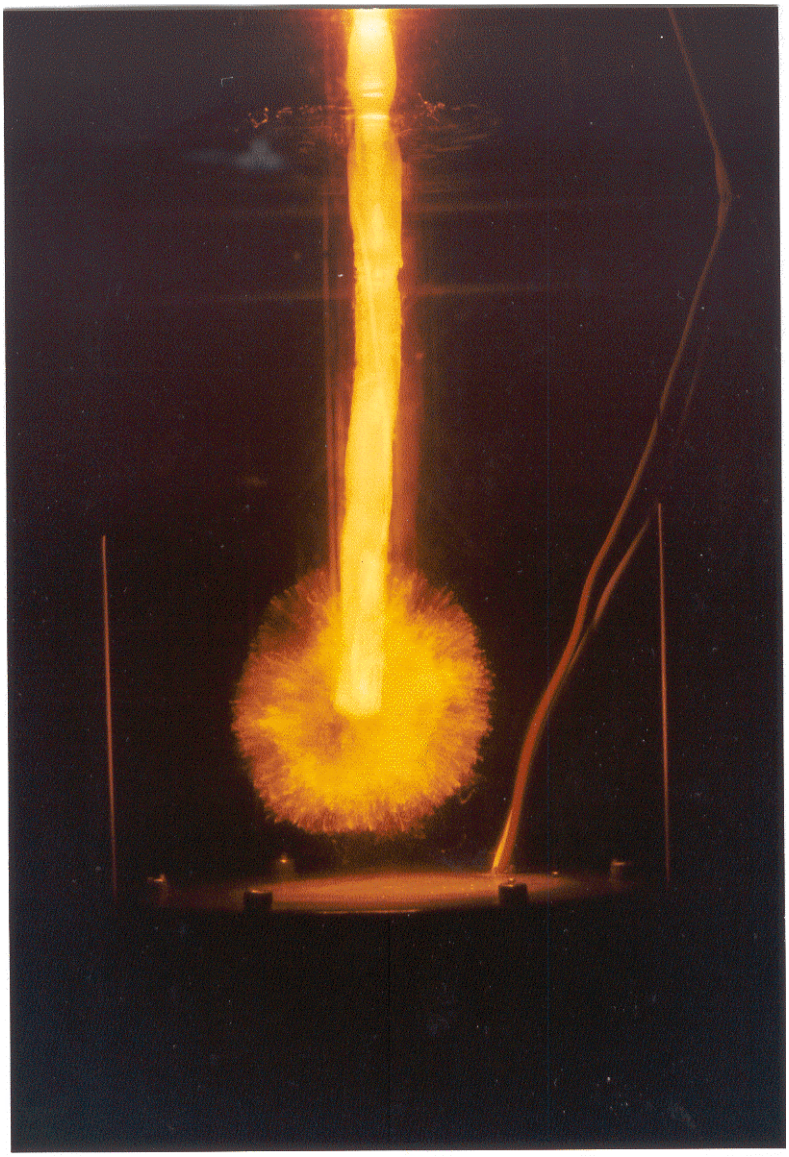

Figure 16. Time-exposed photograph of a spherical steam explosion of a molten ferrosilicon drop triggered with a pressure transient generated by the solenoid-driven impactor. Fiducial rods to either side of the image are 138 mm apart. (C-197-1).

Effects of Alloying

Non-Alloyed Ferrosilicon Drops

The non-alloyed ferrosilicon drops produced the most vigorous explosive melt-water interactions when triggered with either the impactor or the hydrogen-oxygen combustion tube. Typical time-exposed photographs of these explosions are shown in Figures 7 and 16, which were recorded with combustion tube and impactor triggering, respectively (experiments C-154-1 and C-143-1). Both images show fine, ray-like traces that radiate from a central location. The traces are believed to be produced by finely fragmented luminous melt particles that move radially outward from the center of the explosion. Also, in both figures, there is a an additional central luminous zone somewhat larger than the trace of the original drop that appears to be formed by an initial small bubble growth and collapse that occurs just before the growth of the large bubble that carries the fine fragments outward to the final limit. This type of cyclic bubble growth

and collapse has also been observed in the explosions of drops of molten iron oxide (Nelson and Duda, 1981,1982), molten tin (Ciccarelli, 1991; Ciccarelli and Frost, 1994) and molten aluminum (Nelson, 1995).

As an example of the type of dynamic video imaging we recorded with the non-alloyed ferrosilicon drop triggered with the combustion tube, we cite experiment C-170-1. In this experiment, we obtained a good video record that showed the drop to fall for about 400 ms and approach to within about 5 cm of the top of the combustion tube. Then the brilliant flash of light from the hydrogen-oxygen explosion occurred and extinguished one video frame later (16.7 ms). This was followed by the steam explosion of the drop that was quickly obscured by at least 500 ms of brightly luminous fine bubbles in the vicinity of the interaction. Finally, the luminosity decayed to a much lower intensity; this region seemed to be filled with upward rising bubbles and downward falling debris particles. About 1 second after the triggering, a narrow column of discrete bubbles rose from the combustion tube, presumably generated by the unburned gases from the hydrogen-oxygen combustion. And finally, after the bubble activity attenuated, there was a cloud of what seemed to be colloidal material that remained in place for many seconds after the explosion.

The 16 mm film images for experiment C-170-1 show a considerably more detailed view of the explosive interaction. It shows the drop beginning its cyclic growth and collapse when the pressure disturbance from the combustion tube passes it. This occurs well before a high-speed bubble stream emitted from the combustion tube arrives at the drop and partially obscures the view. It is, however, possible to distinguish the later growth of the luminous bubble that contains the fragmenting melt particles from the non-luminous combustion-generated bubbles.

Drops of Ferrosilicon Alloyed with Al and Ca

The time-exposed images of drops of molten ferrosilicon alloyed with Al and Ca as shown in Tables 3 and 4 never produced the fine luminous traces that accompany a vigorous explosion of the type shown in Figures 7, 15 and 16 when they were exposed to either the impactor or the combustion tube triggers. Some images recorded with the hydrogen-oxygen trigger showed a tangled ball of erratically moving coarse images, however. Two of these images are shown in Figures 12 and 13; they were generated by drops that contained 0.34 w/o Al and 0.074 w/o Ca (C-163-1) and 1.4 w/o Al and 0.63 w/o Ca (C-166-1), respectively. (Photographs of the coarse debris generated in these experiments are shown in Figure 27.) As discussed earlier, these drops are thought to have fragmented by Weber-type processes, described by Equation (1), that are caused by the high velocity jet of water and bubbles produced by the hydrogen-oxygen explosion, rather than by true steam explosion processes.

The reflected light images of the experiments with the alloyed drops exposed to the hydrogen-oxygen trigger are difficult to interpret because of the interference by the bubble stream evolved during the interactions. Very little information can be obtained from the video images because of the relatively low framing rate.

The high-speed film of one experiment with the alloyed melt, C-171-1, shows, however, that the melt-water interaction does not seem to occur until the hydrogen-oxygen bubble stream reaches the drop. But then the bubble stream quickly obscures further observation of the melt breakup. Our tentative explanation of this behavior is that Weber breakup of the drops is produced by the water/bubble stream. The drops of melt produced this way are then driven erratically upward to produce the tangled images shown in Figures 12 and 13.

Effects of Water Temperature

During 1997, we carried out nine experiments to test the effects of changing water temperature on impactor-triggered interactions between the molten alloy drops and water. These experiments formed a 3 X 3 matrix generated by three water temperatures—nominally 8 ^{o}C, 20 ^{o}C (room temperature) and 80 ^{o}C—and three ferrosilicon alloy compositions, one without additives and two with Al and Ca additives. In each

experiment, we released one drop or several drops from the same rod several minutes apart into the same water. These experiments are summarized in Table 4.

In these experiments:

- Steam explosions never occurred spontaneously at any water temperature with drops of any of the three alloys studied here.

- Steam explosions could be triggered at the three water temperatures with drops of the molten non-alloyed ferrosilicon from rod F8 (C-133-2). These explosions were most vigorous in the cold water, vigorous in the water at room temperature and mild in the hot water. There was strong indication that many of the fragmented particles burned in the water, accompanied by the generation of hydrogen and fine colloidal material.

- We could not trigger explosions or obtain even coarse fragmentation at any water temperature with drops of the alloy that contained the higher concentrations of Al and Ca (1.4 wt.% Al and 0.63 wt.% Ca, rod F4 (C-121-2); see Table 1).

- At all three water temperatures, the triggering action stripped a few small melt fragments from the drops of the alloy that contained the smaller concentrations of Al and Ca (0.34 wt.% Al and 0.074 wt.% Ca, rod F5 (C-121-3); see Table 1). These small fragments burned in the water with the generation of hydrogen and fine particulate material.

Energetics of the Explosions

In the sections above on triggering with both hydrogen-oxygen explosions and with the mechanical impactor, we discussed the need for imaging the explosions with both reflected light and self-luminosity. The reasons for devoting considerable time and effort to obtaining these images will become apparent in this section.

Perhaps the most important product of our work will be to estimate the damage that could be caused by a large-scale steam explosion of an array of molten ferrosilicon drops in water during industrial granulation. One important element of such an estimate would be the energy transferred to the water by the explosion of each individual drop in the array. A good indicator of this energy is the pressure-volume product of the bubbles that are generated by the steam explosion of a single drop of melt. Thus, measurement of the bubble volumes produced during the explosive interactions of single drops can provide a valuable input into the overall damage potential of the array of drops in a granulation operation.

Bubble volumes can be converted into energies with Equation (2):

$$E\ (J) = 1013\ [\ P_{amb}\ (Mpa) \times V\ (liters)] \qquad (2)$$

where P_{amb} is the ambient pressure against which the bubble grows and V is the volume of the bubble. We assume here that the pressure needed to blow a bubble underwater is not very different from the local barometric pressure plus that of the depth of the water. Because our experiments are performed in relatively shallow water, we can neglect both the pressures added by 200 or 300 millimeters of water and the subtleties at the inner surface of the bubble and equate P_{amb} to P_{atm}, the local barometric pressure. That is, for our present purposes, $P_{amb} = P_{atm} = 0.1$ MPa.

Thus, if we can accurately determine the true dimensions of the steam explosion bubbles from our images of the interactions, we will be able to estimate the amount of energy transferred to the water.

Estimation of Bubble Dimensions

Still Photography. The easiest to record and the highest quality images of the interactions are the time-exposed 35 mm photographs taken in a darkened room. Also, because open shutter photography can record a luminous event at any time during a several minute waiting period, it is particularly well-suited to imaging the explosive interactions produced (always somewhat unpredictably) when drops are released spontaneously. Moreover, these images seem unaffected by the presence of bubbles in the water surrounding the steam explosions; thus, they can be recorded equally well with the hydrogen-oxygen trigger (see Figure 7) or with the mechanical trigger (see Figures 15 and 16).

Open shutter photographs are useful for determining the bubble dimensions for calculations with Equation (2). If we assume the edges of these images represent the outer surfaces of the steam explosion bubbles, we can then measure these edges (using fiducials incorporated in the photographs) to obtain the bubble volumes required for Equation (2).

As an example of the calculation of energy transferred to the water by a steam explosion triggered with the hydrogen-oxygen combustion tube, we have measured the bubble image in Figure 7 (C-189-1). The average outside diameter of the self-luminous image is 75.5 mm. This corresponds to a maximum volume of 0.225 L, which converts with Equation (2) to a maxumum PV bubble energy of 22.8 J. For the debris weight of 1.39 g, the energy transferred per gram of melt is16.4 J/g.

Another example of this calculation is applied to the image of the bubble produced in the impactor-triggered steam explosion shown in Figure 16 (C-197-1). The outside diameter of the self-luminous image here is 58.7 mm. This corresponds to a maximum volume of 0.106 L which converts to a maximum PV bubble energy of 10.7 J. For the debris weight of 1.27 g, the energy transferred per gram of melt is 8.4 J/g.

A third example of this calculation is for the "hemispherical" explosion shown in Figure 15 (C-143-1). This explosion was triggered when the melt drop was in contact with the surface of the mechanical impactor. Here, the horizontal diameter of the hemispherical bubble is 147 mm, corresponding to a maximum volume of 0.832 L (one-half the spherical volume). With Equation (2), this converts to 84.2 J. For debris that weighed 1.24 g, the energy transferred per gram of melt is 67.9 J/g. (In this experiment, there was a discrepancy between the weight of debris recovered from the chamber after the explosion, 1.24 g, and the loss of weight of the rod, 1.53 g. If this latter weight is used, the energy transferred would have been only 55.1 J/g.)

The time-exposed images may not accurately represent the true energetics of a steam explosion bubble, however. There are several aspects of the measurements that concern us:

The images may result from more than one bubble. In both Figures 7 and 16 there are two concentric images that seem to have been formed by the overlap of two bubbles, one smaller and brighter and a second larger and dimmer. In Figure 16, the bright bubble image is almost as large as the darker outer bubble image. We believe the smaller of the concentric images is produced by the formation of an initial bubble generated by the coarse fragmentation of the drop of melt. This bubble collapses quickly, generating a localized shock wave that causes the coarse fragments to begin a second interaction that generates the final, larger bubble, accompanied by fine fragmentation of the melt. The occurrence of several bubbles in sequence during steam explosions of single drops has been reported for molten iron oxide (Nelson and Duda, 1981,1982), molten tin (Ciccarelli, 1991; Ciccarelli and Frost, 1994) and molten aluminum (Nelson, 1995).

As an example of the uncertainty that might arise from the "double bubble," we have also measured the inner image of Figure 16. The outside diameter of the self-luminous inner image is 50.1 mm. This corresponds to a maximum volume of 0.0658 L which converts to a maximum PV bubble energy of 6.7 J. For the debris weight of 1.27 g, the energy transferred per gram of melt by the inner bubble is 5.3 J/g. Thus, if we use only the self-luminous image of an explosive interaction, we can estimate an energy transfer

as small as 10.7 J and as large as 17.4 J (8.4 J/g and 13.7 J/g), depending on whether only the outer image or the outer plus the inner images are used to determine the bubble volumes.

The uncertainty that might arise from the "double bubble" should be less for the image shown in Figure 7 because of the much smaller inner image. In this figure, the outside diameter of the self-luminous inner image is only 34.7 mm. This corresponds to a maximum volume of 0.022 L which converts to a maximum PV bubble energy of 2.2 J. For the debris weight of 1.39 g, the energy transferred per gram of melt by the inner bubble is 1.6 J/g. Thus, if we use only the self-luminous image of an explosive interaction, we can estimate an energy transfer as small as 22.8 J and as large as 25.0 J (16.4 J/g and 18.0 J/g), depending on whether only the outer image or the outer plus the inner images are used to determine the bubble volumes.

The edges of the time-exposed images may not correspond to the outer surfaces of the steam explosion bubbles. In order to address the uncertainties involved with this concern, we believe it important to measure bubbles imaged from the "outside," namely, those taken with reflected light, to compare with those imaged from the "inside," namely, those produced by the self-luminosity of the particles as they fragment. We have, therefore, used both video imaging and high-speed photography with external lighting to record the growth and collapse of the steam explosions of similar drops. Moreover, the time resolution offered by these techniques should help us separate the superimposed bubble images sometimes seen on the time-exposed photographs.

Video Images. A second way to estimate bubble dimensions is with video imaging. This method produces moderate time resolution (60 frames per second for our camera or 16.7 ms per frame) with reasonable image quality in color and with sound. And, as with time-exposed imaging, it requires no careful synchronization with the fall of the drops. Thus, because we have hours of recording time available on a video tape, we can image drops released at any time during a very long waiting period merely by allowing the camera to run continuously during an experiment. Delays of many minutes before a drop forms and is released mechanically or spontaneously can easily be tolerated and still produce usable images.

The wide range of automatic exposure settings available with the video camera allows us to use it as either a primary or a backup imaging system during all experiments: with time-exposed 35 mm photography in a darkened room; with the bright illumination required for the high-speed photography described below; and, very importantly, to capture accidental drop releases at any light level. The primary difficulty with using the video technique with initially low light levels (for example, in a darkened room) is the slow response of the automatic exposure electronics to changing light intensities; this always causes our drop images to be overexposed. Even with the overexposure, however, the self-luminous images can still be used for determining drop behavior and even estimating bubble dimensions with fair time resolution, as shown in the examples in Figure 17 (C-215-1 #1). But when bright illumination is used, as in Figure 18 (C-213-1 #1), reasonably good images of the interactions may be obtained. Unfortunately, the time resolution available with our video camera, 16.7 ms per frame, is considerably slower than the desirable minimum for studying the more vigorous explosions, which usually occur within 10 to 20 ms. (That is, the video camera can record only one or two frames during these more rapid interactions, as shown in Figure 18.)

Video images can also be used to calculate the energy transferred to the water by a steam explosion. For example, we have measured the bubble image in Figure 18b (C-213-1 #1). This steam explosion was triggered with the impactor. The outside diameter of the image is 36.0 mm. This corresponds to a maximum volume of 0.0244 L which converts with Equation (2) to a maximum PV bubble energy of 2.47 J. For the debris weight of 1.30 g (assumed from average debris weights in Tables 2, 3 and 4), the energy transferred per gram of melt is 1.9 J/g.

High-Speed Photography. In this section, we will discuss the use of high-speed photography to achieve faster framing. During 1997, we used the Hycam 16 mm high-speed camera to record ten 100 foot (33 meter) films of our interactions at 1000 frames per second. Most of these had difficulties with exposure and/or with the interference of the bubble streams produced by the hydrogen-oxygen combustion trigger. But the last two films were deemed very successful. One, from experiment C-213-1 #1, produced a good

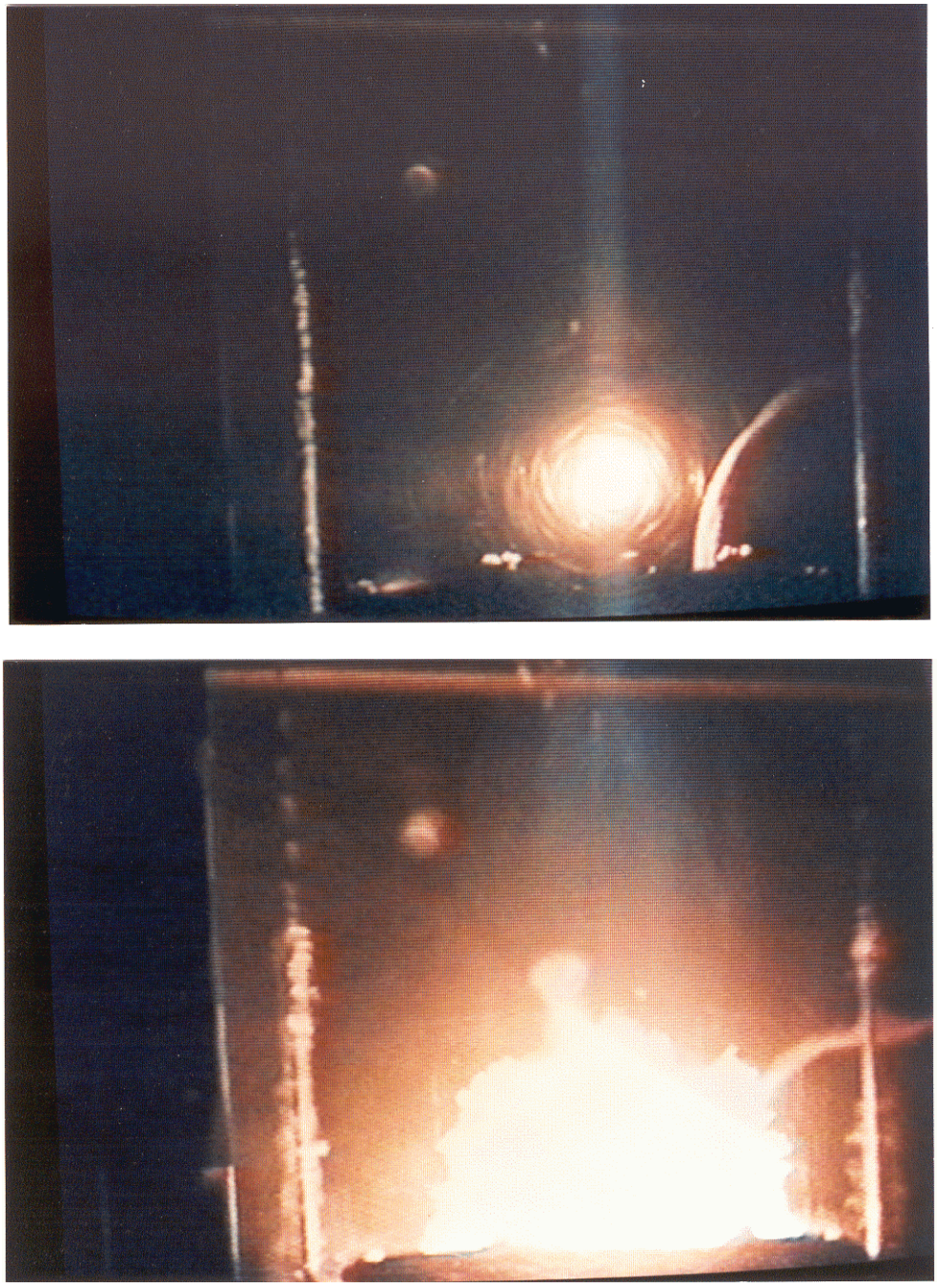

Figure 17(a) (above); Figure 17(b) (below).

Figure 17. Photographs of three consecutive frames from the video record of a steam explosion of a non-alloyed ferrosilicon drop triggered with the impactor. Video images were recorded with the self-luminosity of the melt. Image (a) shows the melt drop as it falls through the water one frame before the trigger. Image (b) shows the drop as it explodes. Image (c) shows the mass of bubbles that form one frame after image (b). Each frame is 16.7 ms apart. Fiducial rods to either side of the image are 138 mm apart. (C-215-1 #1)

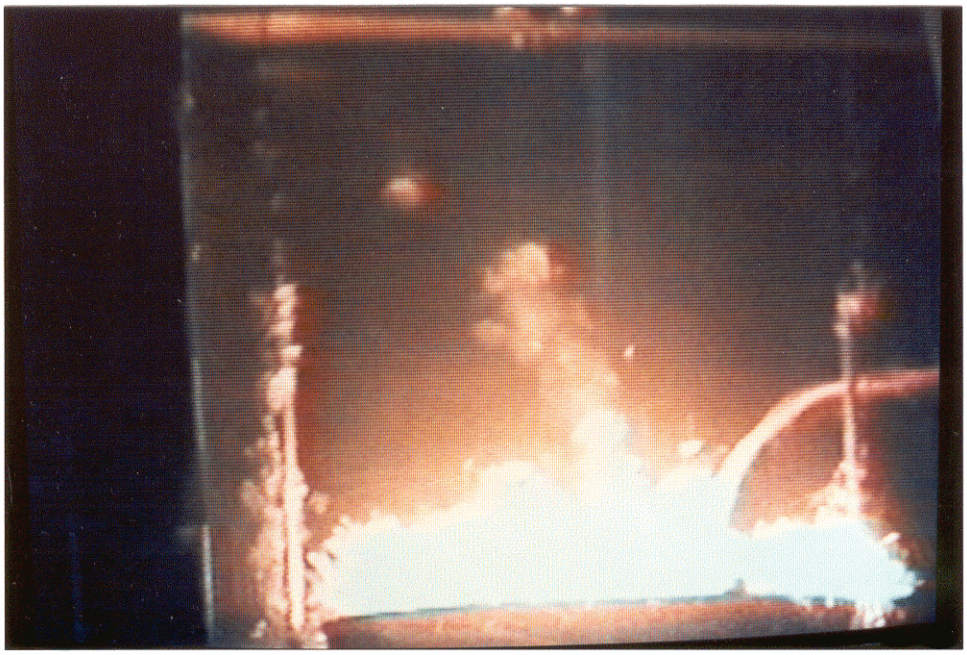

Figure 17(c)

Figure 17. Photographs of three consecutive frames from the video record of a steam explosion of a non-alloyed ferrosilicon drop triggered with the impactor. Video images were recorded with the self-luminosity of the melt. Image (a) shows the melt drop as it falls through the water one frame before the trigger. Image (b) shows the drop as it explodes. Image (c) shows the mass of bubbles that form one frame after image (b). Each frame is 16.7 ms apart. Fiducial rods to either side of the image are 138 mm apart. (C-215-1 #1)

record of an impactor-triggered explosion of a non-alloyed ferrocilicon drop in water at room temperature. The other, C-215-1 #2, produced a good record of a non-alloyed drop similarly triggered in hot water (nominally 80 ^{o}C). In this latter interaction, significant combustion was observed.

Several difficulties accompanied our attempts to use the Hycam for measuring the dimensions of the bubbles produced in the drop explosions (some of these disadvantages have also been summarized in the report of our 1996 work (Nelson et al., 1997a).):

- The inability of the Hycam camera to record spontaneous drop releases. This is caused by the total running time of about 4 seconds for a 100 foot (33 meter) roll of film exposed at 1000 frames per second. Because the camera requires about 1 second to reach full speed, the interaction of the drop must be triggered during the remaining 3 seconds. This has required us to release the drop by mechanical action, namely, with an upward solenoid pull 1 second after starting the Hycam. Fortunately, the ability achieved in the 1997 work to view the formation of the pendant drop through the hole in the side of the furnace tube (see Figure 1) allows us manually to simultaneously start both the camera and a time delay relay slightly before the drop is ready to fall spontaneously. Then the relay activates the drop-release solenoid 1 second later, causing the drop to fall comfortably within the 3 seconds that remain on the film. Triggering with the combustion tube or the impactor was initiated as in the spontaneous drop release experiments in which the photodetector senses the luminosity of the drop as it falls and activates a second time-delay relay that fires the trigger 370 ms later.

The difficulties inherent with recording images on film. These include the costs of the film and its processing (a total of about US$60 per 100 foot roll), the time required for processing at a distant laboratory (several days, using premium transportation), and the need for good projection equipment (a good motion analysis projector costs about US$6000). Also, it is difficult, costly and time-consuming to make enlarged images from the 16 mm frames suitable for reports and visual presentations. In spite of these difficulties inherent with film imaging, we believe the advantages of the high-speed 16 mm

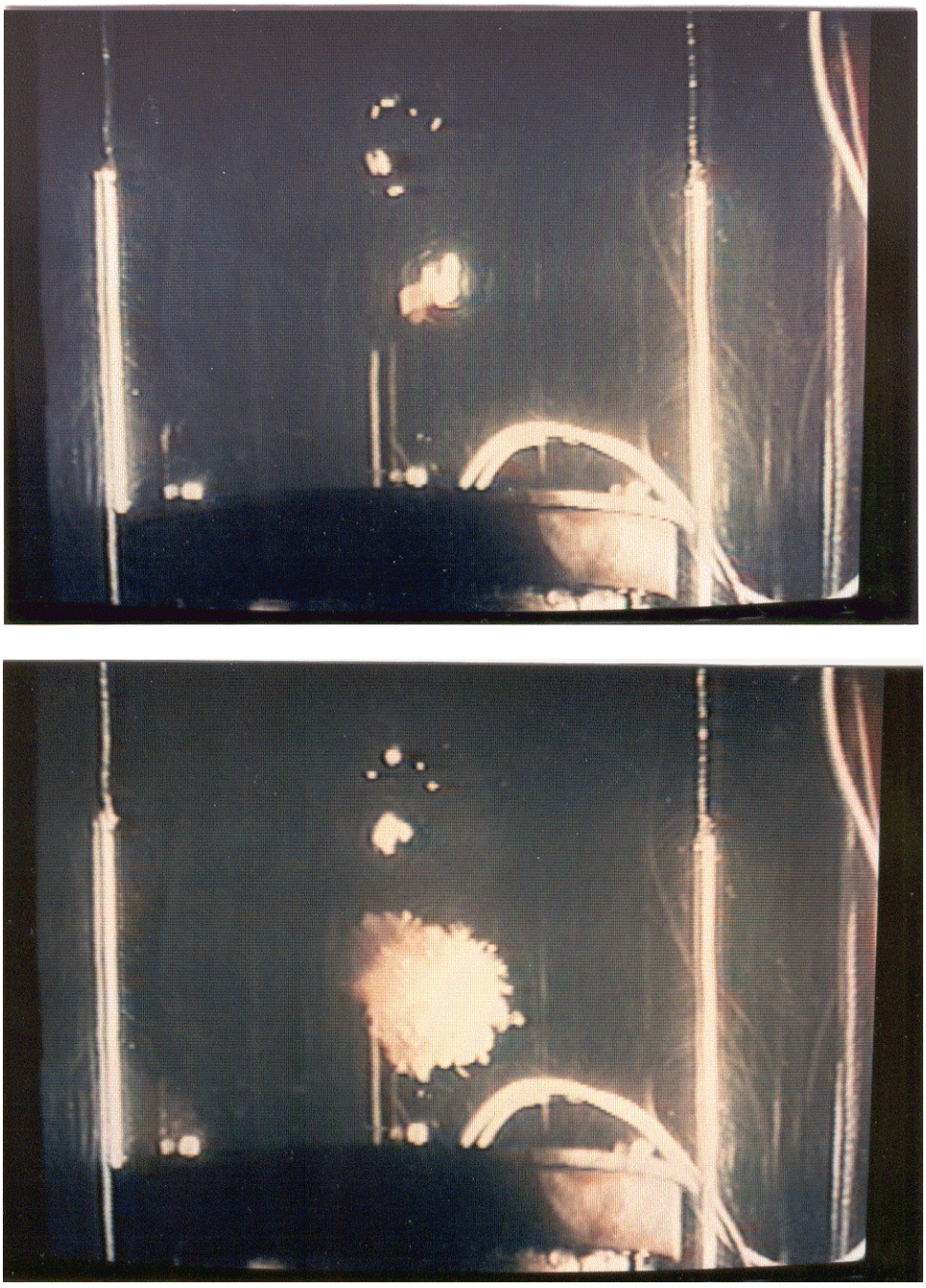

Figure 18(a) (above); Figure 18(b) (below).

Figure 18. Photographs of three consecutive frames from the video record of a steam explosion of a non-alloyed ferrosilicon drop triggered with the impactor. Video images were recorded with reflected light. Image (a) shows the melt drop as it falls through the water one frame before the trigger. Image (b) shows the drop as it explodes. Image (c) shows the mass of bubbles that form one frame after image (b). Each frame is 16.7 ms apart. Fiducial rods to either side of the image are 138 mm apart. (C-213-1 #1).

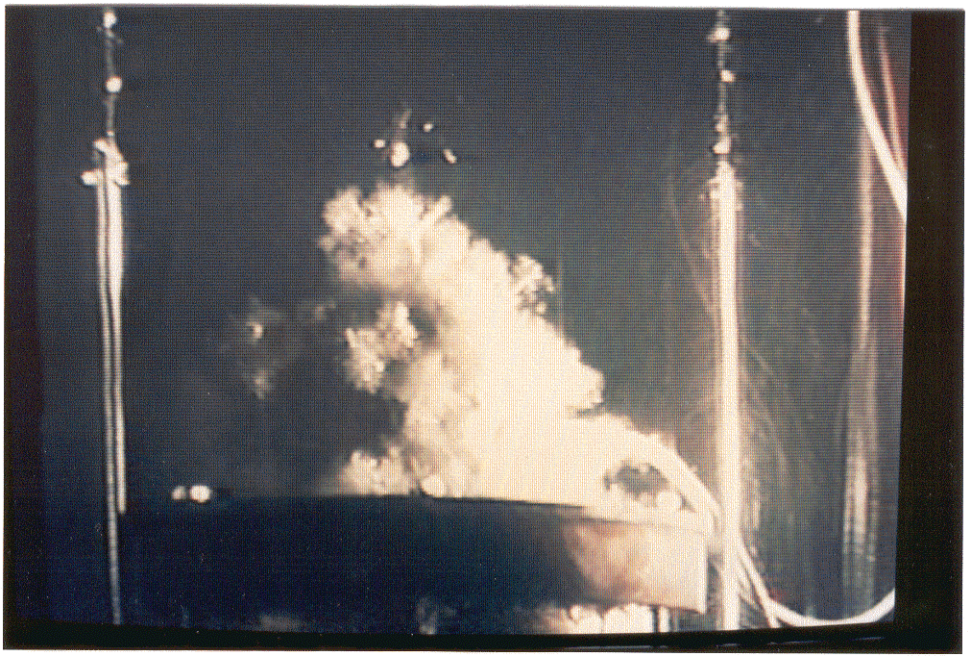

Figure 18(c).

Figure 18. Photographs of three consecutive frames from the video record of a steam explosion of a non-alloyed ferrosilicon drop triggered with the impactor. Video images were recorded with reflected light. Image (a) shows the melt drop as it falls through the water one frame before the trigger. Image (b) shows the drop as it explodes. Image (c) shows the mass of bubbles that form one frame after image (b). Each frame is 16.7 ms apart. Fiducial rods to either side of the image are 138 mm apart. (C-213-1 #1).

camera still outweigh other currently available imaging techniques in the large number (about 3000 frames at 1000 frames/second) of high quality images (that is, with high pixel resolution) in color that can be achieved with good time resolution (the maximum rate of our Hycam is said to be 10,000 frames per second) at fairly reasonable cost.

Three frames enlarged from the film C-213-1 #1, recorded at 1000 frames/second, are presented in Figure 19. These are 3 images selected from 34 photographs taken at high magnification from the film. The individual frames are images recorded 0, 5 and 14 ms after the trigger that show (a) the melt drop 1 ms before the trigger, (b) at the maximum growth of the first bubble, and (c) at the maximum growth of the second bubble. There is some contraction of the first bubble before the second bubble grows to its maximum. (The 34 images enlarged from the Hycam film cover a period of 34 ms; during this same interval, the backup video camera recorded only two new images at 60 frames/second during the same experiment, as shown in Figure 18.)

The high-speed photographic images probably provide the most accurate way to calculate the energy transferred to the water by a steam explosion. For example, we have measured the bubble images in Figure 19b and c (C-213-1 #1). This steam explosion was triggered with the impactor. The outside diameter of the smaller image in b is 34.3 mm, corresponding to a maximum volume of 0.0213 L which converts with Equation (2) to a maximum PV bubble energy of 2.15 J. For the debris weight of 1.30 g (assumed from average debris weights in Tables 2, 3 and 4), the energy transferred per gram of melt is 1.7 J/g for the smaller bubble. The outside diameter of the larger image in c is 65.2 mm, corresponding to a maximum volume of 0.1451 L which converts with Equation (2) to a maximum PV bubble energy of 14.7 J. For the debris weight of 1.30 g (assumed from average debris weights in Tables 2, 3 and 4), the energy transferred per gram of melt is 11.3 J/g for the larger bubble. The total energy for the two bubbles combined is 16.9 J, or 13.0 J/g.

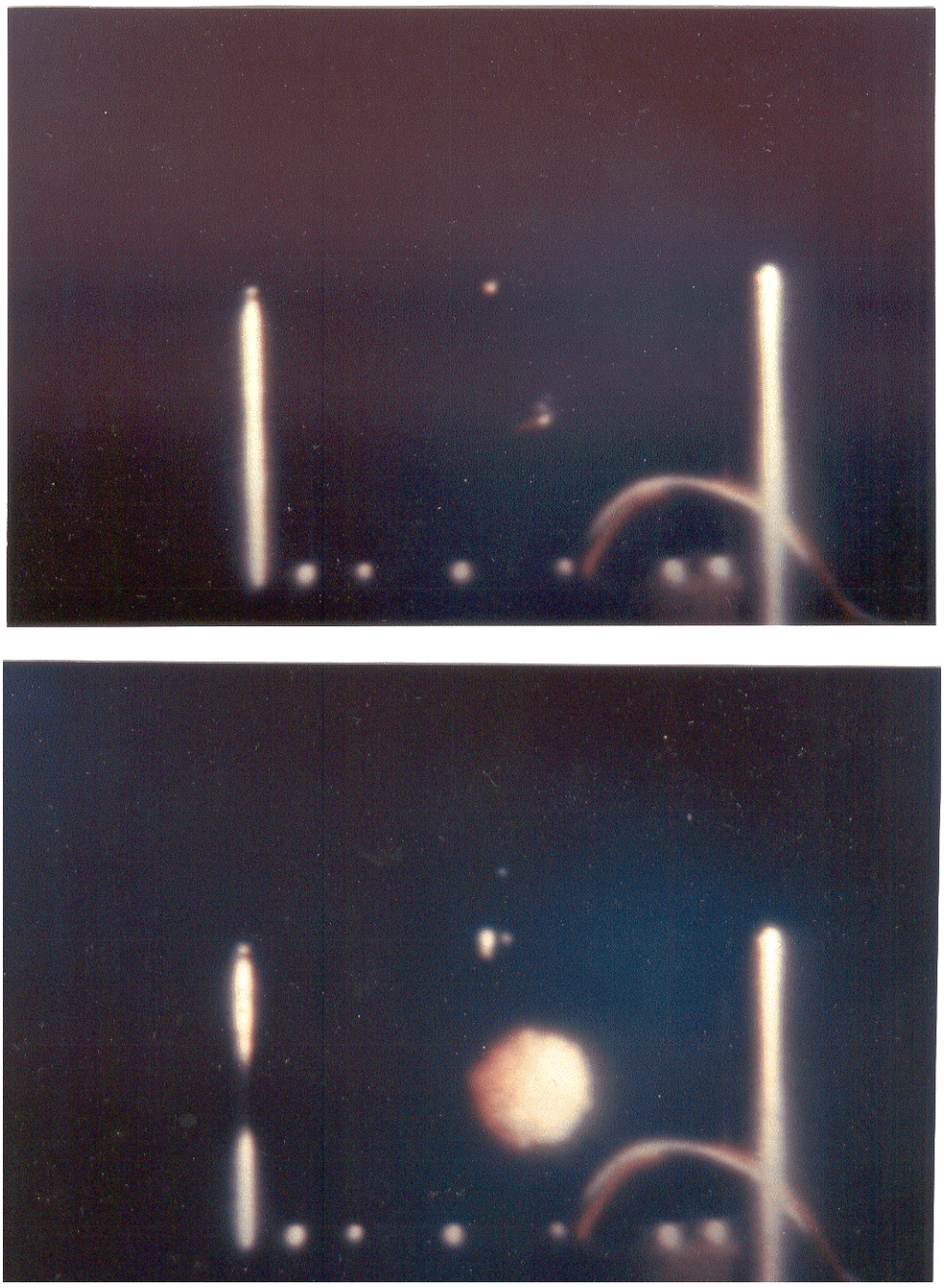

Figure 19(a) (above); Figure 19(b) (below).

Figure 19. Three frames enlarged from the Hycam film C-213-1 No. 1, recorded at 1000 frames/second. The individual frames are images selected at 0, 5 and 14 ms after the trigger that show (a) the melt drop 1 ms before the trigger, (b) at the maximum growth of the first bubble, and (c) at the maximum growth of the second bubble. Fiducial rods to either side of the image are 138 mm apart. (C-213-1 #1).

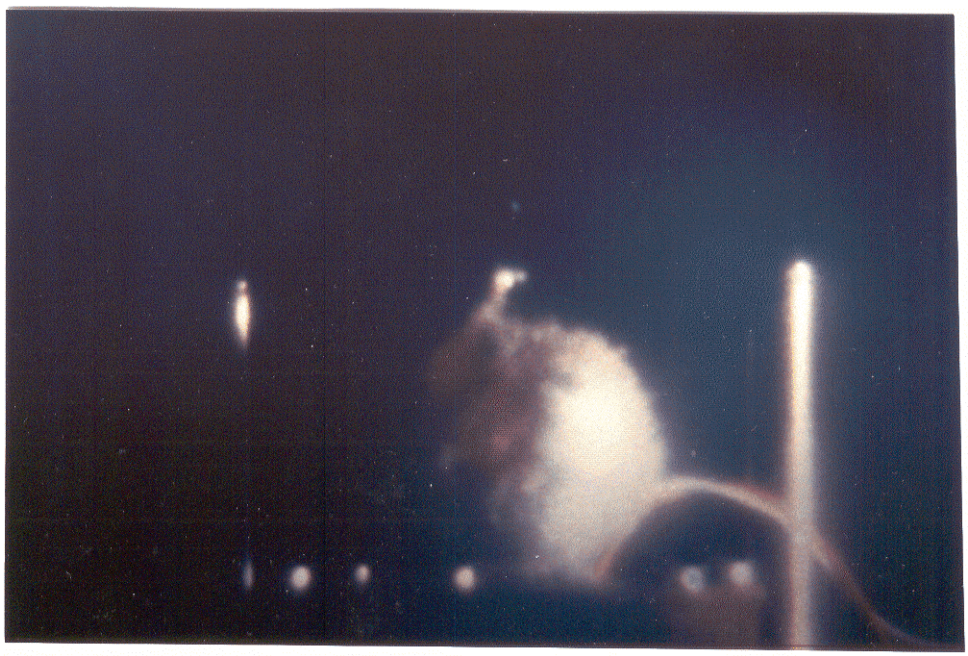

Figure 19(c).

Figure 19. Three frames enlarged from the Hycam film C-213-1 No. 1, recorded at 1000 frames/second. The individual frames are images selected at 0, 5 and 14 ms after the trigger that show (a) the melt drop 1 ms before the trigger, (b) at the maximum growth of the first bubble, and (c) at the maximum growth of the second bubble. Fiducial rods to either side of the image are 138 mm apart. (C-213-1 #1).

It should be noted that the bubble diameter obtained from the video image of the same explosion, shown in Figure 18b, was 36.0 mm, corresponding to a bubble energy of 2.47 J of 1.9 J/g, essentially the same as the values determined for the smaller bubble in Figure 19b. But, because of the slower framing rate of the video camera, the second, larger bubble that grew to a maximum about 9 ms afterward, shown in Figure 19c**,** was completely missed by the video camera. This caused the total energy transferred to the water to be underestimated by about 85%.

Another comparison should be made between the energies estimated from the impactor-initiated self-luminous bubble image in Figure 16 **(**C-197-1) and those estimated from the Hycam films in Figure 19 (C-213-1 No. 1). The outside diameters of the outer and inner bubbles in Figure 16 are 58.7 mm and 50.1 mm, giving maximum volumes of 0.106 L and 0.0658 L, with energies of 10.7 and 6.7 J, energies per gram of 8.14 and 5.3 J/g and total energies of 17.4 J or 13.7 J/g. The latter two comparable values from Figure 19 are essentially identical—16.9 J and 13.9 J/g.

The pressure-volume energetics discussed above are summarized in Table 7.

Combustion

From the experiments performed during both 1996 and 1997, there are strong indications that whenever molten ferrosilicon contacts liquid water, the metal-water chemical reaction occurs. This is observed on our photographic and video images in several ways: generation of hydrogen bubbles, unusual luminosity effects and the deposition of colloidal material in the water during the interaction.

Table 7. Pressure-Volume Energetics of Bubbles Generated by the Steam Explosions of Molten Ferrosilicon Drops

Experiment Number	Estimate	Trigger	Image Used	Diameter (cm)	Volume (liters)	PV (J)	Weight (g)	Energy (J/g)	Remarks
C-189-1	A	$H_2 + O_2$	OS	7.55	0.225	22.8	1.39	16.4	Outer bubble
C-189-1	A	$H_2 + O_2$	OS	3.47	0.022	2.2	1.39	1.6	Inner bubble
C-189-1	A	$H_2 + O_2$	OS			25.0		18.0	Total of both bubbles
C-197-1	B	Impactor	OS	5.87	0.106	10.7	1.27	8.4	Outer bubble
C-197-1	B	Impactor	OS	5.01	0.066	6.7	1.27	5.3	Inner bubble
C-197-1	B	Impactor	OS			17.4		13.7	Total of both bubbles
C-213-1#1	C	Impactor	VCR	3.6	0.024	2.47	1.30 est.	1.9	
C-213-1#1	D	Impactor	Hycam	3.43	0.0213	2.2	1.30 est.	1.7	First bubble
C-213-1#1	D	Impactor	Hycam	6.52	0.1451	14.7	1.30 est.	11.3	Second bubble
C-213-1#1	D	Impactor	Hycam			16.9		13.0	Total of both bubbles
C-143-1	E	Impactor	OS	14.7	0.832	84.2	1.24/1.53	67.9/55.1	Hemispherical explosion

Figure 20. Photograph of a video image of tiny hydrogen bubbles recorded with reflected light 9.2 s after an impactor-triggered steam explosion of a molten ferrosilicon drop. Fiducial rods to either side of the image are 138 mm apart. (C-213-1 #1)

Hydrogen Bubbles

The most significant indication that melt-water combustion is occurring is the release of hydrogen bubbles into the water in the vicinity of the hot, incandescent melt particles. The bubble formation is observed with particles of all diameters ranging from the largest (the melt globules as they are released into the water) to particles of intermediate diameters (as in mild interactions with coarse fragmentation) to the smallest particles (those formed by the fine fragmentation of the melt globule during a triggered explosive interaction). The melt-water reaction also seems to occur with drops of the ferrosilicon alloys (25 wt.% Fe-75 wt.% Si) both with and without added Al and Ca. Because the rate of hydrogen generation is assumed to be related to the surface area of the melt particles exposed to the water, the bubble formation is quite slow for the unfragmented globules and becomes progressively more rapid as the particles become finer.

In the fine breakup associated with a vigorous steam explosion, many tiny bubbles form a few milliseconds after the interaction. These bubbles resemble those released from carbonated beverages. They rise relatively slowly and then break through the surface of the water many milliseconds later. These tiny bubbles are best observed on the video images recorded with reflected light. An example of a video image of these bubbles recorded 9.2 seconds after the steam explosion of a non-alloyed ferrosilicon drop is shown in Figure 20. (C-213-1 #1)

Luminosity Patterns

In a triggered steam explosion that produces fine particles, the interaction is so rapid that it is difficult to separate the luminosity due to combustion from that caused by the rapid breakup and quenching of the hot incandescent melt particles. But when the interaction produces relatively coarse particles, for example, in the hot water experiments, a very distinctive two-stage luminosity pattern is observed. On the video and

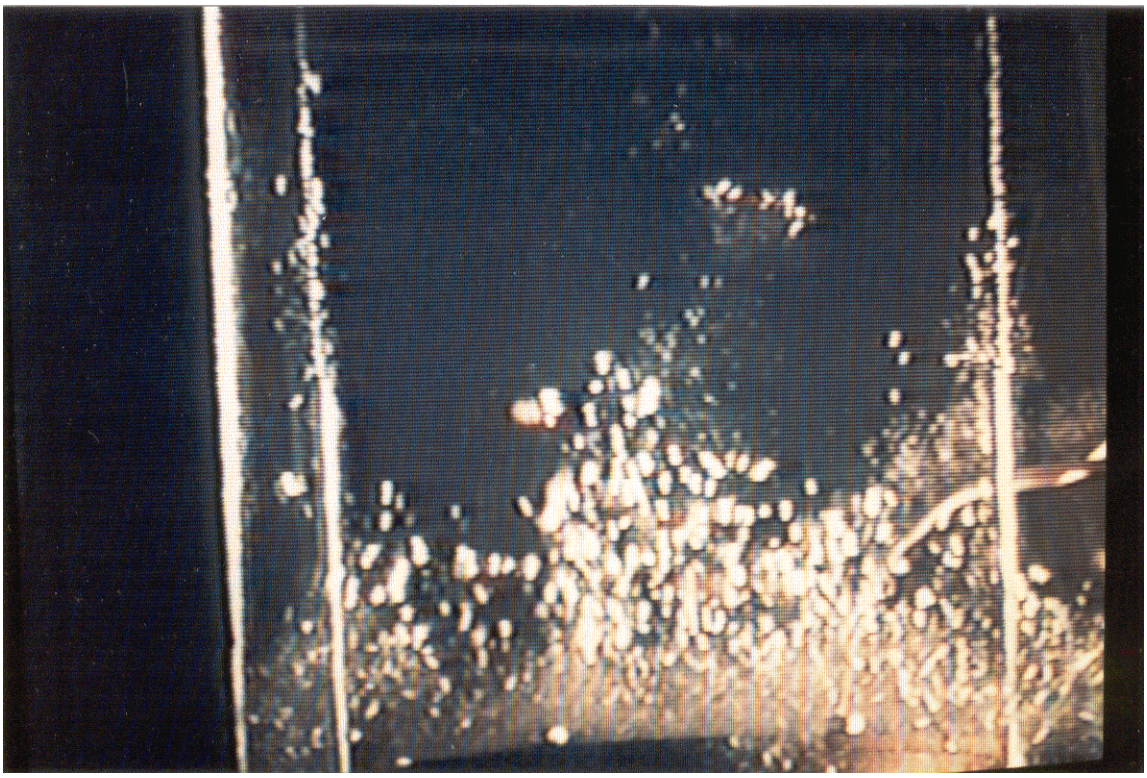

Figure 21. Photograph of a video image of a rising clump of bubbles with burning particles recorded with reflected light 384 ms after an impactor-triggered steam explosion of a molten ferrosilicon drop in 81 ^{o}C water. Fiducial rods to either side of the image are 138 mm apart. (C-215-1 #2).

Hycam images, we can see the drop break up quickly into a clump of large, luminous fragments that slowly rise together many milliseconds after the interaction. (The rise of these burning particles is often slow enough to be seen with the unaided eye.) In this case, the bubbles are large, and inside each one there seems to be a particle that is burning in a self-sustained fashion. Some of these particles may extinguish before they reach the surface of the water, separate from their bubbles and fall to the bottom of the chamber, while their bubbles then continue to rise and ultimately break through the surface of the water. The rise of the clump of bubbles with burning particles 384 ms after the explosion is shown in the reflected light video image in Figure 21. (C-215-1 #2)

With time exposure photography, this slow rise of the clump of particles produces "seaweed-like" images of burning particles. A typical time-exposed 35 mm photograph of these images is shown in Figure 22 (C-203-1), which were formed by the fragmentation and combustion of the melt particles produced from the coarse fragmentation of a non-alloyed ferrosilicon drop in hot water (nominally 80 ^{o}C).

Colloidal Products

Whenever a drop of melt explodes or fragments, we always observe the deposition of colloidal material in the water near the interaction. The colloidal material appears on our reflected light video and photographic images as long lasting turbidity in the water; it can also easily be seen visually. This material seems to have very fine particle sizes because it does not settle from the water, even over a span of several days. Although we have tried several times, this material is difficult to separate from the water by filtration, tending to clog the filter media. (In experiments performed at the end of the 1997 work, we coagulated some of the material by boiling down and evaporating to dryness about 20 L of the turbid water that remained after the experiment in which both a small and large drop of melt exploded (experiment C-213-1). We have not, as yet, analyzed the solid material that was concentrated this way, however.)

Attempts to Identify Combustion Products

We performed a brief set of X-ray diffraction analyses to investigate whether there is a change in the composition of the ferrosilicon particles during underwater combustion. (This work was done collaboratively with Professor C.L. Nassaralla and Mr. Quinn C. Horn of the Department of Metallurgical and Materials Engineering, Michigan Technological University, Houghton, MI.) The objective of this work was to determine whether new compositions of the ferrosilicon melt were generated by the combustion reaction in which oxygen is taken up by the particles as they burn. This type of reaction is indicated schematically by Equation (3):

$$FeSi + H_2O \rightarrow FeSiO + H_2 \qquad (3)$$

(We have not attempted to indicate any specific stoichiometries or compositions in this equation.) To do the analyses, we compared the X-ray diffraction powder patterns of three materials: (a) powdered starting alloy without Al or Ca additives, taken from batch F8 (C-133-2) (see Table 1); (b) the finely fragmented debris from a vigorous steam explosion of melt drops produced from this same rod material in water at 8 ^{o}C (experiment C-205-1) and (c) the coarsely fragmented debris recovered after a mild explosion of drops formed from the same rod material, but in 80 ^{o}C water (experiment C-203-1) in which combustion of drops was known to have occurred (see Figure 22 for the "seaweed-like" images of burning drops produced during this experiment). To obtain the fine powders appropriate for the analyses, these materials were crushed and ground in a mortar as needed.

The X-ray diffraction patterns produced from these three materials are shown in Figure 23. Note that the three patterns seem identical.

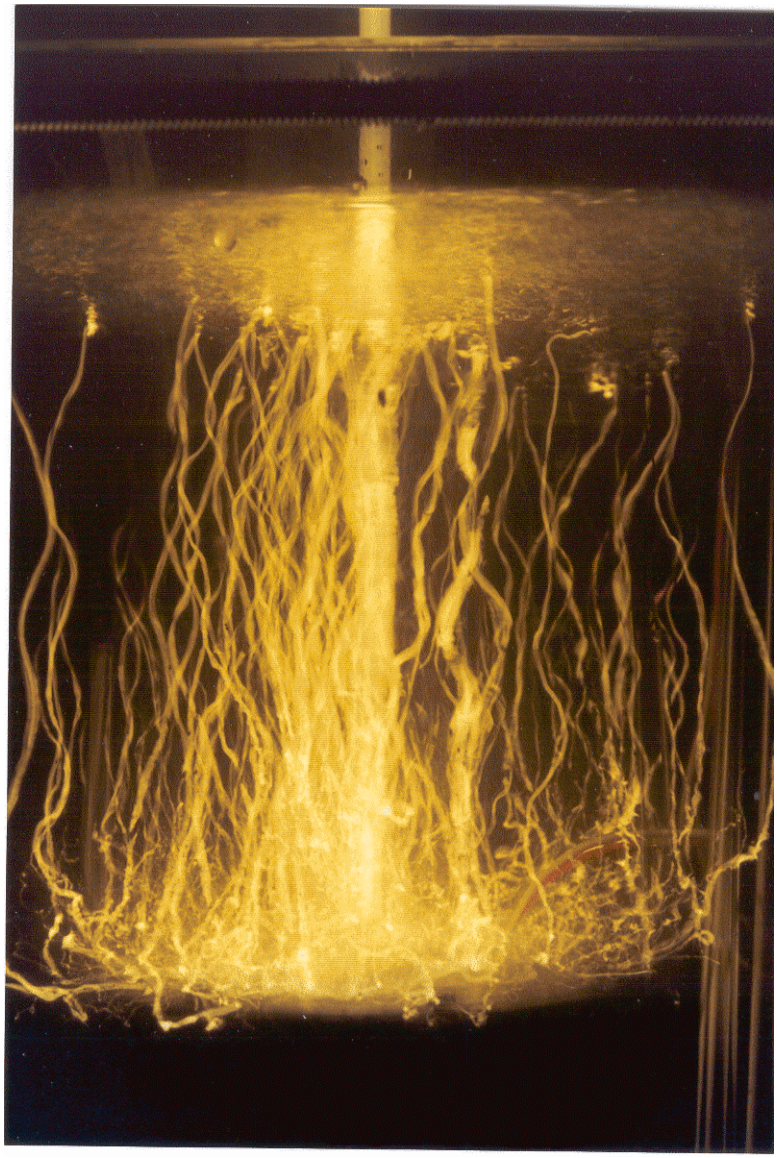

Figure 22. Seaweed-like time-exposed photographic image of the rise of a clump of bubbles with burning particles recorded after an impactor-triggered steam explosion of a molten ferrosilicon drop in 80 ^{o}C water. Fiducial rods to either side of the image are 138 mm apart. (C-203-1).

Effects of Drop Diameter

Part of the investigation planned for 1998 involves the effects of increased drop diameter on the explosive behavior of the molten drops. Some early insight into these future experiments may be obtained from the large drop, Drop No. 2, that fell at the end of experiment C-213-1. The starting material here was the non-alloyed rod F8 (C-133-2) (see Table 1). The rod was fairly short (63 mm) when the experiment began. The first drop, Drop No. 1, had been successfully released by shaking it from the rod with solenoid action to produce the video and Hycam images shown in Figures 18, 19 and 20. Then the rod was lowered further in the furnace to form a second drop that would fall spontaneously and produce an open shutter self-luminous exposure in a darkened room. But instead of a second drop of the size we had been expecting, the support wire gave way and the remainder of the rod, apparently with a large globule of melt attached, fell into the water and landed on the impactor. We did not have time to prepare the camera for a time-exposed photograph as planned; instead our only imaging was the backup video record of the release taken with the room lights on, shown in Figure 24 (C-213-1 #2).

There was a huge explosion with a flash of light that threw water about the room. Afterward, there was much fine debris on both impactor and catcher pan, in addition to a short stub of the original rod (about 17 mm long). The debris and rod, after recovery from the chamber, are shown in Figure 25. We determined the weight of the fine debris to be 9.85 g (combined weight for Drops No. 1 and No. 2). From this total weight, we subtracted 1.30 g, the weight of a typical single drop (see Tables 2, 3 and 4) to estimate that 8.55 g of melt had participated in the second explosion of experiment C-213-1. Then taking the density of the melt to be 3.2 g/cc (Forwald, 1991), we calculated from Equation (4)

$$d(cm) = [0.5968\ W(g)]^{1/3} \quad (4)$$

the diameter of the large drop that had fallen to have been 17.2 mm. A similar calculation indicates that our average drops with weights of 1.30 g have a diameter of 9.2 mm.

Several aspects of the large explosion should be mentioned because they bear directly on the 1998 experiments:

- The 17.2 mm drop fell through the water very rapidly compared to the 9.2 mm drops we had been studying. This was immediately apparent from the video record because after reaching the impactor, the melt globule rested on the surface for 20 video frames before the impactor fired. At 16.7 ms per frame, this corresponds to a rest time of 334 ms out of the total delay time of 370 ms. When this fall behavior is compared to that of Drop No. 1, which was still in free fall several centimeters above the impactor when it fired at 370 ms, it can be seen that the larger drop must have fallen through the water much faster than the smaller drop.

  We estimated the fall velocities from the video images shown in Figure 24 and from the sequence of images from which Figure 18 was taken. We found that the large drop (equivalent sphere diameter = 17.2 mm) fell at about 3.8 m/s while the small drop (our average drop with equivalent sphere diameter = 9.2 mm) fell at about 0.6 m/s. This approximately 6-fold difference between fall velocities may require some changes in our apparatus and experimental procedures in 1998, perhaps requiring the larger melt globules to fall farther through the water to achieve characteristics (for example, melt cooling) analogous to those studied with the smaller drops.

- The vigor of the explosion of Drop No. 2 produced minor leakage of water from the chamber. We believe that even with the reinforcing steel channels added for the studies in 1997, we may be approaching the limit of strengths of the cemented seals used in the construction of the polycarbonate sheet chamber when we study drops as large as 17.2 mm. Thus, in light of these minor failures, the construction and sealing of our chamber should be reviewed carefully for studies with greatly increased drop diameters.

Debris

In the results described above, we have referred to the debris retrieved after an experiment as “fine” when a strong explosion occurred and as “coarse” when a mild explosion occurred. At this stage of our studies, we have not been able to present these descriptions quantitatively. So far, our debris analyses consist of an examination of photographs of the debris particles recorded with a millimeter scale included in the images. We have also examined the debris only with a low power magnifier; a microscope is not readily available.

In Figure 26a, we show an example of “fine” debris photographed as it had landed on the catcher pan after a strong explosion (experiment C-170-1); the explosion had been triggered by a hydrogen-oxygen explosion. Note that the individual particles are almost completely less than a millimeter in longest dimension. The starting material had been a non-alloyed (i. e., low Al and Ca contents) ferrosilicon rod from batch F7 (C-133-1) (see Table 1). In Figure 26b, we show the entire amount of debris recovered from the catcher pan, 1.21 g, photographed in the lower half of a Petri dish.

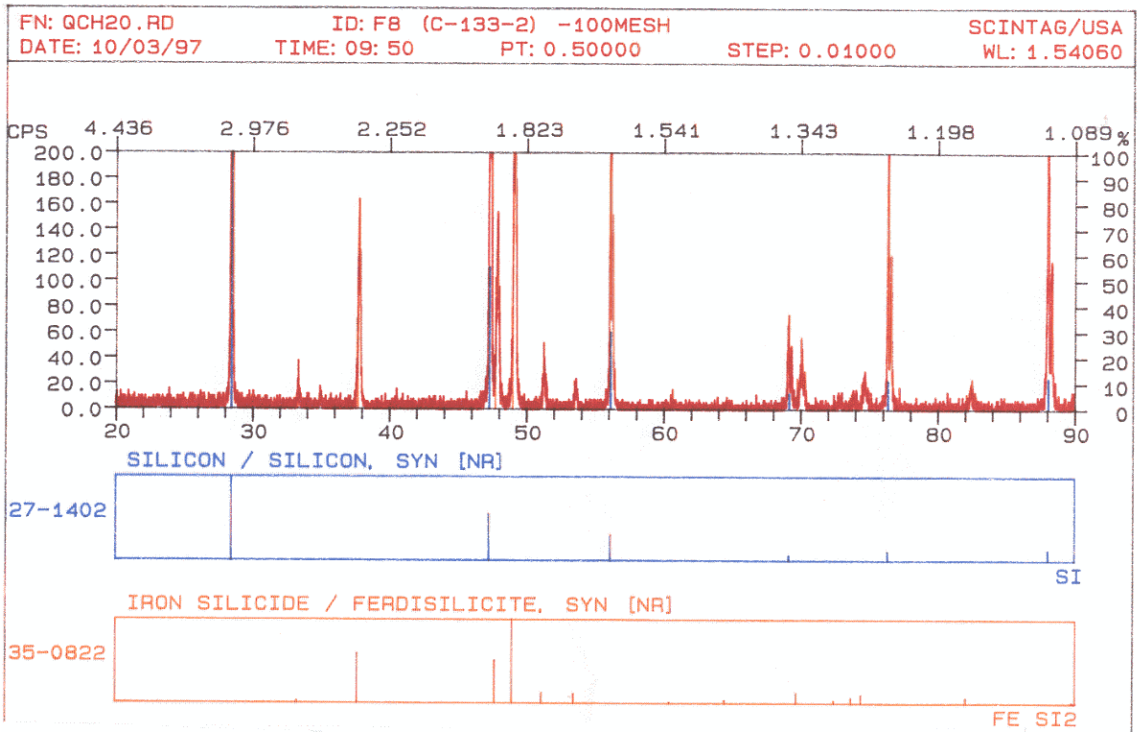

Figure 23(a).

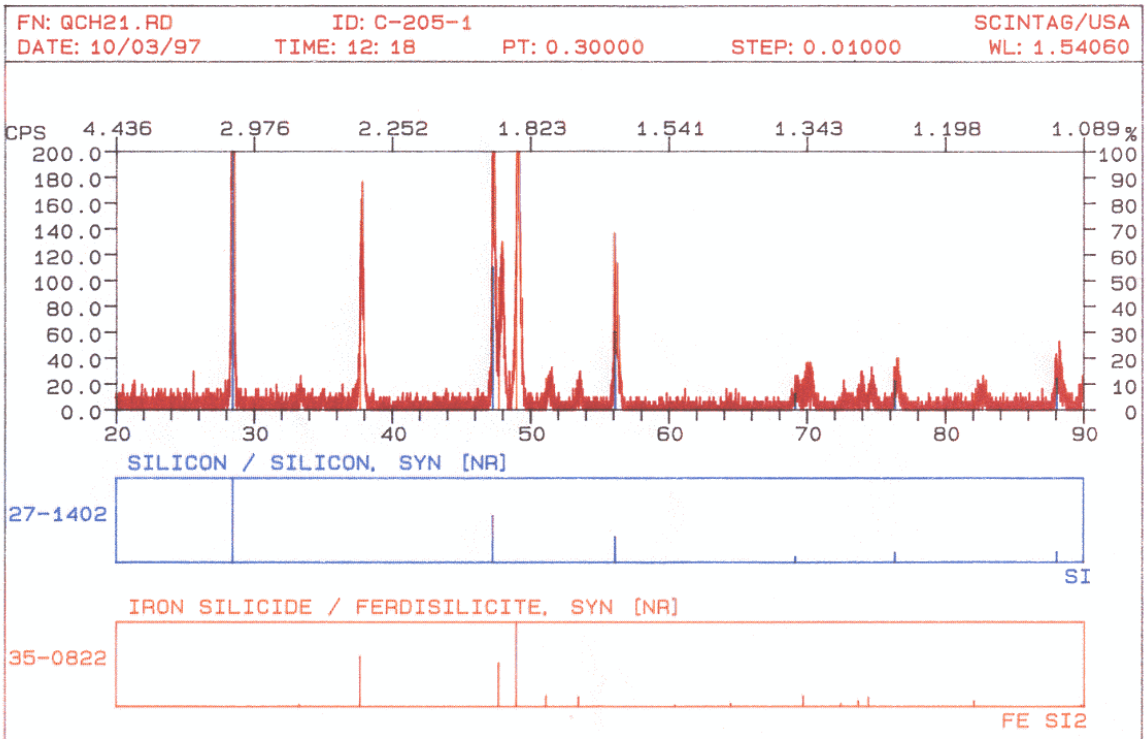

Figure 23(b)

Figure 23. X-ray diffraction powder patterns of: (a) powdered starting alloy without Al or Ca additives, taken from batch F8 (C-133-2); (b) the finely fragmented debris from a vigorous steam explosion of melt drops produced from this same rod material in water at 8 ^{o}C (experiment C-205-1) and (c) the coarsely fragmented debris recovered after a mild explosion of drops formed from the same rod material, but in 80 ^{o}C water (experiment C-203-1) in which combustion of drops was known to have occurred.

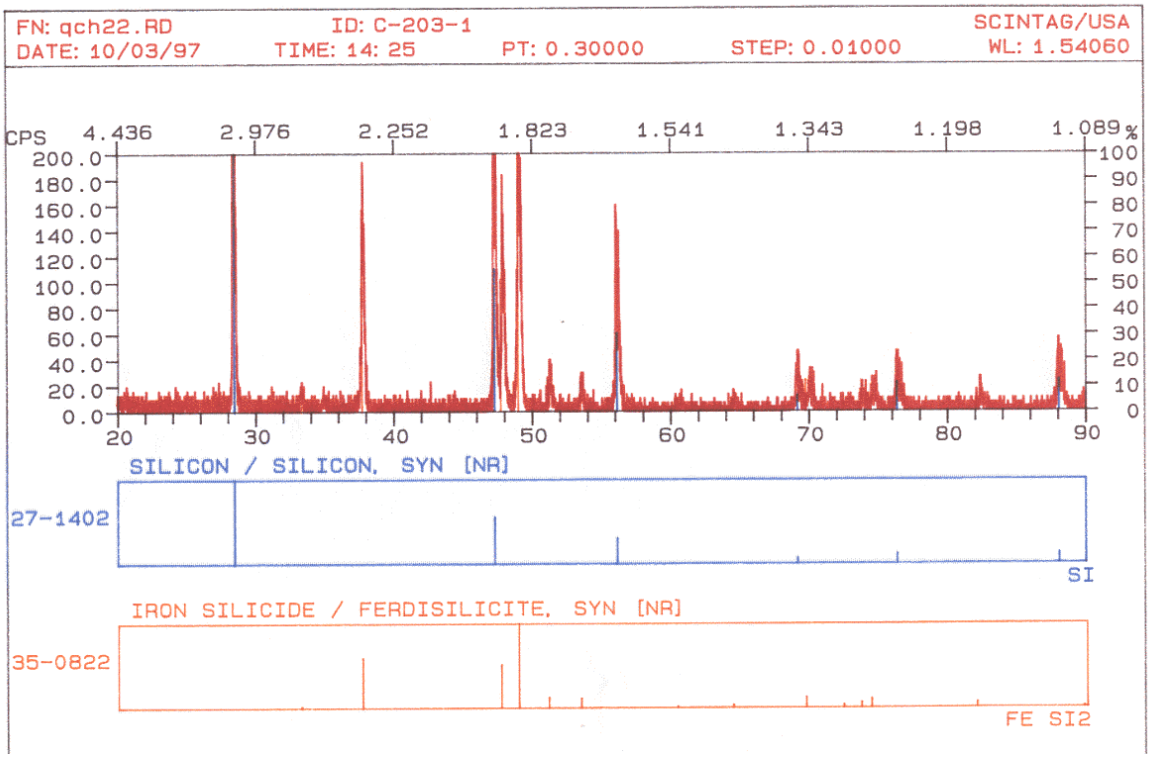

Figure 23(c).

Figure 23. X-ray diffraction powder patterns of: (a) powdered starting alloy without Al or Ca additives, taken from batch F8 (C-133-2); (b) the finely fragmented debris from a vigorous steam explosion of melt drops produced from this same rod material in water at 8 ^{o}C (experiment C-205-1) and (c) the coarsely fragmented debris recovered after a mild explosion of drops formed from the same rod material, but in 80 ^{o}C water (experiment C-203-1) in which combustion of drops was known to have occurred.

In Figures 27a and b, we show typical "coarse" debris recovered from mild melt-water interactions initiated by the underwater explosions of 100 ml of stoichiometric hydrogen-oxygen mixtures. (Both sets of debris were photographed after transfer to Petri dishes.) Time-exposed photographs of the interactions that produced the debris samples have been shown in Figures 12 and 13 above. Note that most of these particles have dimensions on the order of several millimeters, with some chunks as large as 5 millimeters across. The melt drops in both experiments contained Al and Ca additives (in (a), 0.34 w/o Al and 0.074 w/o Ca**;** in (b), 1.4 w/o Al and 0.63 w/o Ca) that have been shown in the 1996 and 1997 work to suppress steam explosions with the fine fragmentation shown in Figure 26. Because of this suppressive effect, breakup of both drops of melt is thought to have been caused by Weber-type processes, not by steam explosions.

If no explosion occurs in the experiment, a dense single frozen globule and occasionally several small satellite drops are recovered. Examples of non-exploding drops formed from non-alloyed ferrosilicon rod F1/F2 (C-133-1) (see Table 1) are shown in Figure 28. In this experiment, C-133-3, for three of the four drops released (spherules 1, 3 and 4), a triggering transient had been applied to the water by the inpactor at a depth of 60 cm and at a time delay of 1000 ms. This is a combination unfavorable for initiating explosions, even though the non-alloyed starting material produced vigorous explosions when the impactor was placed at another depth and activated at another delay time. The fourth drop (spherule 2) was allowed to fall without the triggering transient. Note in Figure 28 that no differences between the spherules are apparent.

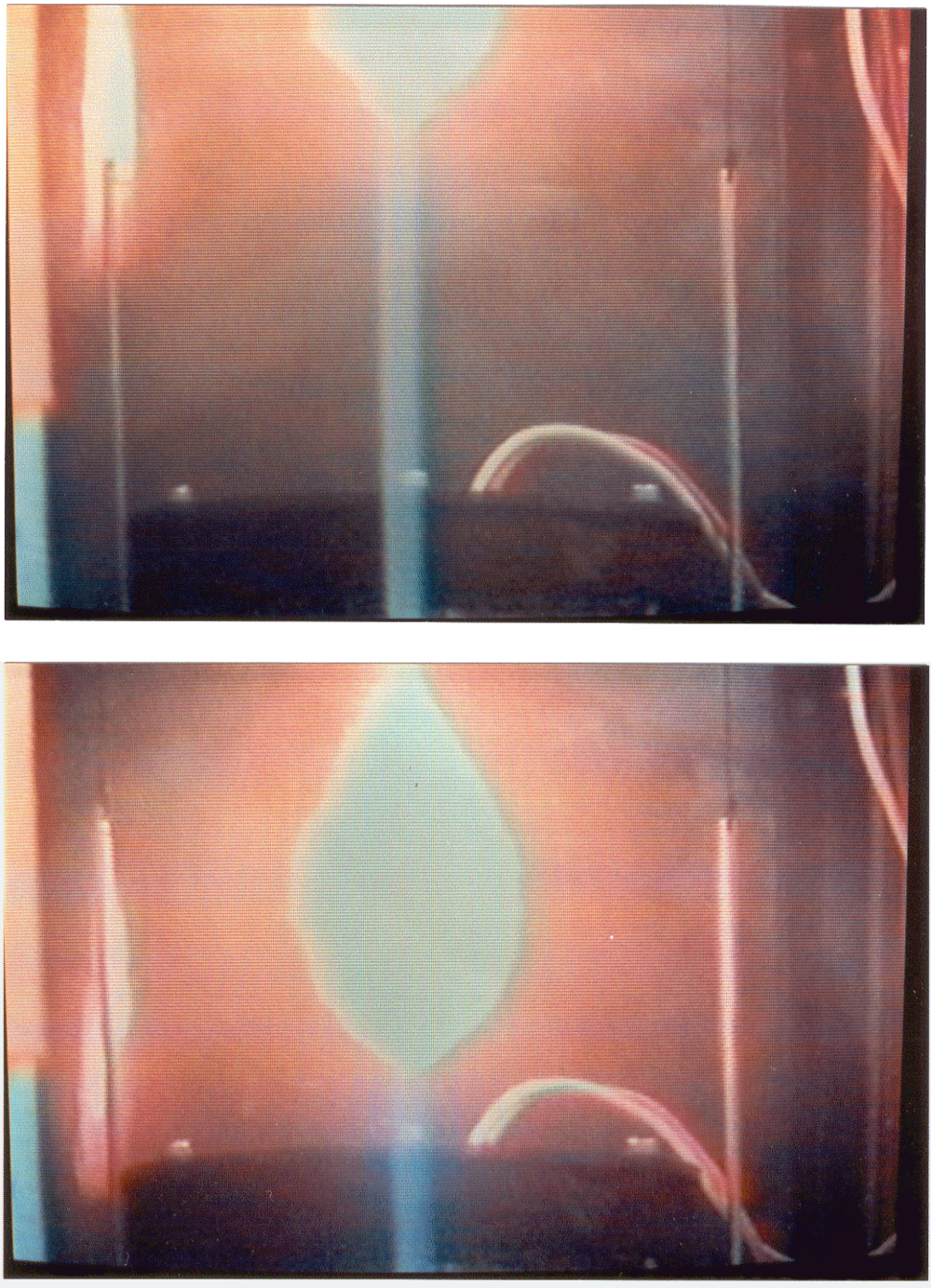

Frame 1 (above); Frame 2 (below)

Figure 24. Photographs of video images of the unexpected release of a large globule of molten ferrosilicon. It landed on the impactor within about 40 ms and exploded very vigorously about 330 ms later. Video frame numbers should be multiplied by16.7 to get times in milliseconds. Fiducial rods to either side of the image are 138 mm apart. (C-213-1 #2).

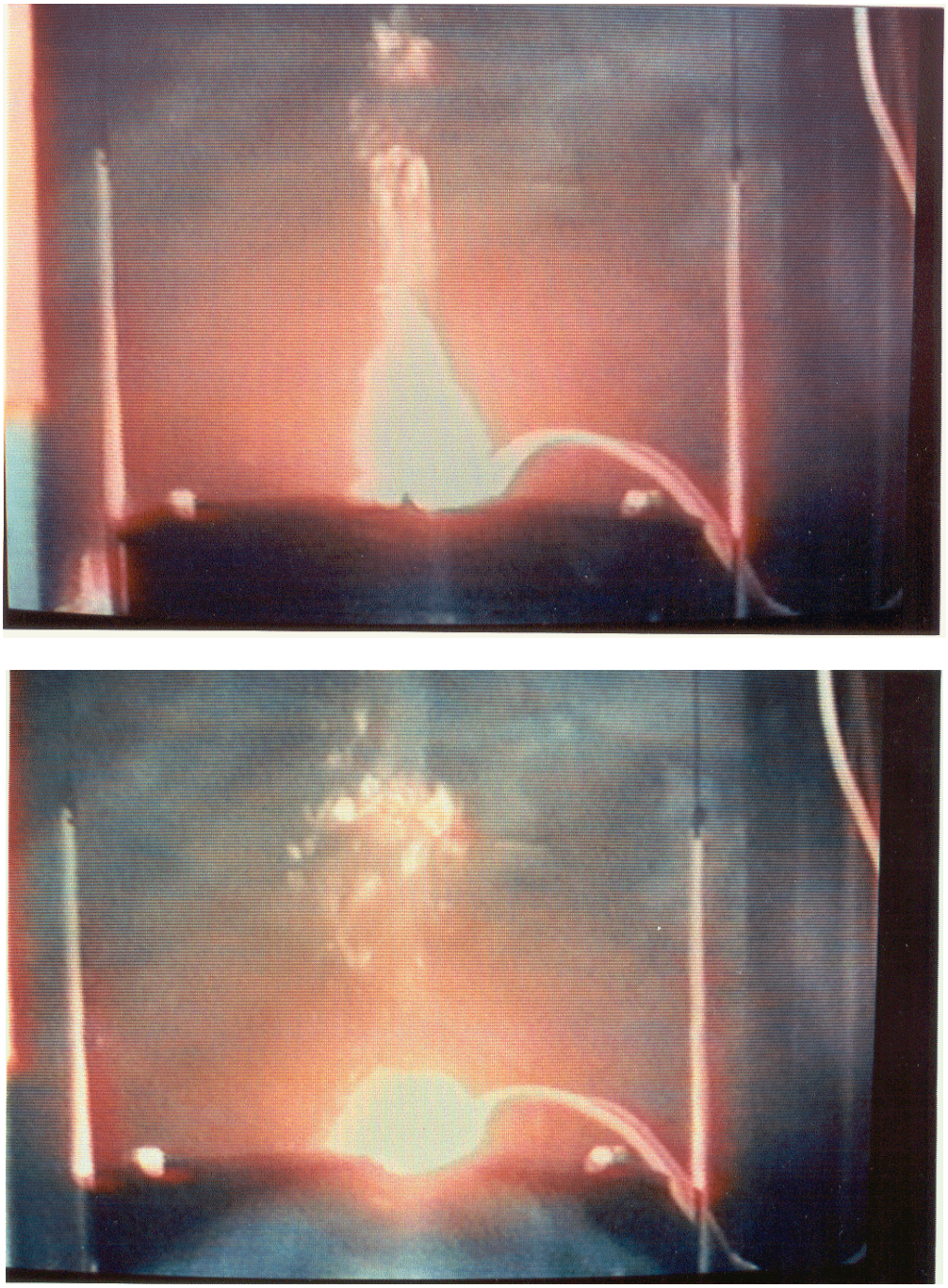

Frame 3 (above); Frame 9 (below).

Figure 24. Photographs of video images of the unexpected release of a large globule of molten ferrosilicon. It landed on the impactor within about 40 ms and exploded very vigorously about 330 ms later. Video frame numbers should be multiplied by16.7 to get times in milliseconds. Fiducial rods to either side of the image are 138 mm apart. (C-213-1 #2).

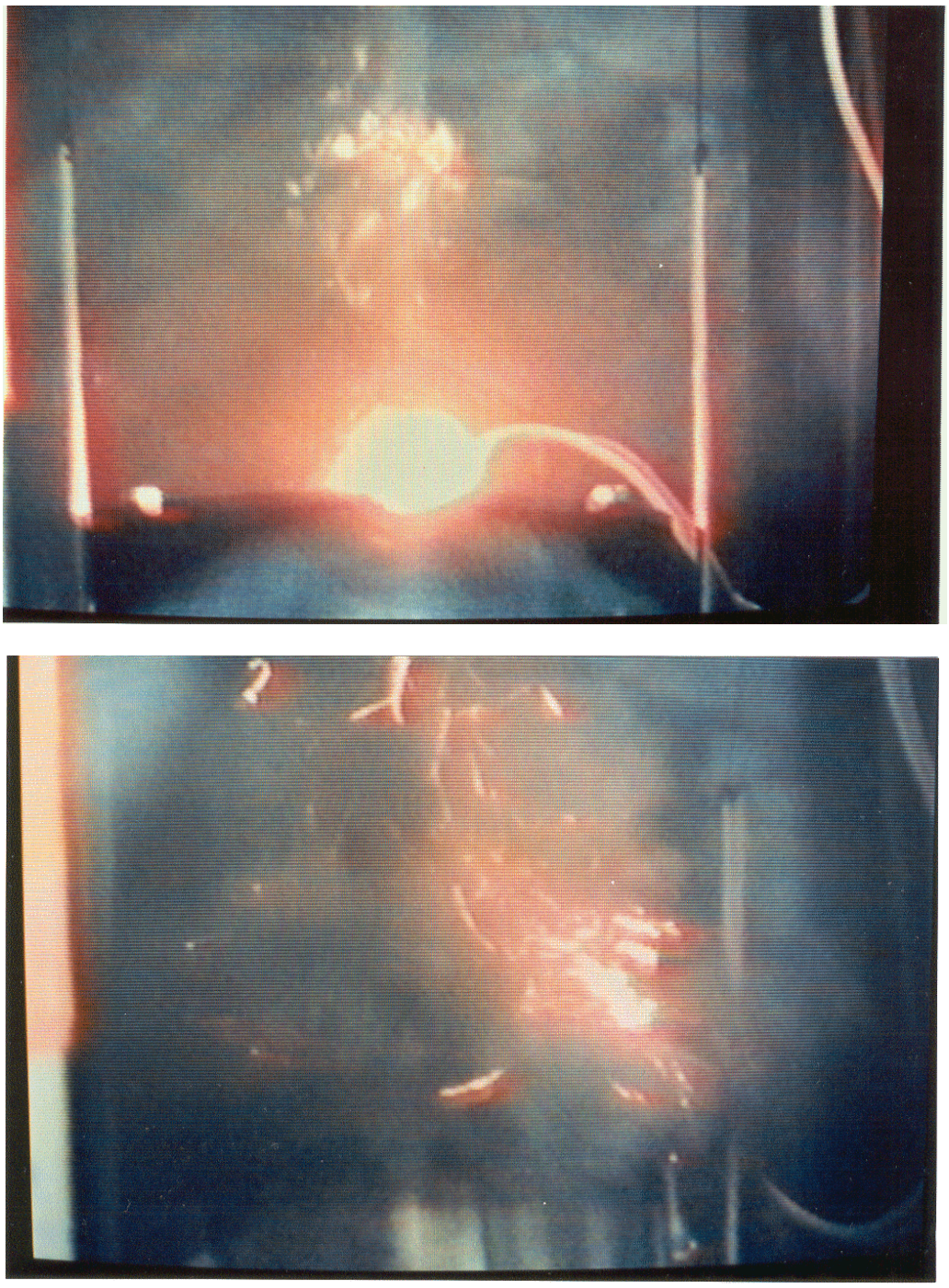

Frame 13 (above); Frame 14 (below).

Figure 24. Photographs of video images of the unexpected release of a large globule of molten ferrosilicon. It landed on the impactor within about 40 ms and exploded very vigorously about 330 ms later. Video frame numbers should be multiplied by16.7 to get times in milliseconds. Fiducial rods to either side of the image are 138 mm apart. (C-213-1 #2).

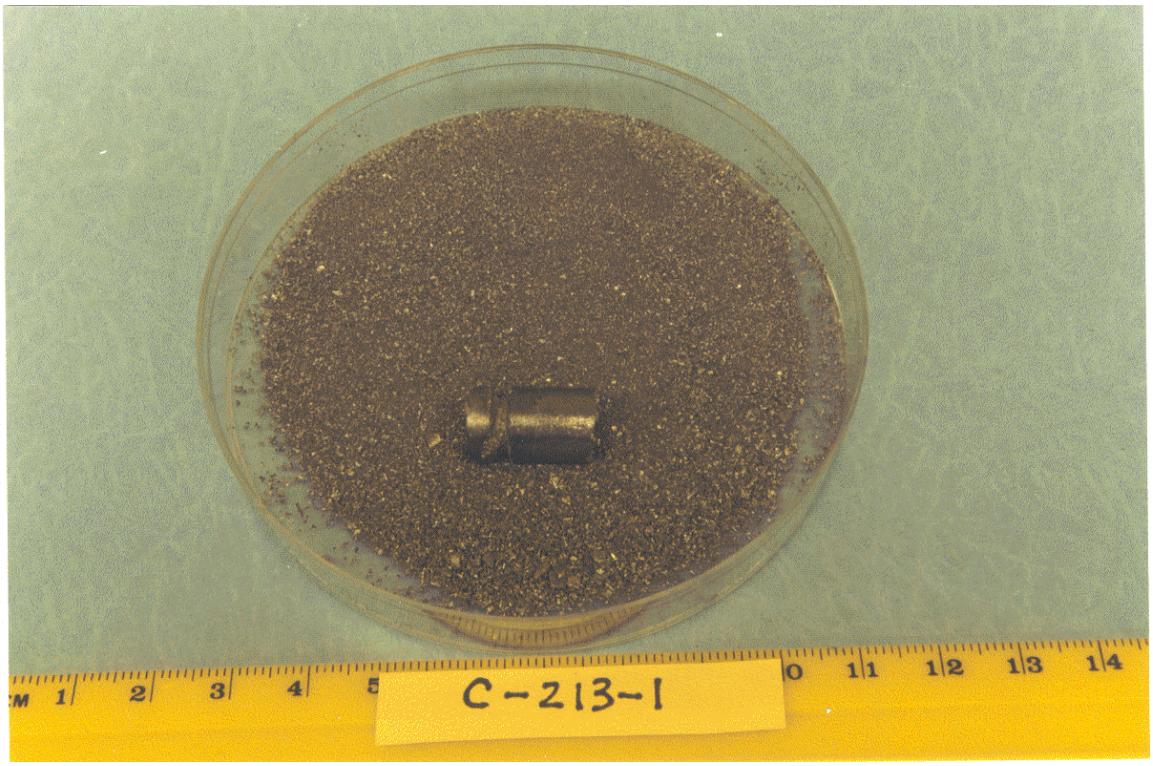

Figure 25. Stub of rod and fine debris recovered from the chamber after the large explosion shown in Figure 24. (C-2-3-1 #2).

We should note that quantitative information about "fine" and "coarse" debris can be presented quantitatively by using sieves to separate various particle size fractions and weighing them. The weights of the various fractions can then be related via statistical treatments to the energetics of the interactions with several melt fragmentation theories. Currently, however, we have neither the facilities nor the mandate to pursue particle size analyses.

Difficulties with One Batch of Rods

Partway through the 1997 experiments, we ran out of the non-alloyed rods from batch F7 (C-133-1). This material behaved well and had been producing steam explosions quite reliably (see Tables 3 and 4). It then seemed a routine matter to switch to the second batch of non-alloyed rod material supplied by the sponsor, F8 (C-133-2). Its analysis is essentially identical to the F7 (C-133-1) material (see Table 1).

The difficulties with the new batch of rods appeared with its very first use, in experiment C-195-1 (see Table 3). This experiment was planned as a special demonstration for a distinguished visitor from SINTEF.

We therefore selected a fresh rod from the new batch. According to our previous procedures, we cut a groove around the upper end of the rod with a tungsten carbide blade to produce the pretest rod shown in Figure 29 (C-195-1 Pretest). Note the distinctive mold markings at the lower tip, namely, the slight webs along each side of the rod and the shape of the tool that made the original mold cavity.

As in all previous experiments, the groove was wrapped with several loops of Type 316 stainless steel wire used to hang the rod in the hot zone of the furnace with the tip of the rod pointing down. In this particular experiment, the furnace was operated at 1490 ^{o}C. Also, we installed a new cylinder of the argon-1% hydrogen mixture used to flush the furnace and region beneath it.

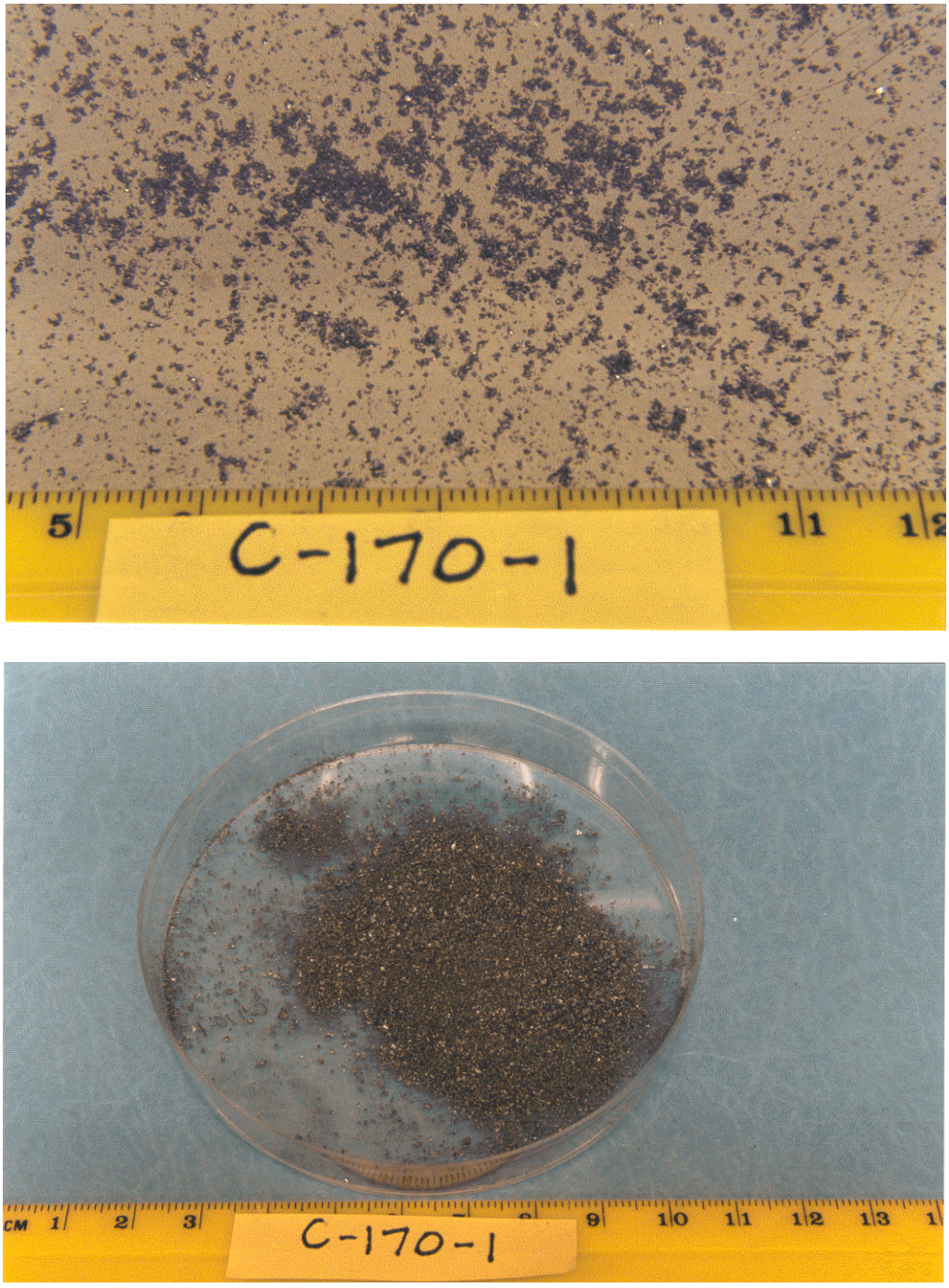

Figure 26(a) (above); Figure 25(b) (below).

Figure 26. Photograph of debris generated during the melt-water interaction of a drop of molten ferrosilicon alloy triggered by the underwater explosion of 100 ml of a stoichiometric hydrogen-oxygen mixture. Alloy, considered non-alloyed, contained 0.020 w/o Al and 0.011 w/o Ca. In (a), a portion of the debris was photographed as it had fallen onto the catcher pan at the bottom of the chamber; in (b), it was photographed after transfer to a Petri dish. (C-170-1)

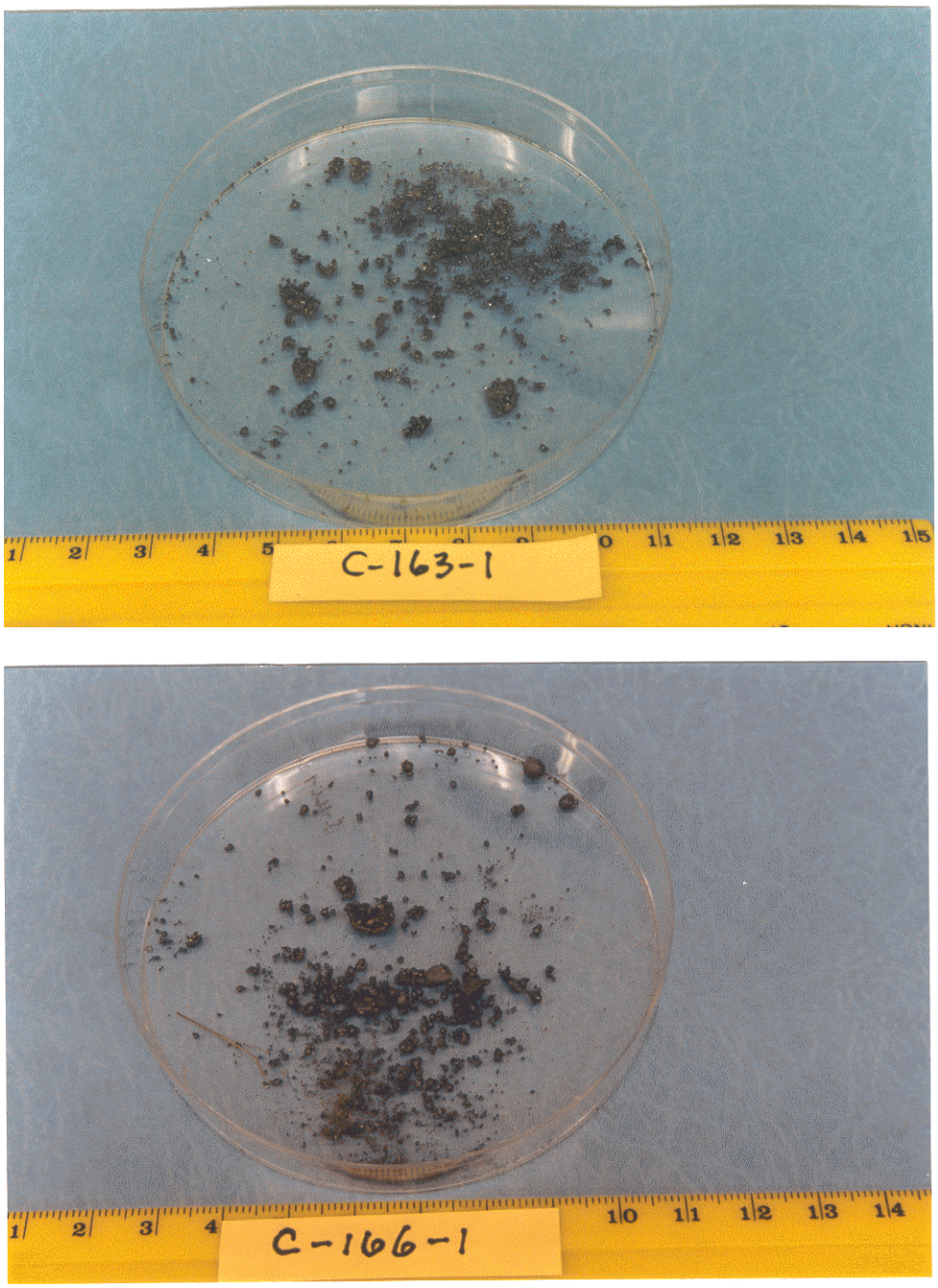

Figure 27(a) (above); Figure 27(b) (below).

Figure 27. Photographs of the coarse debris generated during melt-water interactions of drops of molten ferrosilicon alloys initiated by the underwater explosions of 100 ml of stoichiometric hydrogen-oxygen mixtures. In (a), the alloy contained 0.34 w/o Al and 0.074 w/o Ca (C-163-1). In (b), the alloy contained 1.4 w/o Al and 0.63 w/o Ca (C-166-1). Both sets of debris were photographed after transfer to Petri dishes. Breakup of both drops of melt is thought to have been caused by Weber-type processes, not by steam explosions.

Figure 28. Photograph of the products generated during the melt-water interaction of a drop of molten ferrosilicon alloy with (1, 3 and 4) and without (2) exposure to a triggering transient generated at the underwater surface of a solenoid-driven impactor. The time delay and depth were incorrect for initiating a vigorous explosion. A few tiny satellite drops are not shown. Alloy contained <0.001 w/o Al and 0.001 w/o Ca. (C-133-3).

Figure 29. A fresh rod from the batch F8 (C-133-2). Note the distinctive mold markings at the lower tip, namely, the slight webs along each side of the rod and the shape of the tool that made the original mold cavity. (C-195-1 Pretest).

Figure 30. Time-exposed photograph of a steam explosion attempted with a drop released from the fresh rod of non-alloyed ferrosilicon from the batch F8 (C-133-2) shown in Figure 29. Triggering was attempted with the hydrogen-oxygen combustion tube. Fiducial rods to either side of the image are 134 mm apart. (C-195-1).

Our carefully planned demonstration experiment was then carried out as we had normally performed the previous experiments with the F7 (C-133-1) rods. For the trigger, we chose the hydrogen-oxygen combustion tube with its upper end placed 30 centimeters below the surface of the water and set to fire 350 ms after the drop was released. To record an image of the interaction, we selected open shutter time-exposed 35 mm photography in a darkened room because of the impressive images it can produce.

The results of the experiment were truly disappointing. The explosion we had planned did not occur; instead, the drop merely split roughly in two and produced a few other minor traces. Thus, we did not achieve a dramatic explosion with fine fragmentation that produced images similar to those shown in Figures 7 and 16 in this report. Instead, we produced the ugly time-exposed image shown in Figure 30.

The debris that remained after the experiment was also very coarse, as shown in Figure 31—not the fine powder that forms when a vigorous steam explosion occurs (for example, see Figure 25.)

In the days after our guest departed, we performed a number of other confusing experiments with the F8 (C-133-2) rods. Sometimes we obtained vigorous explosions and sometimes not, even though the conditions seemed identical to those that always produced good explosions with the F7 (C-133-1) rods.

After a few of these strange experiments, a pattern for the failures began to emerge, as outlined in Table 8.

- The first two drops formed from a fresh rod never exploded; the third and subsequent drops always exploded.

- If the lower tip of the rod had broken off before it was used, the remaining rod produced drops that always exploded.

- If the rod was inadvertently hung "upside down" in the furnace (that is, with the lower tip up), the drops that formed always exploded.

We therefore concluded that the lower tips of the rods in batch F8 (C-133-2) have compositions that differ from the rest of the rods in some way that prevents the drops from exploding. (It would be interesting during 1998 to analyze the tips of the rods from batch F8 (C-133-2) to determine the differences in composition that we believe prevent explosions of the drops produced from them.)

A simple solution to the difficulties produced by this batch of rods, then, is to always hang fresh rods in the furnace "upside down," that is with the lower ends at the top. Because of our present method of suspension with Type 316 stainless steel wire, we are unable to produce drops from rods shorter than about 50 mm.

This effectively causes the remainder of the rods to be discarded and prevents us from attempting experiments with the lower tips of the rods.

Figure 31. Debris recovered from the interaction shown in Figure 30. (C-195-1).

Table 8. History of Drops Produced from Rods in Batch F8(C-133-1)
Analysis indicates: Si, 73.9; Fe, 24.9; Al, 0.002; Ca, 0.007 (all weight %)

		Explosion?					
Expt. No.	Drop 1	Drop 2	Drop 3	Drop 4	Remarks	Pretest rod	Posttest rod
C-195-1	No	--	--	--	New F8 rod for SINTEF visitor; also new argon-1% hydrogen	C-195-1 Pretest	C-195-1 Posttest
C-197-1	No	No	Yes	--	New F8 rod; 1st two drops, no explosion at 350 ms delay; 3rd drop exploded at 370 ms	C-197-1-Pretest	C-197-1 Posttest
C-199-1	Yes	Large expl	None	Large expl	F8 rod was used in previous test; 3 good explosions; 3rd drop had oxide on it and did not explode	C-197-1 Posttest	C-199-1 Posttest
C-201-1	Good	Good	Remarks	--	New F8 rod with tip broken off; 1st two drops exploded; on 3rd try, rod fell with explosion	C-201-1 Pretest	Lost
C-203-1	Remarks	Remarks	Remarks	--	New F8 rod with web; 2 drops into hot water. gave no explosions; 2nd new F8 rod with upper end down gave 3 moderate explos. In hot water with combustion	C-203-2 Pretest C-203-1 Pretest #2	Lost C-203-1 Posttest #2
C-205-1	No photo	Good	Good	Good	Four good explosions in ice water	C-203-1 Posttest #2	C-205-1 Posttest
C-211-1	No	No	Yes	--	New F8 rod; 1st two drops, no explosion; 3d drop exploded; Hycam on 1st drop saw no explosion	C-211-1 Pretest	C-211-1 Posttest

DISCUSSION

Impactor vs. Combustion Tube Triggering

Both the mechanical impactor and the hydrogen-oxygen combustion tube have achieved the primary objective of this work—to produce steam explosions of single drops of molten ferrosilicon alloys under conditions that favor their quantitative study. Both generate pressure transients of similar magnitude but with very different degrees of water motion. As our understanding of the processes increases, one of the techniques should provide triggering conditions that most resemble those the individual melt drops might experience during a large scale, drop-to-drop propagation of an explosion through very many melt drops arrayed in water, as in industrial granulation processes.

Although we have not achieved highly reproducible peak pressures with the combustion tube (0.083 MPa at 100 mm, with a standard deviation of ±0.061 MPa; see Table 5), the success rate for initiating explosive interactions was quite high. This suggests that the conditions generated by the combustion tube may successfully replicate the propagation of explosions of drops of molten ferrosilicon drops in the industrial granulation situation. Moreover, the ability to trigger in the presence of Weber-type breakup caused by the high-speed water jet may be an important advantage over mechanical triggering where there is considerably less water motion.

Comments on Combustion Tube Triggering

Although we plan to concentrate mostly on improving mechanical initiation procedures during 1998, we still shall regard the combustion tube as an important alternate triggering source that should be developed further as time permits.

Probably the reproducibility of our combustion tube experiments is poor because the technique relies on a complex deflagration-to-detonation transition (DDT) to produce strong pressure pulses. The ignition of the stoichiometric hydrogen-oxygen mixture initially produces a slow-moving deflagration similar to a candle flame that escalates rapidly with turbulent mixing into a supersonic detonation wave that generates a strong shock wave. The combustion of stoichiometric hydrogen+oxygen has been studied for decades (Strehlow, 1968). These studies suggest that our DDT's are probably quite sensitive to many characteristics of our system. Several modifications of our equipment and procedures, therefore, may produce more reproducible and higher peak pressures and perhaps better triggering:

- Carefully adjust the composition of the gas mixture to the ratio of exactly two volumes of hydrogen to one volume of oxygen. It is likely that our method of determining the individual gas volumes by viewing the meniscus in a 25.4 mm-diameter tube filled with water may produce enough uncertainty in the gas composition to significantly alter the DDT. One way to achieve the exact composition would be to generate the gas mixture by the electrolysis of water, which must produce a gas mixture with the exact 2:1 stoichiometric ratio.

- Close the bottom of the combustion tube. It is possible that the rapid relaxation of pressure in the combustion tube by downward flow of water and bubbles from the essentially open bottom of our combustion volume may contribute to erratic DDT's.

- Alter our smooth-walled combustion tube to produce more turbulence in the flame zone as it moves upward. This has been done by earlier experimenters who inserted an array of obstacles in the tube that stirs the gas mixture as it burns but does not block the path excessively. Typical obstacles are ring-shaped disks with hole diameters about 80% of the tube diameter, or a helix that fits snugly inside the tube.

- Carefully align the combustion tube vertically. In these experiments, we have not paid great attention to the verticality of our tube. It may be that the DDT is sensitive to the exact positioning of the tube.

- Change the dimensions of the tube. In these experiments, we arbitrarily chose a tube with a diameter that would provide a reasonably long combustion path with an initial volume of 100 ml. It is possible that different length-diameter ratios will provide more reproducible shock generation. Increasing the total volume of the tube should be approached cautiously, however, because the explosions with 100 ml of the stoichiometric mixture are already quite vigorous.

Comments on Impactor Triggering

It has been indicated above that the impactor is the most convenient triggering source. It quite reproducibly produces pressure pulses with peaks of 0.422 ± 0.074 MPa normalized to 100 mm (see Table 6) that are about 0.5 ms wide. It is complementary in many ways to the hydrogen-oxygen combustion tube for initiating steam explosions of single drops of melt:

- The impactor can trigger melt drop explosions both at its surface and in the free volume of water above the surface. This provides a broad capability for investigating explosions in the industrial granulation processes, where initiation might occur at underwater surfaces, for example, at tank walls, struts or other underwater structures, as well as at underwater locations away from surfaces.

- The impactor is valuable when it is desired to initiate steam explosions with minimum interference from bubbles. These bubbles arise from two sources: (a) steam bubbles that are emitted with a high-speed water jet from the combustion tube immediately after the hydrogen-oxygen explosion and (b) the bubbles of unburned gases that rise long after the combustion. Both types of bubbles obscure the images of the steam explosion zone. Use of the impactor for triggering eliminates the overall bubble activity in the interaction zone.

- Initiation of explosions where it is desired to measure gaseous hydrogen produced by the metal-water reaction. In most of our ignitions of the stoichiometric hydrogen-oxygen mixtures, the combustion always seems to leave behind some unburned gases. Gaseous hydrogen and oxygen, of course, both would interfere with the analyses of hydrogen produced during the melt-water reaction (see Nelson et al., 1994b). Clearly, triggering the explosions with the impactor would not produce gases that could interfere with these measurements of hydrogen.

- Compared to the combustion tube, which emits a high-speed jet of water and bubbles that travel about 200 mm upward in a few milliseconds, the impactor might prove more valuable for triggering in shallow water. Triggering in shallow water may turn out to be important in steam explosion studies with some of the molten ferrosilicon alloys, especially when Al and Ca are added to the metal, where solid shells are thought to form very quickly after the drops are released. Moreover, the release of drops at temperatures very near the liquidus may also make shallow water attractive for studying steam explosions before solidification begins. It is unlikely that the combustion tube as configured here could be used in water shallower than about 200 mm because the upward jet would probably break through the water surface before the steam explosion could be initiated.

- The impactor has definite advantages where repetitive triggers are needed, for example, when several drops are released one after the other from the same rod during the same experiment. Compared to the combustion tube, which takes about an hour to reset for each firing (i.e., to replace the membrane and exploding copper filament and to recharge with the two gases), the solenoid-driven device resets by gravity after the power source is disconnected and, if desired, can provide repeated triggering pulses as often as a few seconds apart.

- The impactor might prove advantageous in situations where it is desired to quantitatively collect all solid products from a given explosive interaction. We can envision triggering the entire explosion within a strong plastic bag (e.g., made of Kevlar) that also contains the impactor, thus retaining the debris in a relatively small volume of water. This might be especially valuable for studying the very fine colloidal products of the combustion reactions.

- The impactor cannot be modified as readily as the combustion tube, however. While the length, diameter, wall obstacles and gas filling of the combustion tube can be easily changed to modify the pressure pulses, a given impactor design is fairly inflexible in the pulses it can produce. A given design can probably be changed somewhat (say, 10%) by: increasing the voltage applied to it; by changing the weight attached to the armature; or by changing the acoustic impedance of the plate, e.g., by changing the plate thickness, the material of which is made, or its wettability by water. Clearly, there is still much to be learned about the performance of both trigger generators.

Threshold Pressures for Triggering

Compared to experiments with the combustion tube, initiation of an interaction with the impactor provides clean and unobstructed imaging for estimating the magnitude of the pressure transients required to trigger the steam explosion of a drop of molten ferrosilicon. This can be seen, for example, in Figure 16, where the position of the drop at explosion time was determined to be 45 mm above the surface of the impactor. (We used the measured separation of 138 mm between the two vertical fiducial rods at either side of the explosion in Figure 16 to scale the image.) By applying the 1/r relationship that links the distance between the center of the explosion and the impactor to the peak pressure of 0.422 MPa it produces at 100 mm, we estimate the peak pressure of the triggering transient to have been 0.95 MPa at the drop. (This peak pressure is about the same as the 0.71 MPa pulses that successfully triggered the steam explosions of the CO_2 laser-melted drops of iron oxide studied by Nelson and Duda (1981, 1982).)

We believe this to be the first determination of the magnitude of the pressure transient required to initiate the steam explosion of a single molten ferrosilicon drop. Measurements of this sort should be valuable for analyzing (a) the accident conditions that might initiate a large-scale explosion during industrial granulation, and (b) the drop-to-drop propagation of a large explosive wave through an array of many molten ferrosilicon drops in water.

Effects of Al and Ca Additives on the Explosions

One of the major objectives of the 1997 experiments has been to determine the effects of the addition of Al and Ca on the initiation of steam explosions of drops of molten ferrosilicon. We have attempted to initiate explosions of drops of the alloys that contain these additives, using both the impactor and the combustion tube triggering devices.

In each successful explosion reported in Tables 3 and 4, the drops were generated only from non-alloyed starting materials, either rods F7 (C-133-1) or F8 (C-133-1). We have never been able to achieve either spontaneous or triggered explosions with the materials that contain added Al or Ca; see Table 1. The closest we have come to triggering explosive interactions so far with melts that contain these additives has been to achieve very coarse breakup with the intermediate amounts of 0.34 wt.% of Al and 0.074 wt.% of Ca (rod F5 (C-121-3) in experiments C-219-1, C-221-1 and C-223-1 (see Table 4). Some of the particles stripped from the parent drop were seen to burn with the "seaweed-like" pattern, somewhat like that shown in Figure 22.

These observations suggest that a protective solid skin forms on the spherules of melt with the additives that does not seem to form on the non-alloyed ferrosilicon. This skin seems to prevent the vigorous triggering of the explosive interactions, at least at a water depth of about 25 cm for the drop diameters studied here (about 10 mm). It is possible that the Al and Ca are surface active in the molten ferrosilicon, as suggested in our discussions of drop weights above. This may generate a layer enriched with metals that form high

melting point oxides (e.g., alumina that melts above 2000 ^{o}C). On contact with oxidizing conditions, these metals will immediately form crystals to nucleate the ferrosilicon before it can supercool below its liquidus temperature. (An Al-rich layer on commercially granulated ferrosilicon has been observed recently by Horn et al. (1998).) In the absence of the additive metals, the melt will supercool and remain triggerable at temperatures well below the liquidus.

Bubble Energetics

Image Analyses

We have devoted a large part of our efforts during 1997 to estimating the amounts of energy transferred to the water during the steam explosions of the drops of molten ferrosilicon. These are the pressure-volume energies determined from the growth of the bubbles generated by the explosive interactions. We have used three imaging techniques for measuring the bubble growth: time-exposed photography in a darkened room; video imaging at 60 frames per second; and high-speed photographic imaging at 1000 frames per second. The estimated energies have been summarized in Table 7.

Although the number of images analyzed so far is small, several trends are apparent from this table:

- Video images are not reliable for measurements of the bubble growth. This can be seen in Table 7 by comparing Estimate C with Estimate D, determined with video and Hycam imaging, respectively. While the imaging of the first bubble produced comparable results with the two techniques, the slower framing rate of the video camera allowed it to completely miss the second bubble in the interaction and thus grossly underestimate the bubble energy produced in the interaction.

- By comparing Estimates B and D, the imaging technique that is easiest to use, time-exposed 35 mm photography, seems to produce information about maximum bubble growths equivalent to that produced by the most elaborate technique, high-speed photography. Of course, there is no time resolution with the time-exposed images, but the magnitudes of the bubble energies seem comparable to the high-speed images.

- When we compare Estimate A with Estimates B and D, it seems that the hydrogen-oxygen combustion triggers somewhat larger steam explosions than the mechanical impactor. Although this may be true for the one image analyzed, C-189-1, the variability of the peak pressures generated by the combustion technique (see Table 5) suggests that the triggering might also be similarly variable.

- Estimate E suggests that the “hemispherical” explosion initiated at the surface of the impactor may be several times larger than the “spherical” explosions triggered in the free water volume by either the combustion or mechanical trigger. Moreover, the explosion initiated at the surface seems more efficient because only one bubble formed in the “hemispherical” explosion, compared to double bubbles for the “spherical” explosions (compare Figure 15 with Figures 7 and 16). This greater efficiency and transfer of energy to the water could be due to smaller losses of heat into the half solid angle compared to those into the full solid angle.

Again, it should be emphasized that, as yet, too few images have been analyzed; to substantiate the trends just presented, more images must be examined. Although we will have many video images of the bubbles, we plan to concentrate more effort in 1998 on analyzing time-exposed images of the explosions because they seem to offer the simplest way to obtain reliable bubble energies. We will examine both images not analyzed in 1997 and new images obtained in 1998. It may also be possible to measure bubbles more easily on Hycam films because new 16 mm projection equipment may become available during 1998.

Comparisons with Available Melt Energies

In this section, we will make a preliminary comparison of the enthalpy of the molten 25 wt.% Fe-75 wt.% Si ferrosilicon alloy reported by Klevan (1997) with the energies transferred to the water by the steam explosions, as determined by the analyses of the bubble images and summarized in Table 7. As seen in this table, we have obtained maximum pressure-volume energies that range from about 13 J/g to18J/g for the "spherical" explosions and from 55 to 68 J/g for the "hemispherical" explosions. We will use the averages of these extremes, 15.5 and 61.5 J/g, respectively, for our preliminary estimates.

From the graph in Figure 2.4 of Klevan (1997), we estimate the enthalpy of molten 25 wt.% Fe-75 Wt.% Si at the liquidus temperature to be 2300 J/g. Thus, the bubble energy transferred to the water by the "spherical" explosion, 15.5 J/g, is approximately 0.7 % of the total available enthalpy in the melt; also, the bubble energy transferred by the "hemispherical" explosion, 61.5 J/g, is about 2% of the available enthalpy.

These estimates of the energy transferred to the water may be quite conservative, because steam explosions of larger drops may be more vigorous per gram of melt than those of the 9.2 mm drops we have been studying. As we increase drop diameter toward the desired target of 20 mm, the melt mass will increase by $(20/9.2)^3 = 10.3$. If the efficiency also increases with the melt mass, the explosions could become very energetic indeed! (We already have indications in experiment C-213-1 #2 that a 17.2 mm drop [$(17.2/9.2)^3 = 6.3$] may push our current apparatus to its limits.) The drop diameters of 15 mm chosen for the experiments planned for 1998, in which the melt mass will increase by $(15/9.2)^3 = 4.3$, should provide a good test of whether the efficiency will change significantly as the drops become larger.

Also, the considerably larger energy transfer seen in the "hemispherical" explosion produced at the surface of the impactor (Estimate E in Table 7) suggests that wall effects (for example, at underwater structures, struts and the sidewalls of the tank in industrial granulation) might play an important role in the overall energy transfer in a prototypical explosion on large scale.

And finally, a large-scale steam explosion involving thousands of drops may be considerably more efficient in conserving heat than the isolated single drops we have studied. Also, the mechanism of propagation in the large array may produce a more efficient interaction than the simpler single drop explosions might indicate.

For now, then, the value of 1 or 2% should be regarded only as preliminary lower limits that will be refined as we continue our analyses and extend our experiments.

Underwater Combustion of Molten Ferrosilicon

From the various images we have recorded during 1997, we have reason to believe that metal-water reactions always accompany steam explosions of the ferrosilicon alloy drops. The observations consistent with these reactions are the prolonged generation of light, the formation of a cloud of tiny bubbles, presumably hydrogen-filled, and the deposition of colloidal material in the water. While these observations are still mainly interpretive at this time, they form the basis for hypotheses to guide future experiments.

There are two basic pathways for the underwater combustion of metal drops: (a) the oxidation of the metal proceeds by incorporating oxygen into the metal, thus forming liquid and then solid products that contain progressively increasing ratios oxygen to metal (here, Fe and Si) and (b) gas-phase combustion where the metal is vaporized and burns with a flame contained within discrete bubbles. In both cases, gaseous hydrogen is generated. Examples of metals that might burn according to pathway (a) are Fe and Zr, both of which have relatively low vapor pressures and broad ranges of stable O/Me ratios in both liquid and solid phases. Al would be expected to burn underwater via pathway (b) because of its high vapor pressure and inability to form oxides other than Al_2O_3.

The differences between these pathways can best be determined by collecting and analyzing the products of the explosive interactions between metal and water. If oxygen-containing products are found, pathway (a) is probably occurring. If only metallic phases are found in the fine debris particles and combustion is known to have occurred, pathway (b) is likely. Colloidal particles deposited in the water are usually also an indication of gas-phase combustion.

We propose the following hypothesis: that small particles of molten 75 wt.% Si-25 wt.% Fe often burn underwater via gas phase processes to generate gaseous hydrogen, luminosity and to deposit a colloidal product in the water. As these particles burn and generate hydrogen, they become enclosed within individual bubbles that tend to rise due to the buoyancy of the particle-bubble combination. We believe the luminosity is produced as the hot vapors condense at the inside surface of the bubbles. This smoke-like condensate then is taken up by the surrounding water to form the colloidal products. We also suggest that during the burning, oxygen is not incorporated into the melt particles to form FeSiO-type compositions; instead the gaseous oxidizer (steam) reacts only with metal vapor within the bubble to form gaseous oxides.

We base this hypothetical mechanism on observations at both Stoughton and Madison as follows:

- The X-ray diffraction patterns of the starting material and of the debris recovered from explosive fragmentations of the melt in which combustion is believed to have occurred were identical (see Figure 23). This is consistent with the burning away of metal as vapor without forming oxygen-containing particles of melt that would add new phases to the X-ray diffraction patterns. (The underwater combustion of drops of pure aluminum proceeds similarly (Nelson et al., 1995) to leave only metallic aluminum debris particles and colloidal aluminum oxide in the water.)

- Chemical analyses of 1 mm to 2 mm commercial fines produced from 75 wt.% Si-25 wt.% Fe indicate a strong depletion of Si and enrichment of Fe. The final composition of the fines is reported to be 66 wt.% Si-33 wt.% Fe (Horn et al., 1998). We postulate that the depletion of Si results from the sustained gas-phase combustion of the smaller ferrosilicon particles that occurs to a much lesser extent with the larger drops during industrial granulation.

- This mechanism is also consistent with the observation that when drops of nonexploding alloyed molten ferrosilicon are released into hot water, fewer fines are generated than when they are released into colder water (Nelson et al., 1997a). We believe the slower cooling in hot water allows more time for the smallest melt particles to burn away completely. This, then, accounts for the smaller amounts of fines.

- The deposition of colloidal material in the water near the combustion is consistent with the properties of the oxides of both Si and Fe. Both metals can precipitate very stable colloids during a number of chemical processes that start with the metals in homogeneous solutions (for example, during the neutralization of an acidic solution). Silica gel is probably the most familiar example of a metal-based oxidic material that forms very stable colloidal suspensions in water.

As yet, we have little quantitative information to support this hypothetical explanation of the combustion of ferrosilicon drops. Several lines of investigation might provide important information about the mechanism: measurements of the amounts of hydrogen generated, collection and analyses of the colloidal combustion products, and, possibly, spectral analyses of the radiation emitted during the combustion.

Comments on Future Studies

We add here a few final comments that may bear on future work, including that planned for1998:

Release of Drops at the Liquidus. In the experiments performed in both 1996 and 1997, the melt always has intentionally been released at or very near the liquidus temperature because (a) the pendant drop procedure inherently cannot produce melt at higher temperatures and (b) this temperature can provide a

convenient and reasonably well known fixed point for optical pyrometry. Also, the pendant drop procedure provides a very simple experimental situation for high temperature studies in which the melt is supported on solid of the same composition, thus eliminating the need for compatibility with another solid for support or containment.

Unfortunately, however, the release of drops at the liquidus always limits us to the study of the interactions of supercooled melts. Thus, the inability to achieve steam explosions of drops with Al and Ca additives may have to do more with the inability of the melt to remain liquid below the release temperature in our experiments than with some intrinsic "nonexplosive" properties of the melt.

We should, then, also think about experimenting with the melts, both with and without Al and Ca additives, at release temperatures higher than the liquidus. Also, this would very likely simulate actual granulation conditions more realistically. The release of melt at higher temperatures, of course, will require a procedure different from the pendant drop technique. One possibility would be to use a bottom-draining crucible (Nelson et al., 1995) or a tilting crucible (Nelson et al., 1988) similar to those used for the release of drops of superheated molten aluminum. A suitable crucible material may be difficult to find, however.

Varying Drop Diameters. In the 1998 studies, we have mutually agreed to study the effect of drop diameter on the explosions of the same three alloys—non-alloyed, and with two levels of Al and Ca additives. We have tentatively decided to use drops produced from rods of 15 mm diameter for comparison with those released from 10 mm rods in 1996 and 1997. These diameters have been selected primarily because 10 and 15 mm rods are most easily prepared in Trondheim.

There is the possibility that we may want to study drops with diameters different from those produced from 10 and 15 mm rods (for example, if the explosions or fall velocities of the larger drops seem excessive). Then it will be necessary to produce either smaller or larger rods. We should consider the possibility of preparing rods with square cross sections by sawing them from larger billets of the three alloys. Also, we could probably study drops between 10 and 15 mm by grinding the 15 mm rods to smaller diameters. We realize the ferrosilicon materials are hard and brittle and difficult to work. But UW shop personnel assure us there are specialized machining techniques available to cut and grind materials of this hardness.

There might be an additional benefit in working with rods prepared from larger initial billets, namely, to eliminate or minimize the occasional localized deviations in composition we believe to have caused our difficulties with rods of batch F8 (C-133-2).

Compositional Analyses. There are several situations in which we believe additional analyses of the starting materials or products might be helpful. One might be to investigate the difficulties with the starting materials just mentioned. A second might be to examine the composition of the colloidal combustion products deposited in the water. Although X-ray diffraction immediately comes to mind as a way to examine this latter material, its crystallite size might be too small to produce good diffraction patterns. We therefore suggest that inductively coupled plasma mass spectrometry (ICPMS) be considered as an additional analytical scheme for making quantitative elemental analyses of the various materials encountered in these studies.

CONCLUSIONS

The experiments performed during 1996 and 1997 have established that the pendant drop technique can provide a simple, inexpensive and reproducible way to prepare single drops of molten ferrosilicon alloys at their liquidus temperatures. Three 75 wt.%Si-25 wt.% Fe alloys were studied, one without and two with Al and Ca additives. The drops can be released into liquid water either spontaneously or with mechanical shaking to investigate quantitatively the steam explosions that sometimes occur during industrial granulation processes.

Because 10 mm drops of the three alloys always freeze benignly in the water without exploding spontaneously, we have developed two low-cost schemes to generate pressure transients in the water that will trigger their explosions—hydrogen-oxygen combustion and mechanical impact. Each method has advantages and disadvantages. Even though the combustion technique is not highly reproducible, it triggers explosions of drops in free fall very effectively. But it also generates a high velocity water jet with bubbles that can obscure imaging and mechanically fragment the drops; the jet also may burst through the surface of the water if it is too shallow. The impactor also can initiate explosions, either while the drops are still falling through the water or after they land on its steel surface. Moreover, the transients it produces are quite reproducible and without strong water motion or bubbles that interfere with imaging of the interactions. Transients with peak pressures of about 1 MPa will trigger explosions of molten drops of non-alloyed ferrosilicon when they are about 45 mm above the impactor.

Increasing the water temperature decreases the vigor of the explosions of the non-alloyed drops, causing coarser fragmentation. Our experiments have also established that Al and Ca additives effectively suppress explosions of 10 mm ferrosilicon drops in cold as well as hot water, even when the drops are exposed to the strongest triggering transients.

Whenever molten ferrosilicon contacts liquid water, the metal reacts chemically with the water. When an explosion or other fragmentation of the melt occurs, the particles formed usually burn with a self-sustained combustion that releases bubbles of hydrogen and colloidal material into the water. Also, the particles rise in the water as they burn, often forming distinctive luminous patterns on time-exposed photographs.

By measuring the photographic and video images of the bubbles produced by the steam explosions, we are able to estimate the pressure-volume energy transferred to the water by the exploding ferrosilicon drop. We have determined this energy to be 1% or 2% of the available enthalpy of the melt.

Larger drops fall through the water more rapidly than smaller drops; for example, a 17.2 mm drop of molten ferrosilicon falls about 6 times faster than a 9.2 mm drop. This and other aspects of larger drops will be studied further during 1998.

ACKNOWLEDGEMENTS

This work was supported by SINTEF Materials Technology, Trondheim, Norway, via a contract monitored by Dr. Trond Bergstrøm, Process Metallurgy and Electrochemistry Division.

FINAL NOTE

This document originally was submitted to the sponsor, SINTEF Materials Technology, Trondheim, Norway, on March 15, 1998, as the draft final report that describes the research performed at the University of Wisconsin-Madison during 1997. Three informal letter reports that describe this work also have been submitted to the sponsor on July 1, 1997 (Nelson et al., 1997b), September 1, 1997 (Nelson et al.,1997c) and December 31, 1997 (Nelson et al., 1997d).

Related research has been performed at NTNU, the Norwegian Technological University, Trondheim, Norway, under the direction of Professor Johan Kr. Tuset, and has been described in the thesis "Steam explosions during granulation of Si-rich alloys: Effect of Ca- and Al-additions" by Kjetil Hildal, dated 25 March, 2002. It may be accessed via the Internet link http://www.ub.ntnu.no/dravh/000057.pdf.

REFERENCES

Anderson, R.P., and Armstrong, D.R., 1981, "Experimental Study of Small-Scale Explosions in an Aluminum-Water System," presented at the Winter Annual Meeting of the American Society of Mechanical Engineering, Washington, DC, November 15-20, and published in Fuel-Coolant Interactions, ASME HTD-Vol. 19, 31-40.

Arakeri, V.H., Catton, I., Kastenberg, W.E., 1978, "An Experimental Study of the Molten Glass/Water Thermal Interaction Under Free and Forced Conditions," Nucl. Sci. Eng. 66, 153-66.

Beck, D. F., Berman, M., and Nelson, L. S., 1991, "Steam Explosion Studies with Molten Iron-Alumnia Generated by Thermite Reactions,"in Dynamics of Detonations and Explosions: Explosion Phenomena, edited by A. L. Kuhl, J. -C. Leyer, A. A. Borisov, and W. A. Sirignano, Progress in Astronautics and Aeronautics 134, 326-355.

Buxton, L.D., and Nelson, L.S., 1975, Core Meltdown Experimental Review, SAND74-0382, Sandia National Laboratories, Albuquerque, NM, Chapter 6.

Ciccarelli, G., 1991, Investigation of Vapor Explosions with Single Molten Metal Drops in Water Using Flash X-ray, Thesis, Department of Mechanical Engineering, McGill University, Montreal, Quebec, Canada.

Ciccarelli, G. and Frost, D.L., 1994, "Fragmentation Mechanisms Based on Single Drop Steam Explosion Experiments Using Flash X-ray Radiography," Nucl. Eng. Des. 146, 109-132.

Corradini, M.L., Kim, B.J., and Oh, M.D., 1988, "Vapor Explosions in Light Water Reactors: A Review of Theory and Modelling," in Progress in Nuclear Energy, 22, pp. 1-117.

Cronenberg, A.W., and Benz, R., 1980, "Vapor Explosion Phenomena With Respect to Nuclear Reactor Safety Assessment," in Advances in Nuclear Science and Technology, Lewins, J., and Becker, M., eds., Plenum Press, New York, NY.

Dullforce, T.A., Buchanan, D.J. and Peckover, R.S., 1976, "Self-Triggering of Small-Scale Fuel-Coolant Interactions: I. Experiments," Journal of Physics D: Applied Physics, 9, pp. 1295-1303.

Epstein, S.G., and Miller, R.E., 1987, "Causes and Prevention of Molten Aluminum-Water Explosions," Light Metals 1987, The Metallurgical Society of AIME, Warrendale, PA, pp. 693-698.

Flory, K., Paoli, R., and Mesler R., 1969, "Molten Metal-Water Explosions," Chemical Engineering Progress, 65, pp. 50-54.

Forwald, K., 1991, Private communication via Dr. Young Lee, Elkem Research, Pittsburgh, PA.

Horn, Q. C., Nassaralla, C. L., and Heckel, R. W., 1998, "Microstructural Study of Granulated Ferrosilicon with 75 wt.% Silicon," Draft Manuscript Prepared for INFACON 8.

Kim, B., and Corradini, M.L., 1984, "Recent Film Boiling Calculations: Implication on Fuel-Coolant Interactions," Fifth Int. Meeting on Thermal Nuclear Reactor Safety, Karlsruhe, W. Germany, Vol. 2, pp. 1098-1107.

Klevan, O. S., 1997, Removal of C and SiC from Si and FeSi during Ladle Refining and Solidification, Dr. Ing. Thesis, Department of Metallurgy, The Norwegian University of Science and Technology, Trondheim, Norway.

Kondo, S., Togo Y., and Iwamura T., 1976, "A Simulation Experiment and Analysis on the Effects of Incoherence in Fuel Coolant Interaction," PNC N251, 76-12, 285-305.

Nelson, L.S., and Duda, P.M., 1981, Steam Explosion Experiments with Single Drops of Iron Oxide Melted with a CO_2 Laser, Sandia National Laboratories, Albuquerque, NM, NUREG/CR-2295, SAND81-1346.

Nelson, L.S., and Duda, P.M., 1982, "Steam Explosion Experiments with Single Drops of Iron Oxide Melted with a CO_2 Laser," High Temperatures, High Pressures, 14, 259-281.

Nelson, L.S., and Duda, P.M., 1983, "Steam Explosions of a Metallic Melt as its Degree of Exidation Increases: Fe, $FeO_{1.0}$, and $FeO_{1.2}$," Proc. Int'l Mtg. on Thermal Nuclear Reactor Safety, Aug. 29 - Sept. 2, 1982, Chicago, IL, U.S. Nuclear Regulatory Commission, Washington, DC, NUREG/CP0027, Vol. 2, 981-986.

Nelson, L.S., and Duda, P.M., 1985, Steam Explosion Experiments with Single Drops of Iron Oxide Melted with a CO_2 Laser, Part II," Parametric Studies, Sandia National Laboratories, Albuquerque, NM, NUREG/CR-2718, SAND82-1105.

Nelson, L. S., Eatough, M. J., and Guay, K. P., 1988, "Why Does Molten Aluminum Explode at Underwater or Wet Surfaces?," in Light Metals 1989, P. G. Campbell (ed.), The Minerals, Metals and Materials Society, pp. 951-961, Warrendale, PA.

Nelson, L.S., Fuketa, T., Eatough, M.J., Vigil, F.J., Szklarz, D.D., Wong, C.C., and Hyndman, D.A., 1992, Steam Explosions of Single Drops of Thermite-Generated Melts: 25 and 50 Weight Percent Aluminum-Iron Oxide Initial Mixtures, SAND90-0511, Sandia National Laboratories, Albuquerque, NM.

Nelson, L.S., Hogeland, S.R., and Utash, J.L., 1994a, Bubble Growth, Shock Waves and Flow Transients Produced by Underwater Capacitor Discharges, SAND93-0765, Sandia National Laboratories, Albuquerque, NM.

Nelson, L. S., Duda, P. M., and Hyndman, D. A., 1994b, "Interactions Between Drops of a Molten Aluminum-Lithium Alloy and Liquid Water," Metallurgical and Materials Transactions B, 25B, 623-625.

Nelson, L.S., 1995, "Steam Explosions of Single Drops of Pure and Alloyed Molten Aluminum, " Nucl. Eng. Des.155, 413-425.

Nelson, L. S., Duda, P. M., Hyndman, D. A., Allison, D. K., and Hyder, M. L., 1995, Thermal and Ignition Type Steam Explosions of Single Drops of Molten Aluminum, Westinghouse Savannah River Company, Engineering & Construction Services, Aiken, SC, Report WSRC-RP-95-718.

Nelson, L. S., Bonazza, R., and Corradini, M. L., 1996, Formation of 10-20 mm Drops of Molten Ferrosilicon, University of Wisconsin-Madison, Fusion Technology Institute Report UWFDM-1027.

Nelson, L. S., Bonazza, R., Brooks, P. W., and Corradini, M. L., 1997a, Quenching 10-20 mm-Diameter Drops of Molten Ferrosilicon in Water and on Solids, Informal Letter Report to SINTEF Materials Technology, Trondheim, Norway, March 13, 1997.

Nelson, L. S., Brooks, P. W., Bonazza, R., and Corradini, M. L., 1997b, Generation of Pressure Transients for the Initiation of Steam Explosions of Single Drops of Melt, Informal Letter Report to SINTEF Materials Technology, Trondheim, Norway, July 1,1997.

Nelson, L. S., Brooks, P. W., Bonazza, R., and Corradini, M. L., 1997c, Release of Molten Ferrosilicon Drops into Water: Effects of Triggering and Alloying, Informal Letter Report to SINTEF Materials Technology, Trondheim, Norway, September 1, 1997.

Nelson, L. S., Brooks, P. W., Bonazza, R., and Corradini, M. L., 1997d, Release of Molten Ferrosilicon Drops into Water: Part 2. Effects of Triggering, Alloying and Water Temperature, Informal Letter Report to SINTEF Materials Technology, Trondheim, Norway, December 31, 1997.

Nygaard, L., Brekken, H., Lie, H.U., Magnussen, Th. E., and Sveine, A. 1995, "Water Granulation of Ferrosilicon and Silicon Metal," in INFACON 7, Trondheim, Norway, June 1995, Eds.:Tuset, Tveit and Page, Publishers: FFF, Trondheim, Norway.

Peppler, W., and Till, W., 1986, "Mechanisms Observed During Triggered Fragmentation of a Droplet of Molten Alumina in Water," Proc. Int. Conf. Sci. Technol. Fast React. Safety 2, 497-502.

Pilch, M., and Erdman, C. A., 1987, " Use of Breakup Time Data and Velocity History Data to Predict the Maximum Size of Stable Fragments for Acceleration-Induced Breakup of a Liquid Drop", Int. J. Multiphase Flow 13, (6) 741-757

Reid, R.C., 1983, "Rapid Phase Transitions from Liquid to Vapor," Advances in Chemical Engineering 12, 105-208.

Schins, H., 1986, "Characterization of Shock Triggers Used in Thermal Detonation Detonation Experiments," Nucl. Eng. Des. 94, 983-998.

Sharon, A., and Bankoff, S.G., 1981, "Fuel-Coolant Interactions in a Shock Tube with Initially-Established Film Boiling," PCH, PhysicoChem. Hydrodyn. 2,177-202.

Shoji, J., and Takagi, N., 1983, "An Experimental Study of Small-Scale Vapor Explosions for Molten Tin Dropped Into Water," Bulletin of the Journal of the Society of Mechanical Engineers, 26, 215, 791-796.

Strehlow, R. A., 1968, "Gas Phase Detonations: Recent Developments," Combustion and Flame 12, 81-101.

Vinet, B., Garandet, J. P., and Cortella, L., 1993, "Surface Tension Measurements of Refractory Liquid Metals by the Pendant Drop Method Under Ultrahigh Vacuum Conditions: Extension and Comments on Tate's Law," J. Appl. Phys. 73, 3830-34.

APPENDIX A

Hypothesis: Weber Breakup Determines the Maximum Product Sizes Produced During the Industrial Granulation of Molten Ferrosilicon in Water

It has been reported that the maximum diameters of the products achieved during the industrial water-granulation of molten ferrosilicon alloy (75 wt.% Si-25 wt.% Fe) are about 20 mm (Nygaard et al.,1995). In this appendix, we present preliminary evidence that suggests this maximum granule size is determined by the Weber breakup of all molten drops larger than about 20 mm as they fall through the water.

As indicated in the main part of this report, the Weber number, W_e, given in Equation (A-1), is a measure of the likelihood that a drop of liquid will break up when exposed to a high-speed flow of another fluid:

$$W_e = \rho V^2 D/\sigma \qquad \text{(A-1)}$$

where ρ is the density of the streaming fluid, V is the velocity of the fluid stream past the drop, D is the diameter of the drop, and σ is the surface tension of the drop material. Also, it is shown in the main part of this report that when a 9.2 mm (0.0092 m)-diameter melt drop with a surface tension of 750 dynes/cm (0.75 N/m) (Klevan, 1997) is exposed to a water jet with a density of 1.0 g/cc (1000 kg/m^3) travelling at 8.4 m/s, the Weber number is 875. According to Pilch and Erdman (1987), when the Weber number is greater than 350, the molten drop is very likely to break up catastrophically, provided its viscosity is not too high, and the time it is exposed to the flowing stream is not too short. Nonexploding ferrosilicon drops (with Al and Ca additions) were seen to break up in this manner, as shown in Figures 12 and 13 in the main part of this report.

This same treatment can be applied to drops of melt of other diameters released in free fall into water (Okkonen and Sehgal, 1998). For example, the large ferrosilicon drop produced accidentally in our experiment C-213-1 #2 had a diameter estimated to be 17.2 mm and fell through the water at 3.8 m/s. Equation (A-1) gives a Weber number of 331, just below the threshold value of 350. No breakup would be expected here, and none was observed. (The fall distance here was only 200 mm, however, so the lack of breakup in this short a fall time may not be overly significant.)

If we apply this same fall velocity of 3.8 m/s to a 20 mm drop of molten ferrosilicon, the Weber number is 385. This exceeds the critical value of 350, and the drop is likely to break up during its fall. The fall velocity of the 20 mm drop is probably greater than 3.8 m/s, suggesting an even greater Weber number and an even greater tendency to break up.

We can also use equation (A-1) to calculate the fall velocity of a 20 mm-diameter drop that would be required to produce a Weber number of 350, the threshold value for breakup. This velocity is 3.6 m/s.

From the discussion given above, then, it seems that if the diameter of a molten ferrosilicon drop is greater than 20 mm when it is released into water, it will fall through the water at a velocity of 3.6 m/s or greater. This will cause it to fragment into smaller particles by Weber-type processes. We believe this to be a likely explanation for the absence of frozen particles larger than about 20 mm in the industrial granulation process.

A similar maximum diameter of particles recovered from the industrial water-granulation of silicon has been reported to be about 15 mm (Nygaard et al.,1995). It would be interesting to apply the Weber criterion to this metal with its lower melt density. To determine the Weber number in this exercise, it would be necessary to measure the velocity of 15 mm-diameter (and larger, if possible) drops of molten silicon as they fall through water.

Open shutter, time-exposed photographs of the drops would confirm the Weber breakup of large drops of both silicon and ferrocilicon as they fall through water. The usefulness of this technique for recording Weber-type breakup of molten ferrosilicon drops is indicated in Figures 12 and 13 in the main part of this report.

REFERENCES FOR APPENDIX A

Klevan, O. S., 1997, Removal of C and SiC from Si and FeSi during Ladle Refining and Solidification, Dr. Ing. Thesis, Department of Metallurgy, The Norwegian University of Science and Technology, Trondheim, Norway.

Nygaard, L., Brekken, H., Lie, H.U., Magnussen, Th. E., and Sveine, A. 1995, "Water Granulation of Ferrosilicon and Silicon Metal," in INFACON 7, Trondheim, Norway, June 1995, Eds. Tuset, Tveit and Page, Publishers: FFF, Trondheim, Norway.

Okkonen, T., and Sehgal, B. R., 1997, "Experiments on Melt Droplets Falling into a Water Pool," in Proceedings of the OECD/CSNI Specialists Meeting on Fuel-Coolant Interactions, May 19-21, 1997, Tokai-Mura, Japan, Eds. Akiyama, M., Yamano, N., and Sugimoto, J., Japan Atomic Energy Research Institute, Tokai-Mura, Japan, JAERI-Conf 97-01 1 (Part II), NEA/CSNI/R(97)26, pp. 658-673, January, 1998.

Pilch, M., and Erdman, C. A., 1987, "Use of Breakup Time Data and Velocity History Data to Predict the Maximum Size of Stable Fragments for Acceleration-Induced Breakup of a Liquid Drop", Int. J. Multiphase Flow 13, (6) 741-757.